Mediating gold nanoparticle growth in nanoreactors

Contrôle de la croissance des nanoparticules d'or dans des nanoréacteurs

A Thesis Submitted to the Division of Graduate Studies
of the Royal Military College of Canada
by

Vishva Shah

In Partial Fulfillment of the Requirements for the Degree of
Master of Applied Science

September 2016

Acknowledgements

I would like to thank my supervisors Dr. Cecile Malardier-Jugroot and Dr. Manish Jugroot for their constant support and encouragement. This thesis and work would not have been possible without their invaluable guidance and time. I would also like to thank other members of the group including Ms. Xia Li, Mr. Matt Mctaggart and Dr. Deborah Durbin for sharing their expertise and guiding me for further improvement.

I would also like to thank Dr. Andreas Korinek and Dr. Carmen Andrie at the Canadian Center for Microscopy at McMaster University for their help with the use of TEM instruments. My gratitude also goes to Mr. Bob Whitehead and Ms. Neda Bavarian for their excellent instrumental support.

Lastly, I would like to take this opportunity to thank my parents who have always provided their support regardless of the circumstance. Without them, none of this would be possible.

Abstract

Nanosystems have drawn inspiration from biological systems with many years of evolutionary optimization and biomimicry in many materials has been obtained by using whole organisms, their individual components or soft organic polymeric materials. Biomimetic nanoreactors in aqueous environment have proven to affect both thermodynamics and kinetics of a reactor due to the confinement effect occurring in small cavities. This has been demonstrated using poly(styrene-*alt*-maleic anhydride)-gold (SMA-gold) nanoreactors that utilize the two hydrophobic and hydrophillic active centers to initiate and catalyze reactions that are thermodynamically unfavourable and require high temperatures and pressures.

This thesis introduces various methods to mediate the interaction of gold nanostructure growth within the nanoreactor. The new properties of gold at the nanoscale have favoured applications in a variety of fields from catalysis to targeted drug delivery. Interestingly, the reactive nature of gold nanoparticles allows its use as an active center for nanoreactors. This study shows that Gold (I) chloride reacts with the hydrophilic domain of SMA and produces metal gold crystals of 30-50 nm in size, as well as with the hydrophobic cavity to produce metal gold clusters, 2-3 nm in size. The control of the environment surrounding the active center (hydrophilic versus hydrophobic domains) is essential for the development of tailored nanoreactors. The control of the interaction between the polymer and gold was obtained by modifying the nature of the polymer, adding external energy and using a coupling agent such as thiophene known to form stable bonds with gold.

It was found that the presence of monomethyl ester in the polymer intensifies the interaction of gold on the hydrophilic domain while producing larger gold crystals (both hexagonal close pack (hcp) and face centered cubic (fcc)) and slightly smaller gold clusters. Sonication was found to disrupt the whole self-assembly process and completely eliminate the interaction of gold with SMA in the hydrophobic cavity producing exclusively monoatomic hcp gold crystals. Moreover, it was shown that thiophene, when mixed and stabilized with either polymer or gold was successfully able to control the interaction between polymer-gold, minimizing or completely eliminating the interaction of gold on the hydrophilic domain, producing smaller gold crystals and maximizing its interaction in the hydrophobic cavity producing greater number of gold clusters. Contrary, when the polymer and gold were stabilized before the addition of thiophene, it was able to promote the interaction of gold with the hydrophobic cavity without disrupting the interaction on the hydrophilic domain to a great extent.

This thesis also demonstrates the unique properties of the nanoreactors with gold and platinum nanostructures by enhanced pyrrole polymerization and recommends the best system requiring the lowest amount of activation energy. Lastly, the thesis attempts to increase the biocompatibility of the system by

attaching a linker, an amino acid. Computational modelling with basic experimental characterization determines the ideal candidate for the nanoreactor formation and allows the study of its interaction with gold in future.

This study discusses the formation of a nanoreactor via self-assembly with catalytic centers in hydrophilic or hydrophobic environments and provides ways to control the reaction on either of the centers by modifying the reactive environment. The ability to control the interaction of gold with the hydrophobic or hydrophilic cavity offers tremendous potential for many applications from drug delivery to nanocatalysis in hydrophilic and hydrophobic confinement. Applications of this system range from using the entire nanoreactor with metallic compositions for catalysis or drug delivery or simply use it as an environmentally friendly synthesis vehicle for the formation of gold or platinum structures for diagnostic or therapeutic applications.

 Résumé

Les systèmes biologiques, ayant été optimisés grâce à l'évolution pendant de nombreuses années, ont inspirés le développement de nanosystèmes. L'imitation de systèmes biologiques dans de nombreux matériaux a été obtenue en utilisant des organismes entiers, leurs composants individuels ou des matériaux formés de polymères organiques souples. Les nanoréacteurs en milieu aqueux imitant les propriétés des systèmes biologiques, se sont avérés affecter à la fois la thermodynamique et la cinétique d'une réaction en raison de l'effet de confinement se produisant dans les petites cavités. Cela a été démontré en utilisant des nanoréacteurs composés de poly(styrène-*alt*-maléique anhydride) combinés a l'or (SMA-Au) qui utilisent deux centres actifs hydrophobes et hydrophiles pour initier et catalyser des réactions qui sont thermodynamiquement défavorables et nécessitent des températures et des pressions élevées en l'absence de confinement.

Cette thèse présente différentes méthodes de médiation de la croissance de nanostructures d'or à l'intérieur des nanoréacteurs. En effet, les nouvelles propriétés de l'or à l'échelle nanométrique ont favorisé son utilisation dans une variété de domaines en passant de la catalyse à l'administration ciblée de médicaments. De plus, la nature réactive des nanoparticules d'or permet son utilisation en tant que centre actif pour nanoréacteurs. Cette étude demontre que le chlorure d'or (Au(I)) interagit avec le domaine hydrophile de SMA et de produit des cristaux de 30 à 50 nm d'or métallique. Il interagit également avec le domaine hydrophobe pour produire des nanoclusters d'or métalliques, 2-3 nm. Le contrôle de l'environnement entourant le centre actif (hydrophile par rapport à des domaines hydrophobes) est essentiel pour le développement de nanoréacteurs sur mesure. Le contrôle de l'interaction entre le polymère et l'or a été obtenu en modifiant la nature du polymère, par apport d'énergie externe et en utilisant un agent de couplage tel que thiophène qui forme des liaisons stables avec l'or.

Cette étude a permit de démontrer que la présence de l'ester monométhylique dans le polymère intensifie l'interaction de l'or sur le domaine hydrophile tout en produisant de plus gros cristaux d'or (à la fois hexagonal compact et cubique face centree) et réduisant légèrement l'interaction de l'or sur le domaine hydrophile (plus petits nanoclusters d'or). De plus, l'apport externe d'énergie par sonication perturbe l'ensemble du processus délicat d'auto-assemblage et élimine complètement l'interaction de l'or avec SMA dans la cavité hydrophobe produisant exclusivement des cristaux d'or hexagonaux compacts fins (monoatomiques). En utilisant un médiateur tel que le thiophène, il est démontré que le thiophène, lorsque mélangé et stabilisé avec la matrice de polymère ou avec l'or, est capable de contrôler l'interaction entre le polymère et l'or, minimisant ou éliminant complètement l'interaction de l'or sur le domaine hydrophile produisant des cristaux d'or plus petits et d'optimisant l'interaction dans la cavité hydrophobe produisant plus grand nombre de nanoclusters d'or. A l'inverse, lorsque le polymère et l'or ont été stabilisés avant l'addition du thiophène, on a pu favoriser l'interaction

d'or avec la cavité hydrophobe sans perturber l'interaction entre le domaine hydrophile dans une large mesure.

De plus, cette thèse montre les propriétés uniques des nanoréacteurs combinant des catalyseurs d'or et de platine impliquant une amélioration de la cinétique de polymérisation de pyrrole et permettant ainsi la sélection du meilleur nanoréacteur avec la plus faible énergie d'activation. Enfin, la thèse tente d'accroître la biocompatibilité du système par modification de la matrice de polymère avec un acide aminé. La modélisation atomique combinée à la caractérisation expérimentale préliminaire ont permis de déterminer le candidat idéal pour la formation de nanoréacteurs; ce qui permettra d'étudier son interaction avec de l'or dans le futur.

Cette étude décrit la formation d'un nanoréacteur par auto-assemblage avec des centres catalytiques hydrophiles ou hydrophobes, et fournit des moyens pour contrôler la réaction sur l'un des centres en modifiant l'environnement réactif. La capacité de contrôler l'interaction de l'or avec la cavité hydrophobe ou hydrophile offre un énorme potentiel pour de nombreuses applications de l'administration ciblée de médicaments à la nanocatalyse en confinement hydrophile et hydrophobe. Les nanoréacteurs peuvent également être utilises comme véhicule de synthèse respectueux de l'environnement pour la formation de nanostructures d'or, de platine pouvant être utilisées pour des applications diagnostiques ou thérapeutiques.

Contents

List of Tables

List of Figures

Acronym List

Acronym	Full form
AA	Amino acids
Au	Gold
AuCl	Gold chloride
BPA	4-N-(3,5-ditetradecyloxybenzoyl)-aminobutane-1-hydroxy-1,1-bisphosphonic acid disodium salt
cAMP	Cyclic Adenosine Mono-phosphate
CCMV	Cowpea chlorotic mottle virus
CSA	Camphorsulfonic acid
DDC	Dicyclohexylcarbodiimide
DDS	Drug Delivery Systems
DFT	Density functional theory
DMSO	Dimethyl Sulfoxide
DNA	Deoxyribonucleic acid
DOX	Doxorubicin
DTT	Dithiothreitol
Dtxl	Docetaxel
DZ	Double zeta
E-DNA	Electrochemical deoxyribonucleic acid
EPR	Enhanced permeability and retention
fcc	Face centered cubic
FTIR	Fourier transform infrared spectroscopy

GGA	General gradient approximation
GNPs	Gold nanoparticles
GNRs	Gold Nanorods
GTO	Gaussian type orbitals
GUV	Giant Unilamellar vesicle
HA	Hydroxyapatite
hcp	Hexagonal close packing
HF	Hartree Fock
HIV	Human immuno virus
HPCVL	High performance computing virtual laboratory
HPLC	High performance liquid chromatography
IR	Infrared spectroscopy
LDA	Local density approximation
LED	Light emitting diodes
LUV	Large unilamellar vesicle
MLV	Multilamellar vesicle
NHS	N-hydroxysuccinimide
NMR	Nuclear Magnetic Resonance
NPs	Nanoparticles
PBS	Phosphate buffer saline
PEG	Polyethylene glycol
PEO	Poly ethylene oxide

PiPrOx	poly(2-isopropyl-2-oxazoline)
PNIPAAM	Poly(*N*-isopropylacrylamide)
PPy	Polypyrrole
Pt	Platinum
Py	Pyrrole
RGD	Arginine-glycine-aspartic acid
SAM	Self-assembled monolayers
S-b-4VP	Poly (styrene-*block*-4-vinylpyridine)
SCF	Self-consistent field
SDS	Dodecylsulfate
SEM	Scanning electron microscope
SMA	Poly(styrene-*alt*-maleic anhydride)
SPR	Surface plasmon resonance
STO	Slater type orbitals
SUV	Small unilamellar vesicle
SV	Split Valence
TEM	Transmission electron microscopy
TZ	Triple zeta
UV-Vis	UltraViolet-Visible Spectroscopy

1. Biomimicry at the nanoscale

1.1 Introduction

Bioinspired nanoscale structures have led to the development of new materials with novel properties.[1] For example, spiders have inspired the synthesis of flexible hair and fire beetles have inspired infrared sensors based on flexible membranes.[1] Comparatively, hydrogels are inspired from dynamic materials that change their volume and shapes in response to external stimuli.[2] Most biological systems found in the human body depend on self-assembling nanostructures that respond to their chemical environment. Biological systems commonly sense and send signals to other systems or actively work towards attempting to alter the environment for efficient and selective action.[3] Biological systems have had years of evolution to optimize and perform essential functions, including energy production and storage, material transport, and waste removal. Hence, nanosystems have drawn inspiration from natural systems with millions of years of evolutionary optimization. Biomimicry; bios meaning life and mimests meaning imitate, takes nature's best ideas and tries to replicate them by using materials to solve human problems.[4]

Biological organisms use available natural materials to assemble highly functionalized large structures and sensing and processing systems.[5,6] Moreover, they have had many years of evolution to optimize systems and pack them efficiently in terms of physical structure, physiology, and repair along with survival strategies. They also have the ability to adapt and pass down their genetic materials to the next generations. Hence, biomimicry either by adapting natural molecules to new purposes or completely recreating the chemical or physical properties of biological systems in new materials offers great potential for the development of novel systems with unique properties. Natural organisms or naturally obtained components have been used for detection purposes.[7] For example, caged canaries have been used by miners to detect methane in coal mines.[7] The Canary is very sensitive to methane, an odourless poisonous gas, and hence a canary dying would indicate the area not being safe for work.[7] Similarly, Daphnia, small freshwater crustaceans, have been used to provide an indication of water quality as their response to toxicants can very readily be monitored.[8] However, using whole organisms or part of natural components comes with restrictions in terms of cost, the variability in results, or damage to the organisms themselves, generating a need to either use natural components or synthetic systems that can provide similar results without the drawbacks.

Components of biological systems can also be used for various applications, minimizing cost and ethical issues surrounding using whole organisms. Researchers have developed a sensor in which, B cells found in

vertebrate immune systems, are engineered to express a single antibody that binds to an antigen causing a release of Ca^{2+} ions detected by an aeqorin protein in B cells resulting in an emission of blue-green light.[9,10] Another example includes using a mammalian signalling pathway from rats and inserting it into the outer membrane of yeast cells.[11] The rat olfactory proteins stimulate increased cellular level of cAMP and the yeast are genetically engineered to respond by making green fluorescent protein.[11] Cells and tissues have been observed to behave very differently outside the host compared to inside and hence whole organisms provide a better picture of the actual system. Moreover, using biological components still require an accompanying life support system raising more complications in terms of what it can be paired with or how it can be used.

Non-biological synthetic systems can incorporate bio-inspired functions and architectures while allowing a wider range of operating environment in terms of conditions such as pH or temperature. Polymers are often used in non-biological systems because of their simple synthesis, low cost and tuneable properties.[12] Similar to biological systems, polymers containing hydrophilic and hydrophobic groups are also known to self-assemble in different structures.[13] There are many types of copolymers (Figure 1) including random copolymers, alternating copolymers or block copolymers with various properties such as conductivity or non-conductivity. Conductive polymers are known to exhibit highly reversible redox behaviour with the ability to tailor them to specific needs for their application by incorporating antibodies, enzymes, and other biological moieties.[14] Copolymers have the ability to form different architectures (Figure 2)[15] creating various active centers including hydrophobic and hydrophilic.[16] Copolymer arrangements originate from different interactions including hydrogen bonding or hydrophobic interactions allowing one to effectively mimic reaction conditions produced by proteins. For example, block copolymers are known to self-assemble to produce different nanoarchitectures in selective solvents.[17] The nanoarchitectures obtained by block copolymers can be controlled by varying factors including chain length, ratio of block lengths, polydispersity, temperature, time or concentration.[18] The size and the properties of the cavities produced by various morphologies are crucial in determining potential applications especially in drug delivery. Typically, block copolymers are known to produce larger nano or micro structures when compared to alternating copolymers and hence produce larger cavities.[17] For example, the diameter of the cavities produced by nanotubes by block copolymer and alternating copolymers were found to be between 9 nm[18] and 3 nm[19], respectively. The large cavity of the structures produced using block copolymer prevents confinement effects which play a significant role in influencing the reactivity inside the polymeric template.[20] For example, alternating copolymer includes sequential incorporation of monomers in a chain and therefore has uniform interactions allowing for higher stability in the structure. The higher stability and smaller cavities present in structural architectures formed by alternating copolymer creates confinement effect providing non-polar molecules an

opportunity to gather within the hydrophobic cavities for enhanced catalysis. Moreover, the surface groups of a polymeric structure are also essential since the polymer is able to respond to environmental stimuli including pH, light or temperature. Hence, polymers can be tuned to adsorb or shed solvent molecules by responding to environmental stimuli.
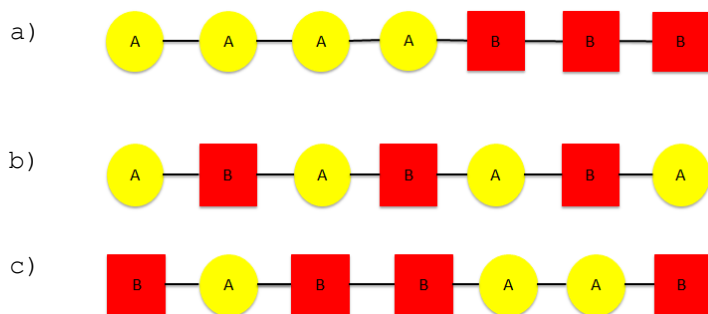
Figure 1: Schematic representation of a) block, b) alternating and c) random copolymers
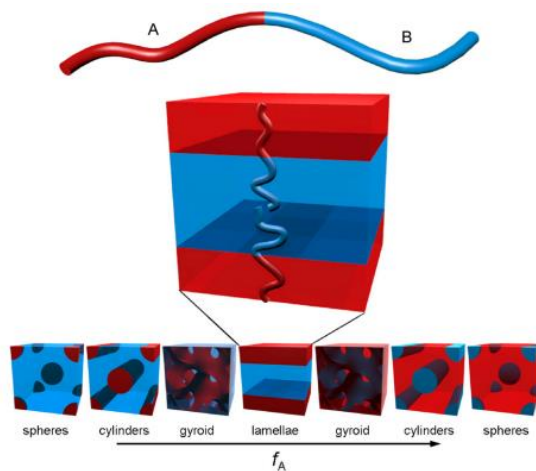
Figure 2: Various morphologies of block copolymers achieved by various conditions (Reproduced from Ref. [15] with permission from the Royal Society of Chemistry)

3

Naturally occurring organisms, individual components or synthetic architectures produce nanoarchitectures through self-assembly of small molecules. It is important to note that as the size of the system decreases the atomic interactions dominate and give rise to novel properties. While synthetic systems do ease the characterization process by isolating only one type of interaction, in an actual system, many interactions play a role that is hard to mimic entirely. It is important to study both including altering the natural biological systems as well as using completely synthetic polymeric systems to truly understand both the micro and macro forces that give rise to properties. Therefore, this review surveys various methods of biomimicry including using biological systems with slight modification for various applications and using novel polymeric systems both using self-assembly to fulfill their appropriate functions. It is important to note that although materials discussed in this report could be utilized for various other applications such as catalysis, energy collection and storage or chemical remediation, they have most commonly been used for bio-medical applications. Therefore, the primary focus of this review will be on discussing the many applications in biomedicine enabling us to better study and understand the concept of biomimicry. Biomimicry commonly involves modifying natural systems such as liposomes and DNA to exploit their properties for better targeted applications.

1.2 Altering the natural biological systems

1.2.1 DNA origami

In 1982, Seeman proposed using DNA as a construction material for various nanostructures.[21] This idea became the foundation for what is known today as "DNA origami" invented in 2006 (Figure 3).[21] The DNA origami involves folding of a long single stranded DNA into a customized shape with short synthetic strands to bind the whole structure together. [22] This method takes advantage of the self-recognition properties of DNA due to the complimentary base pairing between segments of oligonucleotides. One of the main advantages for using DNA for biomedical application includes that it naturally exists in our body minimizing the toxic effects and immune response reactions.
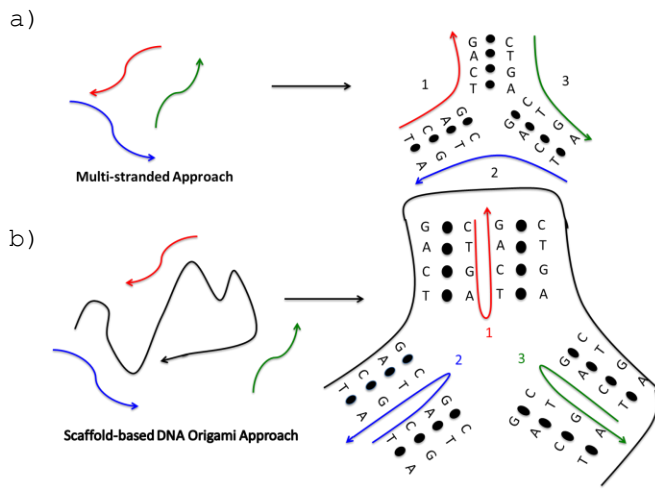
Figure 3: Schematic representation of the two approaches used to build DNA architectures a) Multistranded approach involves oligonucleotides that are designed to self-assemble with each other b) DNA origami technique involves a scaffold that is folded into a desired shape by using many shorter strands

The self-assembly and recognition properties of DNA can be used to create various shapes for drug delivery. Some of the shapes generated by this method include tetrahedrons or cubes with controllable lids (Figure 4) .[23–25] Later, various other structures including nanocages or tubes have been created and uptaken by biological cells both *in vivo* and *in vitro*.[25–28] Ko et al., have conjugated functional agents such as folate for cancer cell targeting and cyanine dyes as a fluorescence imaging agent to the DNA strands.[27] The DNA strands along with conjugated agents have shown good uptake in biological cells and no toxic effects.[27] Comparatively, Walsh et al., demonstrated that DNA nanocages remain intact even inside the cells 48 hours after transfection and can be used for drug loading.[25] Even after promising drug delivery studies by DNA scaffolds, the practical applications are limited because of the restrictions associated with properties of DNA. The structure of DNA leaves limited room for optimization of properties, which is mandatory for their full exploitation, giving rise to the need to develop other systems.
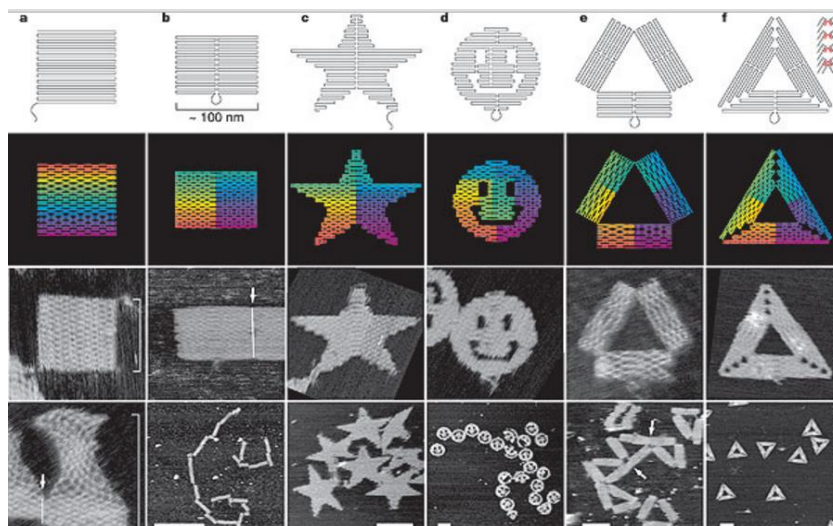
Figure 4: Various architectures produced by DNA origami (Reproduced from Ref. [23] with permission)

1.2.2 Liposomes and their applications

Liposomes are made of phosholipds, which self enclose to form spheres of lipid bilayers with an aqueous core (Figure 5).[29] They were first described by Bangham[26] et al., and then understood as a potential drug delivery system in 1970's.[30] Liposomes are typically amphiphilic in nature allowing for incorporation of both hydrophobic and hydrophilic drugs (Figure 5). Some of the advantages associated with liposomes include improved solubility of encapsulated drugs, prevention of chemical or biological degradation by enzymes, since its materials are naturally found in the body, reduction of non-specific binding of drugs, enhanced intracellular uptake, sustained release and their versatility giving one the ability to modify surface ligands.[31] The classification of these liposomes can be done on the basis of its structure, method of preparation, composition and application. Liposomes have been extensively used in the field of drug delivery. Takahisa et al., synthesized calcium phosphate-binding liposomes for effective therapy against metastatic bone diseases.[32] Specifically, they synthesized an amphiphatic molecule with a bisphosphonate head group able to recognize and bind to hydroxyapatite (HA) found in bones. [32] Figure 6 shows the results of the binding assay performed with the BPA liposomes and HA found that at a concentration of 5 mg/ml, both 5% and 10% mol BPA liquid, almost all of the liposomes bound to HA.[32] Comparatively, liposomes with 0% BPA show no binding proving that surface modification plays a crucial role.[32] The liposomes were then loaded with doxorubicin, a drug commonly used to treat cancer, with 10% BPA-liposome showing good suppression of tumor cells (Figure 6B). [32]
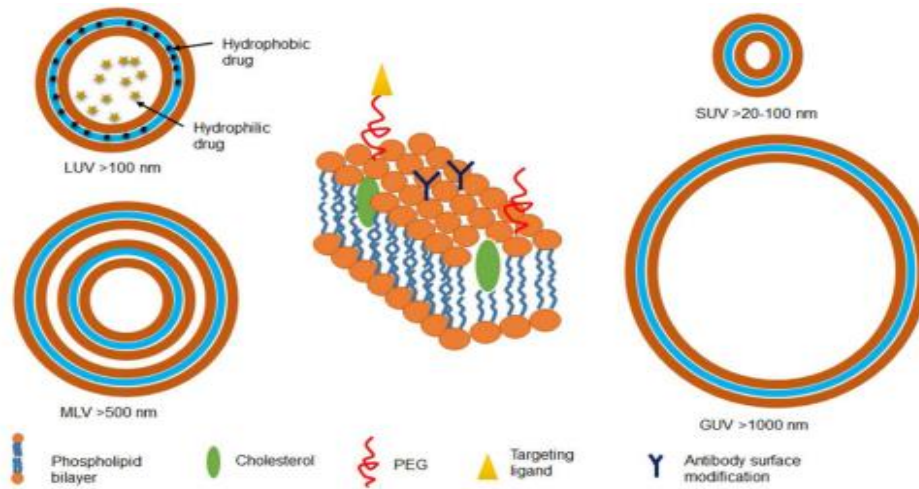
Figure 5: Schematic representation of various types of liposomes based on size and lamellarity (Reproduced from Ref. [29] with permission)
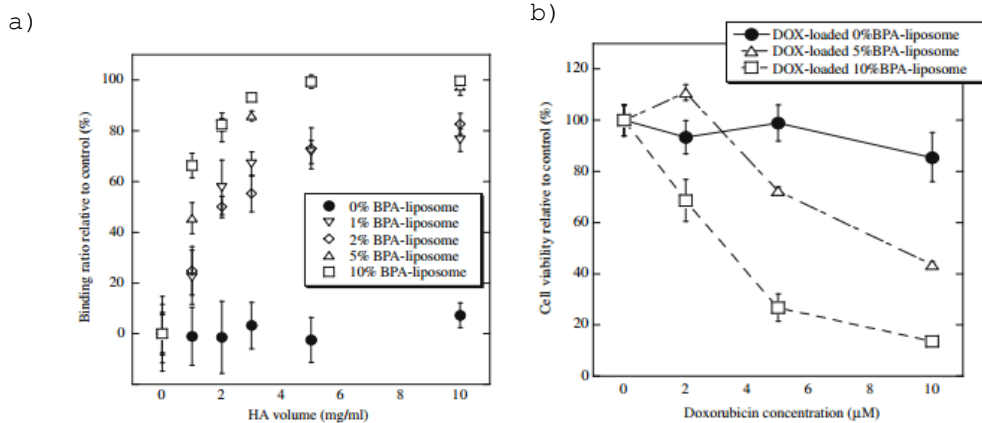
Figure 6: a) Affinity of BPA-liposomes to HA determined by measuring light-scattering intensities of the supernatant b) a comparison of cytotoxicities of DOX-loaded liposomes with and without BPA as a function of initial drug concentration (Reproduced from Ref. [[32]] with permission)

Comparatively, to improve the liposomal systems alone, they have commonly been coupled with gold nanorods (GNRs) to create a hybrid system that allows for better visualization.[33] This hybrid system was designed to allow deep tissue detection therapy and monitoring in living animals.[33] Gold has also been

7

extensively used in bio-medicine because of its unique electronic, magnetic and optical properties at the nanoscale.[34] Since gold has many electrons, it has the ability to intensely scatter and emit these electrons proving its potential for visualization and diagnostic applications. Gold nanorods have two differentiated surface plasmon bands offering powerful optical properties allowing for in vivo deep tissue imaging.[33] The UV-Vis for GNRs-liposome hybrids can be observed in Figure 7a with two characteristic surface plasmon bands from GNRs at 512 nm (axial) and 792 nm (longitudinal).[33] The two fold intensity increase observed in the hybrid system compared to gold nanorods alone could be due to a more hydrophobic environment surrounding GNR's. The Liposome-GNR hybrid can be observed in a cryosection of mouse brain tissue (Figure 7b) and tumor tissue (Figure 7c). Although successful treatment options have been studied, liposomes, also have their limitations including short half–life, leakage, and fusion of the encapsulated drugs and expensive materials.[35] In general, for truly mimicking a biological system, great control over factors such as temperature and pH is required, generating a need for development of synthetic systems that provide just that along with complete biocompatibility and cost efficiency.
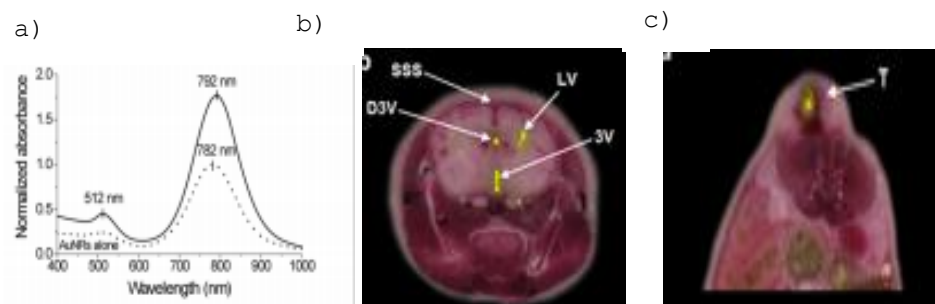
Figure 7: a) UV-vis absorption spectra of Liposome-GNRs hybrid b) Fluorescence image after injection of 5μL of hybrid into dorsal ventricle of mouse brain, section of brain tissue c) Fluorescence image after injection of 25μL of hybrid into cryosection of tumor tissue showing Liposome- GNR's hybrid (Reproduced from Ref. [33] with permission)

1.3 Modifying synthetic systems

1.3.1 Polymers and Polymeric Systems

Living organisms are designed to produce various structured macromolecules to satisfy functions being carried out in today's industrial era including energy collection, storage and transport of materials, and disposal of waste products.[37] These natural macromolecules or polymers have created an inspiration among the scientific research community to make these processes more efficient. However, the lack of performance experienced by several polymeric drug

carriers during preclinical and clinical development processes can be explained by inadequate pharmacokinetic/biodistribution profiles and difference in their toxicities, generating a need to study such systems in greater detail. Polymers, specifically, have played a major role in the advancement of drug delivery by ensuring controlled release of therapeutic agents and other hydrophilic and hydrophobic drugs in various dosages. Modern technology has been very beneficial in effectively designing these polymer-based systems to hold and transport bioengineered cargo to create long-term therapeutic effects and exert specific biological functions. With the expansion and the availability of a large number of polymers, consideration for their selection and design for drug delivery is necessary.

1.3.2 Selection of Polymers

The selection and design of polymers is a very challenging task due to the current diversity of structures. Thorough understanding of the surface diversity and various bulk properties of the polymer can ensure that the desired chemical, mechanical and biological functionality is achieved.[38] Furthermore, surface properties such as hydrophobicity and hydrophilicity, smoothness and lubricity govern the biocompatibility with the human body in addition to influencing physical properties such as durability and biodegradability.[38] Moreover, polymers that need to be used for longer periods of time must be water repellent in nature to avoid degradation that leads to toughness changes and loss of mechanical strength. Bulk properties of polymers also need to be taken into account for controlled delivery systems including molecular weight, solubility based on the site of action and the release mechanism.[38] Natural systems commonly are able to adapt to the surrounding environment and respond to various changes in a person's body. Hence, if a polymer is to have any type of bio-medical applications, it must be able to respond to a stimulus.

1.3.3 Responsive polymers

Responsive polymers can sense changes in their environment and respond to the stimulus such as pH, temperature, and ionic strength. Synthetic polymer systems are used for many applications including biointerfaces that mimic natural surfaces[39], drug delivery systems[40], coatings, and are able to respond to their environment[41,42]. Materials that mimic muscles in the human body[43] and thin films and particles are able to sense small concentrations of analytes[44]. [45] (Figure 8)
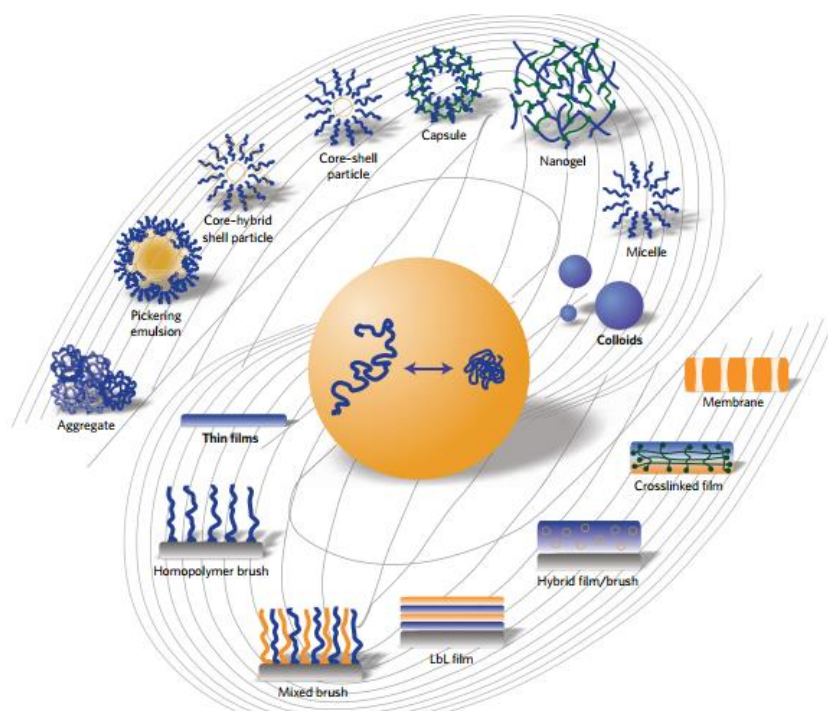
Figure 8: Various nanostructures stimuli- responsive polymer materials. These materials mainly rely on phase behavior change in thin films and nanoparticles (Reproduced from Ref.[45] with permission)

1.3.3.1 Smart and self-healing coatings

Polymer coating systems are applied on metal surfaces to produce a dense barrier against external species. The structure of the coating can be programmed in the formulation that responds to external stimuli and self-assembles with desired properties. Motornov *et al.* used hybrid responsive nanoparticles consisting of silica core with grafted mixed block copolymer brush of Poly (styrene-block-4-vinylpyridine) (S-b-4VP).[46] These responsive shells were used to stabilize the secondary aggregates of the particles of appropriate size and morphology.[46] The coating is originally hydrophilic upon casting and evaporation of water but then becomes superhydrophobic when heated to above glass-transition temperature.[46] Comparatively, another group of researchers, while developing self-healing polymers to protect metals from cracks or corrosion, programmed the particles to release encapsulated agents in a controlled way.[47] They also incorporated nanocapsules for rapid release of repairing agent after being triggered. The proposed mechanism of action can be observed in Figure 9, which was then tested by exposing a surface to salt water for 120 hours.[47] The results can be observed

with the control samples showing very fast corrosion and the self-healing surface showing no signs of corrosion even after a long exposure (Figure 10). [48] Smart coatings are often used for the development of biointerfaces.
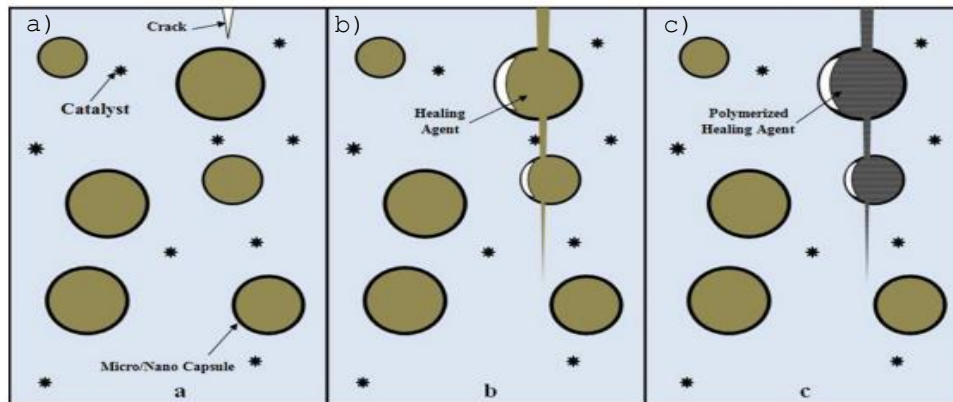
Figure 9: Schematic demonstrating the automatic healing concept where nanoencapsulated healing agents are embedded within the matrix containing a catalyst capable of initiating the healing agent. A) Cracks form due to damage b) the crack ruptures the nanocapsules triggering the release of healing agent c) healing agent comes in contact with the catalyst, triggering the polymerization to seal the crack (Reproduced from Ref. [47] with permission)
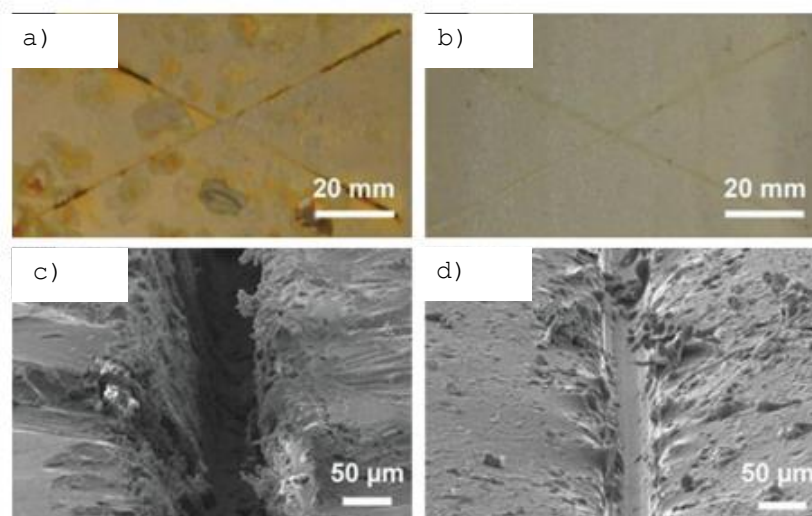
Figure 10: Corrosion evaluation of self-healing coatings after 120h of immersion in salt water a) Optical image of control sample with epoxy vinyl ester matrix and adhesion promoter b) Optical image of self-healing coating consisting of matrix , adhesion promoter, catalyst and healing agent c) SEM image of the control coating d) SEM image of the self-healing coating (Reproduced from Ref. [48] with permission)

1.3.3.2 Biointerfaces

Reconstructable thin polymer films are known to undergo dynamic changes in response to the changes in the living system and as a result have been useful in many biological and biomedical applications.[45] The tuning and switching adhesion between bio interfaces and the proteins or other cells have been researched to provide a better understanding of cell and protein control.[45] Moreover, it was seen that exposing and masking functional moieties played an important role in the presentation of regulatory signals and modulation of the biomolecule activity. The dynamic control of the permeability of nano membranes or the interactivity of the biomolecule with surfaces has given an opportunity for bioseparation.[45] For instance, Ebara *et al*., used stimulus-responsive PNIPAAM copolymers to expose or mask arginine-glycine-aspartic acid (RGD) recognition sequences for cell binding.[49] Comparatively, another group of researchers designed biocompatible nanovalves controlled by pH stimulation based on a [2]pseudorotaxane composed of a curcubit[6]uril ring that encircles a bisammonium stalk.[45] The mode of action of the valve relied on the pH-dependent binding of curcubit[6]uril with the bisammonium stalk.[50] Neutral and acidic pH valves prevented the nanoparticles from escaping by trapping them. Deprotonation

of the stalk upon addition of a base resulted in the dethreading of the ring and release of the contents trapped inside it as observed in Figure 11.[41,50] Similarly, another recent development in this field was the E-DNA sensors, which are comprised of a surface-confined DNA stem loop, labeled with an electro active reporter as a hybridizing sensing element (Figure 12a).[41] In the absence of a target sequence, the stem loop holds the redox moiety in proximity to the electrode, producing a large Faradic current. Upon hybridization with the complementary nucleic acid, the stem loop is disrupted increasing the distance between the redox moiety and the electrode. This produced a measurable reduction in current that can be related to the presence and concentration of the target sequence as seen in Figure 12.[41] Stimuli responsive polymers that are able to respond to external stimuli offer tremendous potential not only for biointerfaces but also drug delivery systems. Extensive research is being conducted enabling the synthesis of polymeric nanostructures with unique properties for enhanced drug delivery for various drugs, especially for improving cancer treatment.
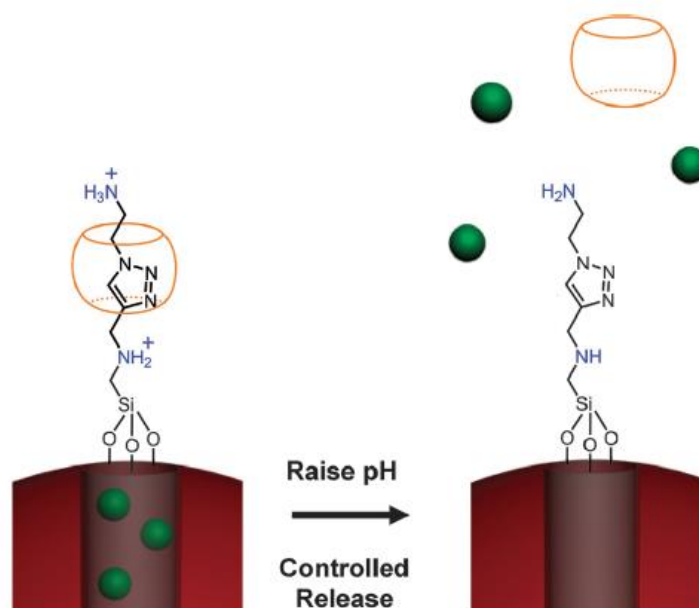
Figure 11: Structural and graphical representation of a pH-controlled nanovalve powered by mesoporous silica nanoparticles and a curcubit[6]uril-dialkylammonium pseudorotaxane as a gate keeper. Controlling the Ion-dipole interaction between the curcubit[6]uril ring and the bisammonium stalk enables the contolled release of cargo. (Reproduced from Ref. [41] with permission from the Royal Society of Chemistry)
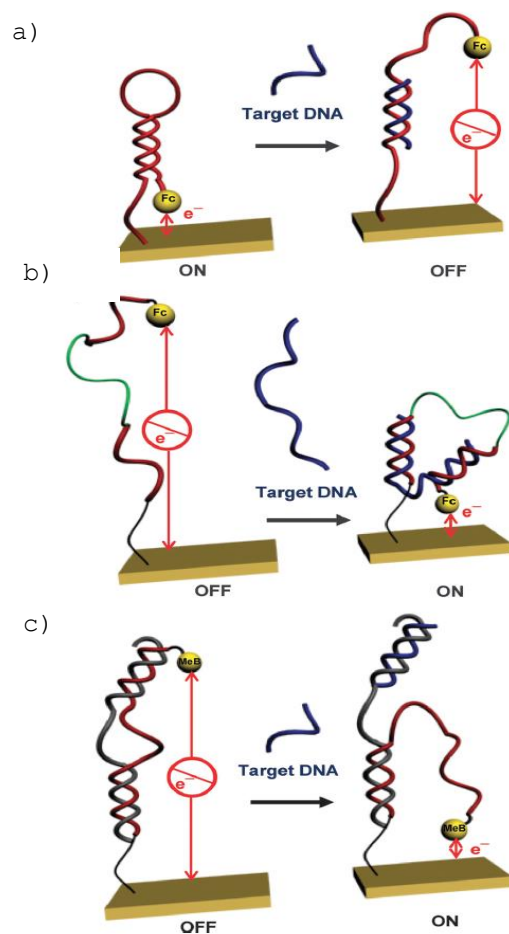
Figure 12: (a) Signal OFF state of an E-DNA sensor comprised of a surface-confined stemp-loop oligonucleotide that holds the ferrocene group in close proximity with the gold electrode. (b) Hybridization with the target sequence reduces the distance between the ferrocene group and the electrode thus decreases electron transfer efficiency. (c) Signal ON state of an E-DNA sensor where hybridization with target sequence results in a large detection signal (Reproduced from Ref. [41] with permission from the Royal Society of Chemistry)

1.3.3.3 Polymeric systems for the development of nanostructures

Among the various methods used for the treatment of cancer, carrier systems are currently being investigated to couple with chemotherapy for efficient delivery. Drug release must be stimuli responsive, which can be divided in three categories: physical (light, electric, magnetic, ultrasound, temperature), chemical (pH, ionic strength, solvent), or biological (enzymes and receptors).[51] Various types of polymers have been used to formulate different nanostructures depending on the desired properties. For example, linear dendritic block copolymers composed of linear PEO block were used for fabrication of pH responsive micelles for drug delivery.[52] It was shown that the encapsulated agent can be stored in prepared micelles at pH 7.4 and released at pH 5 with gradual disintegration of micelles into unimers.[52] Expanding on this study another group of researchers developed dual stimuli responsive block copolymers by copper-mediated click reactions between PiPrOx and poly (benzyl ether) dendrimers exhibiting sharp thermal transitions and a wide range of pH dependent thermal transition temperatures.[53]

Stimuli-responsive nanogels have also been investigated and make up another promising material for drug delivery. Oishi et al., developed nanogels from a crosslinked, pH sensitive polyamine core surrounded by PEO chains that were conjugated to ligands recognized by cell-specific receptors.[54] These nanogels were uptaken by cells through receptor mediated endocytosis.[54] In an endosome with acidic conditions, the nanogels swelled and released the drugs. Another group of researchers developed nanogels that have the ability to mimic biological viruses and are able to migrate from cell to cell leaving some cargo behind.[55] These nanogels consist of drug loaded copolymeric core with PEO serum albumin double shell decorated with folate groups.[55] Just like the previous study; the drug release is triggered by pH change by entry into the endosome. However, the swollen nanogels disrupt the endosomal membranes and escape encountering a less acidic pH environment and hence shrinking back to their initial size to migrate to another cell just as a virus.[55]

Instead of travelling from cell to cell exhibiting virus like behavior, nanoparticles (NPs) are known to increase local accumulation inside the tumor cells. NPs have also been observed to improve homogeneous spatial distribution and enhance the intracellular localization of drugs. Many disulfide based NPs have been proposed for gene delivery or cancer therapy. These systems are designed to remain stable in the bloodstream and protect against extra cellular degradation with fast release upon reduction after cellular uptake.[56] Wu et al., have developed a novel cysteine poly (disulfide) based library with simple synthesis mechanism.[56] Specifically each structure includes one disulfide part offering the redox responsiveness and one diacid part offering the ability to fine tune properties (Figure 13).[56] The NP's are absorbed into the cancerous cells which inturn release their drugs resulting in cell apoptosis (Figure 13). The group optimized the ratio between the cysteine (diacid containing segment) and the number of methylene

groups in the diacid repeating units. [56] The structures produced were found to be spherical in shape via TEM (Figure 14b). To test the cell viability the NPs were encapsulated with 10% docetael (Dtxl) and exposed for 4 and 48 hours to hela cells.[56] Overall, it was observed that the drug loaded NPs had anticancer affects similar to free Dtxl. By increasing the exposure time to 48 hours, both the free drug and Dtxl showed great improvement in inhibition of cell growth (Figure 14 a/b).[56] Lastly, in Figure 14d NP's in PBS show that 60% of the drug is released over six days, which is drastically different in the presence of DTT confirming the redox promoted discharge of payload.[56]

Polymeric systems are often coupled with metallic systems to fully exploit the potential of hybrid systems.[57,58] Hybrid metal-polymer systems have shown great potential with their unique properties and many applications ranging from use in nano-devices such as nanowires, medical imaging agents, drug delivery agents to the development of an immunoassay.[57–59] The main advantage of combining the metal and polymer includes improved properties for applications in fields including photonics[60] or electronics[6]. Many studies have been conducted successfully combining metals and organic compounds for drug delivery systems or medical imaging applications such as using gold with hollow hybrid nanospheres for drug loading as well as a contrast agent in cancer-cell imaging.[57,60–62] Gold nanoparticles (GNPs) in particular have been very commonly used because of their unique properties and many promising applications in the field of biomedicine.[63–65]
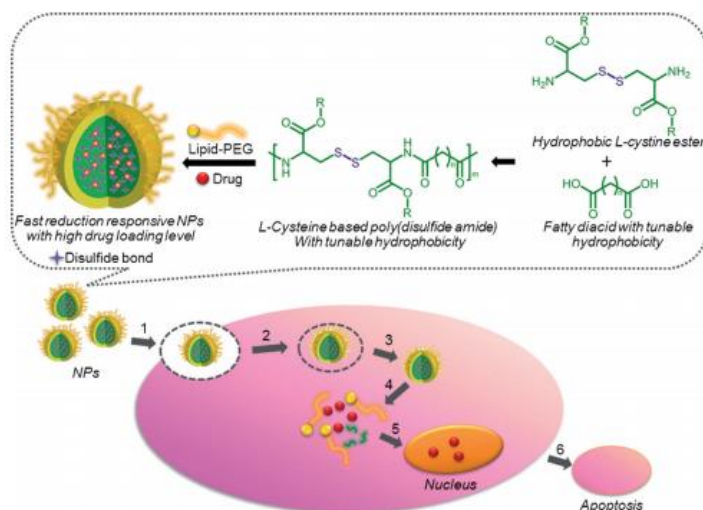
Figure 13 : Illustration of L-cysteine based drug delivery system for docetaxel (Dtxl) (Reproduced from Ref. [56] with permission)
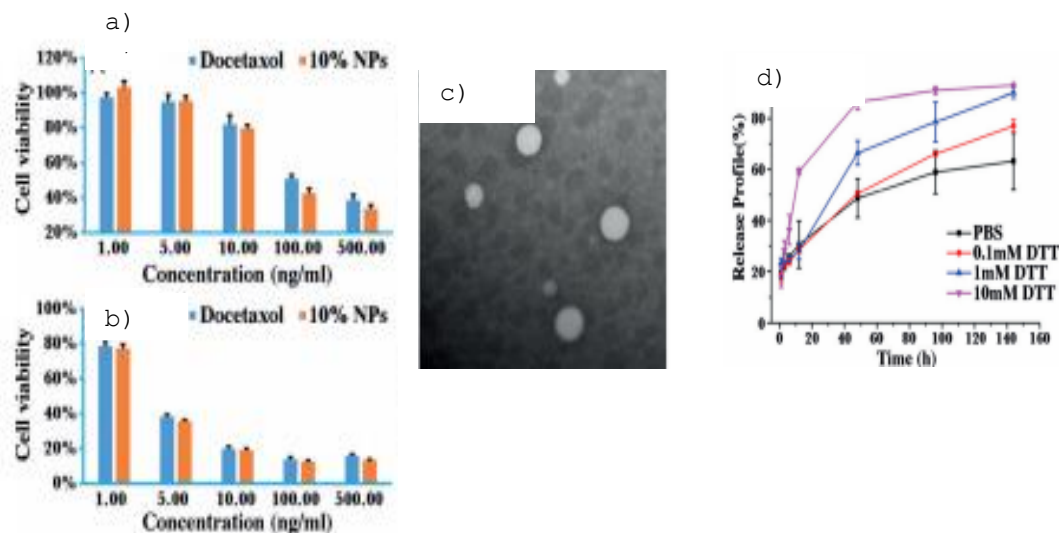
Figure 14: Cys-8E NPs with 10 wt% Dtxl a) cell viability after treating hela cells with NP's for 4h b) cell viability after treating hela cells with NP's for 48 h c) TEM image of 20% Dtxl loaded NPs d) Cumulative release of DTxl from Cys-8E NPs (Reproduced from Ref. [56] with permission)

1.4 Gold and applications in bio-medicine

1.4.1 Gold in Hybrid systems

GNPs have been used in many visualization and bioimaging methods to identify chemical and biological agents.[66,64] Since 1971, electron microscopy has been used to detect the biospecific interactions by the use of GNPs mainly because of their high electron density.[67] GNPs can have high scattering and emit secondary electrons and have found an application in Transmission electron microscopy (TEM).[64] GNPs are used for labelling purposes which are then very easy to detect by the use of TEM. Recently, GNPs have also gained popularity in optical microscopy, especially confocal laser microscopy. Confocal microscopy involves detecting micro objects with the help of an optical system, which ensures that light emission is recorded only when it comes from objects located in the system's focal point.[64] This allows one to scan the samples based on their height and to create 3D images. The use of GNPs in the antibody conjugates allows real time detection of gold penetration into living cells.[64] The detection is usually very accurate as it allows detection upto the level of a single particle or estimates their number.[64] A confocal image can be obtained from, for example, detection of fluorescence emission.[66] The main advantage of this method is that it increases contrast through

the reduction in the background signal and involves the excitation of the luminescence and simultaneous absorption of two or more photons.[66] Example includes the two-photon luminescence of GNPs, which enables molecular markers of cancer to be visualized inside the cells.[64]

GNPs have the ability to change color while interacting with proteins. This has led to the development of many colorimetric methods for protein determination. Dykman *et al*. have used colloidal gold conjugated trypsin as a specific agent for proteins.[64] Colorimetric assays have also been used for the detection of DNA.[68] Two methods have been suggested including the use of GNP conjugated with thiol-modified single-stranded DNA or aptamers or the use of unmodified GNPs.[64] Both of the methods have been used by various researchers and have been successful in the detection of DNA by increasing its sensitivity. Moreover, GNPs have also found use in immunoassay. Immunodot assay is mainly used to analyze the membrane- immobilized antigens and in some cases allows for the quantitative determination of antigen. [64]Khlebstsov *et al.,* used gold nanoshells as biospecific labels in dot assays whereas Bogatyrev *et al.,* were the first to perform a dot assay of whole bacterial cells with the reaction products being visualized by immunogold markers.[64]

GNPs have also been widely used in therapy due to the fact that they have an absorption maximum in the visible or near-IR region and get very hot when irradiated with the corresponding light. The main principle is to have gold conjugates be near or inside the target cells causing them harm due to high amount of heat and eventually causing cell death. The thermal treatment for cancerous cells has been used for many studies and includes hyperthermia or local heating.[66] Hyperthermia typically involves heating to 45 degrees for 1 hour whereas local heating can go up to 70 degrees.[64] Local heating is not typically used because it causes irreversible damage by using extreme temperature and damages the cell membrane permeability as well as protein denaturation. Since it uses harsh temperatures as well as causes irreversible damage there is a chance of it affecting the healthy cells, thus making it harmful and imposing limitations on its use. Laser radiation which enables controlled and limited injury to the tumor tissues, has also been popular, however, it is not very selective resulting in a rise of high powered lasers for effective tumor cell death.[64] Photothermal therapy, where agents help to achieve selective heating, has been proposed as well.[66] The use of GNPs in photothermal therapy was first proposed in 2003 and called plasmonic photothermal therapy.[66] Pitsillides et al. used 20-30 nm gold nanospheres irradiated with 20 ns laser pulses, 532 nm to create local heating and assist with selective damage to cancer cells.[69] This technique can be especially useful in chemotherapy-resistant tumors. Some of the challenges associated with this include the choice of NP with the most suitable optical properties, the enhancement of NP accumulation in tumors to lower the potential toxicity, development of methods for delivery of optical radiation to the targets as well as the search for alternative radiation sources, with a combination of high permeability and the possibility of heating the

GNPs.[64] There are also some problems which require more studies including the biocompatibility, chemical interaction with the physiological environment, circulation period in the blood, penetration in the tumor, interaction with the immune system as well as excretion of the GNPs.[66]

Another aspect of using GNPs for therapeutic purposes includes using them as drug carriers.[63–65] GNPs have the ability to conjugate with a variety of antitumor substances and can be used as drug carriers.[64] Conjugation is usually done by physical adsorption preparations using alkanethiol linkers.[68] To ensure efficient delivery, target molecules are applied along with active substances for better anchoring and penetration. Other substances such as antibiotics or antibacterial agents have also been employed to deliver GNPs.[65] A group of researchers have prepared a stable vancomycin-colloidal gold complex and showed its effectiveness towards various vancomycin resistant strains such as *Escherichia coli*, *Enterococcus faecium* and many more.[70] Moreover, it has also been suggested that GNPs serve as effective means for gene delivery of genetic material to the cytoplasm and the cell's nucleus to correct the structure and function of improperly functioning genes.[66]

Along with the many applications of GNP's, they have also been used for the production of antibodies.[64] Some researchers have shown that the introduction of complete antigen along with colloidal metals promotes the production of antibodies.[64] Antibody biosynthesis is typically induced by substances such as proteins, polymers, polysaccharides which have developed structures. If the substance is small and does not have a developed structure it usually does not elicit an immune response. However, in the case of GNPs this is overcome by chemically attaching such substances to high molecular weight carriers which makes it possible to obtain the desired immune response for the antibody production. The antibodies against glutamate by the use of colloidal gold NPs were first observed in 1986, by Japanese researchers.[64] This technique was then further developed by many researchers to obtain antibodies for various substances including amino acids, biotin, recombinant peptides, influenza, antibiotics, transmissible gastroenteritis virus and the peptides for the surface protein of malaria.[64] In all of these studies GNPs were conjugated with various substances and then mixed with Freund's adjuvant for animal immunization. Figure 15 demonstrates an example of successful therapy in mice. In the study, mice were injected with cancer cells.[71] Laser irradiation was performed 72 hours after injection of PEG-coated gold nanorods or control (saline buffer).[71] It can be observed that irridation without particles and just plain buffer does not have a destructive effect whereas GNR's with laser is found to completely destroy the tumor. (Figure 15)
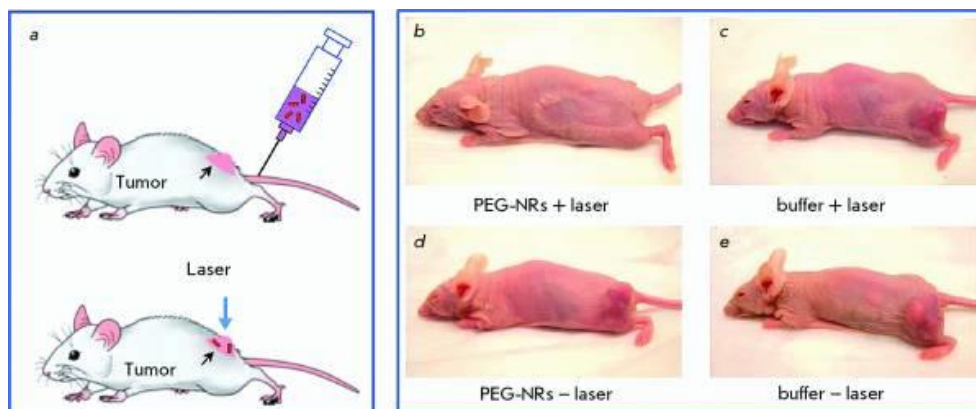
Figure 15: Photothermal therapy of mice injected with tumor cells. Laser treatment was performed 72 hours after injection of PEG coated gold nanorods. It can be observed that controls do not have a destructive effect whereas GNPs with laser completely destroy the tumor (Reproduced from Ref. [63] with permission)

The use of GNPs for therapeutic purposes is not limited to only cancer and has been used for many other diseases such as Alzeimers, HIV, Hepatitis B, and Tuberculosis. [65] While trying to tackle Alzheimer's, the Mirkin traditional method, which consists of GNP-nanoprobe cross-linking known for protein detection, was used for measuring the concentration of amyloid- beta- derived diffusible ligands, a potential Alzheimer's disease marker present at low concentrations in the cerebrospinal fluid of affected individuals. [65] For HIV, GNPs were found to inhibit the HIV fusion and therefore a screening assay has been developed for HIV-1 protease by the use of single walled carbon nanotube- GNPs modified electrode.[65] GNP-nanoprobe has also found an application in detection of Mycobacterium tuberculosis. Gold has also been used for anti-bacterial therapy.[65] Laser induced overheating effects, with bubble formation around clustered GNPs, cause bacterial damage and this has been used for selective killing of gram positive Staphylococcus aureus by targeting the bacteria surface using 10-20 and 40 nm GNPs conjugated with anti- protein A antibodies. [65]

1.4.2 Gold and its unique history

Gold is unique because of its properties, history and the role it has played in society. Traditionally, gold was of interest to researchers due to four main properties, including its metallic yellow color, resistance to corrosion, malleability and high density. The high corrosion resistance and density were the main reason for its use in production of gold nuggets as well as jewellery. The medicinal purposes of gold were first discovered by Chinese, Indian and Arabic scientists who used gold solution or liquid gold for a variety of medical purposes in the fourth century.[64] Gold was later studied by the alchemist's laboratories in Europe

where a scientist used gold to treat some mental disorders where auric chloride was reduced by alcohol or oil plant extracts.[64] In 1920's, the use of gold for the treatment of cancer was first proposed and many publications have shown some success in detection and treatment of cancer via gold nanoparticles.[65]. Gold nanoparticles (GNPs) are the most stable metal nanoparticles and have unique electronic, magnetic and optical properties.[34] The special optophysical properties enable very sensitive detection of biomarkers.[72] GNPs also have very easy and simple preparation and could be detected by various methods. GNPs, because of their unique properties, accumulate at sites of tumor growth and enter cells faster than small molecules.[64] GNPs can convert light into heat allowing for highly specific thermal ablation of infected tissues.[65,66] Moreover, GNPs can also act as a shield for unstable drugs and act as a vehicle for their delivery to the target site.[66] Gold nanoparticles typically range from 1 to 120 nm providing them with an advantage over proteins and small molecules, to be able to perturb through and modify cellular processes.[66] GNPs can also provide clinical laboratory with more sensitive, faster and cost effective assays making them a promising tool for many medical applications.[72] Overall GNPs can be used for targeting, detection, diagnostic and therapeutic applications simultaneously making them of great interest to the scientific community and opening new spectra of applications in a variety of fields.[66]

1.4.3 Properties of GNPs

GNPs are usually spherical nano-sized particles ,but they could also have a dielectric core and thin gold shell surrounding it, known as the gold nanoshells.[72] A GNP consists of few gold atoms, usually less than 300 for the maintenance of the unique optical properties.[72] The properties of GNPs include enhanced absorption and scattering mainly due to the Surface Plasmon Resonance (SPR).[65] SPR occurs when an electromagnetic radiation of a wavelength larger than the diameter of GNPs hits the particles and induces resonant oscillations of the metal free electrons.[72] The oscillations lie within the visible frequency and account for the strong absorbance and scattering properties of the GNPs.[72] The SPR phenomenon can be affected by factors such as the distance between the GNPs, the particle shape and size and the refractive index of the medium.[72] The solution containing gold nanoparticles ranges from blue-green to red to colourless giving it an advantage to be used in a colorimetric assay.[65] This color change is due to the plasmon resonance phenomenon where small monodisperse GNP solution absorb the light in blue-green spectrum where the red light is reflected whereas as the particle size increases the wavelength associated with the plasmon resonance phenomenon shifts to longer wavelengths resulting in absorption of the red and reflection of the blue or purple color.[65] As the particle size increases even more the surface plasmon resonance shifts to the infrared portion of the spectrum and all the visible lights are reflected giving the solution a clear or translucent color.[65] The color change can also be seen when salt is added, making the GNP solution neutral,

causing aggregation, resulting in a blue color. Moreover, aggregation of the GNPs can be minimized by coating it with various substances such as polymers, small molecules or biological molecules. When the GNPs bind to target, they aggregate resulting in larger size and allowing for easier detection due to the change in the optical signal.[65]

1.4.5 Synthesis of Gold nanoparticles

The synthesis of gold nanostructures uses complicated methods and harsh chemicals typically using a reducing agent. There are three commonly used methods for the synthesis of gold nanostructures including citrate reduction, Burst Schiffrin method and seed growth method each with their own advantages and disadvantages. The methods will be discussed further in the sections below.

1.4.5.1 Citrate reduction

Citrate reduction was introduced by Turkevitch in 1951 and lead to GNPs of 200 nm.[73] Turkevitch used chloroauric acid as the source for gold in water. Reduction of gold derivatives in water for the synthesis of GNPs has been one of the most commonly used methods. In 1973, Frens obtained GNPs in the range of 16 to 147 nm by varying the ratio between the reducing and stabilizing agents.[34] The methods proposed are still very commonly used and variations usually include varying the amounts of components or adding stabilizers. The GNPs can be stabilized by using various ligands, surfactants, polymers, dendrimers or biological molecules.

1.4.5.2 The Burst-Schiffrin Method

The Burst-Schiffrin method involves a two phase synthesis and stabilization by a variety of compounds, usually thiols.[34] The main advantage associated with this method includes that it allows for synthesis of thermally and air stable GNPs with low dispersity and controllable size.[74] Burst-Schiffrin synthesis typically uses chloroauric acid, a thiol, tetraoctylammonium bromide and sodium borohydride in water-toluene for the production of thiolate-GNPs.[65] Moreover, the solubility of the GNPs is controlled by the terminal groups of the thiolate ligands.[65] One can alter the terminal groups and change the GNPs from an aqueous to an organic phase depending on the terminal groups.[65] Another method for the synthesis of gold nanoparticles include the use of dendrimers containing a pre-organized number of ligands leading to dendrimer encapsulated GNPs.[65] This method allows one to control exactly the number of metal atoms in the GNPs.[65] Another group of researchers have also synthesized gold nanoparticles by using PEG sorbitan fatty acid esters functionalized with the lipoic acid.[65] This method is known to produce very stable GNPs which are stable from pH 1-14 and under a very high concentration of sodium chloride, up to 5M.[65] The shapes of the nanoparticles are not always found to be spherical and involve various methods for the synthesis of gold nanorods, gold nanocubes as well as gold nanocages.[65]

Moreover, gold nanosheets have also been investigated and studied by researchers due to their higher surface area and reusability in terms of their catalytic capabilities due to their large size.[65]

1.4.5.3 Seed growth method

Seed growth method is typically used when GNPs with larger size are required.[34] Seeding growth allows one to control the size of the nanoparticles and allows for the formation of larger GNP, typically 50-200 nm.[72] In this method, small mono-dispersed particles are initially prepared by other methods and are then used as seeds for the preparation of larger GNPs.[72] The reducing agents used in this method are typically weak since they need to reduce the metal ions only in the presence of seeds.[72] Moreover, the exact size of the NPs can be controlled by adjusting the metal ions to seed ratio.[72] A study done by Perrault et al. reported the synthesis of GNPs in the 50-200nm range.[75] In this study initial GNP were prepared by citrate reduction and hydroquinone was used as a reducing agent to allow for the growth of smaller GNPs into larger GNPs.[75] It was also reported in the study that reducing the number of seeds will result into larger GNPs.[75]

Various sizes of gold nanostructures produced by different synthesis methods are summarized in table 1. The size and the shape of the gold nanostructures play a crucial role in its properties. A group of researchers have discovered that changing the shape of GNPs to gold nanorods (GNRs) allows for deeper penetration under the skin, allowing targeting cancers such as breast cancer. Deeper penetration under the skin implies that the laser power could be reduced to have the same effect in terms of damaging the cells.[76] Sayed *et.al* have discovered that by changing the spheres into rods, the frequency to which nanoparticles respond can be lowered from the visible light spectrum to the infrared spectrum.[76] The nanorods then usually are conjugated to an antibody that can bind to a receptor protein such as epidermal growth factor receptor providing selective binding for entry into the cancer cell.[76] Overall, for treating cancer that is very close to the skin the GNPs work just as well but for other types of cancer cells that are deeper in the skin, gold nanorods provide a better alternative. Hence, the shape and the size of the gold nanostructures are observed to modify its properties to a great extent. It is essential to develop a bio-compatible synthesis strategy that does not involve harsh chemical or complicated synthesis protocols for the formation of gold nanostructures. More important is to establish control levels on the shape, size and the crystal structure produced resulting in altered properties.

Table 1: Summary of the various sizes of GNPs obtained from different methods

Methods	Size of GNPs produced	Reducing Agents
Citrate reduction method	16-147 nm, Monodispersed (16-50 nm) Polydispersed (50-147 nm)	Trisodium citrate dihydrate
Burst Schiffrin method	1.5-5.2 nm	Sodium borohydride
Seed growth method	50-200 nm	Hydroquinone

1.5 Objectives of thesis

Considering the use of gold in the field of biomedicine and the effect of altering the shape and the size of the gold nanostructures on its properties, it becomes crucial to not only develop novel methods to produce stable and water soluble gold nanostructures, but to also control the way they interact with the polymeric template. This study investigates using a polymeric template as the means of generating nanostructures and attempts to control this interaction in various ways including external energy, altering the nature of the polymer as well as using a coupling agent such as thiophene.

Choosing Poly (styrene-alt-maleic anhydride)

Poly (styrene-*alt*-maleic anhydride) (SMA) is used as a polymeric template because of its unique self-assembled structures, pH responsiveness and biocompatability (Figure 16).[77] SMA is an amphiphilic copolymer, which self-assembles into nanotubes and nanosheets, depending on the molecular weight of the polymer.[78–80] The nano architectures produced are highly dependent on maintaining the linearity of the polymeric backbone, a structure that is only obtained at pH 7 (Figure 17).[77] These nanoarchitectures are known to form a hydrophobic cavity in the middle of approximately 3 nm and a hydrophilic domain on the outside.[80] It has previously been shown that SMA nanotubes are formed from the association between eight SMA polymers through π-π stacking with the diameter of the hydrophobic cavity of 3 nm and a hydrophilic domain on the outside.[80] The nanotemplates generated by SMA are unsupported and induce a confinement effect due to the small size of the cavity, promoting reactions that are not possible in bulk. The confined space produced within the hydrophobic cavity has shown to induce reactions such as polymerization of pyrrole that are otherwise not thermodynamically favoured in free space. [16,20]
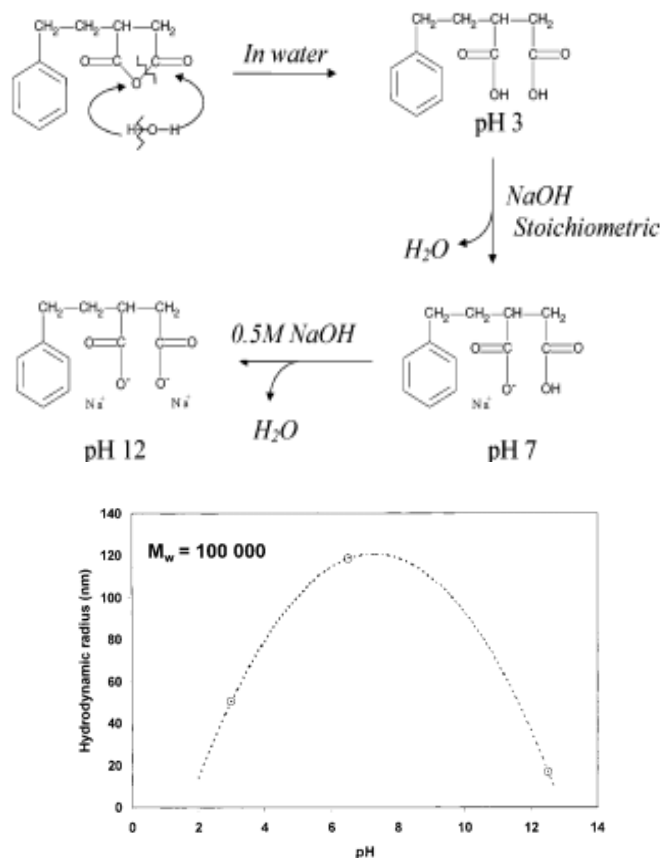
Figure 16:a) pH responsiveness of SMA demonstrated at three different pH values (Reproduced from Ref. [77] with permission) b) the effect of pH on the hydrodynamic radius of the assemblies produced by SMA (Reproduced from Ref. [81] with permission)

In addition, metal nanoparticles can be synthesized within the polymeric template. Indeed, platinum (II) chloride, under the confinement of SMA has previously been observed to produce well dispersed and stable metal platinum nanoparticles, less than 3nm in size.[79] It is important to note that no reducing agents were involved in the synthesis of platinum nanoparticles within the hydrophobic cavity making it very stable and environmentally friendly.[79] The use of reducing agents in the solution creates problems including remaining in the solvent due to a very hard reduction process along with toxic characteristics associated with the reducing agents narrowing the possibility of applications in biomedicine.[82] Moreover, the hydrophobic cavity of SMA was also found to

promote the spontaneous polymerization of pyrrole.[20] Combining the two results, it was also found that using the SMA-platinum nanoreactor, along with pyrrole led to faster kinetics of pyrrole polymerization and an overall threefold increase in the reaction rates.[16] Therefore, the template, SMA provides an option for environmentally friendly synthesis and reduction of metal salts under confinement effect without the use of any reducing agents. This template is a good candidate for the synthesis of novel nanoreactors with gold active centers.

Chirality	Optimised structure	Backbone representation
SR RR SR		
SR SR SR		
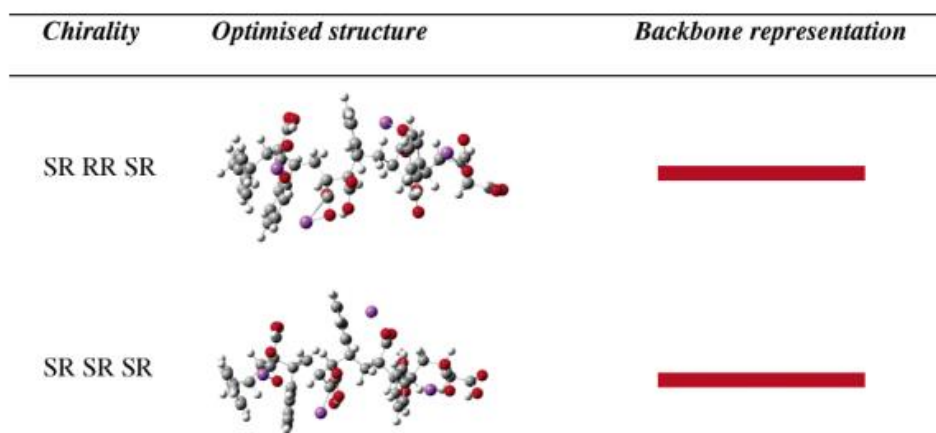
Figure 17: Optimized quadrimers of SMA at pH 7 showing a very linear backbone (Reproduced from Ref. [77] with permission)

The primary purpose of this research investigation is to use the polymeric system described previously and exploit the confined hydrophobic and hydrophilic active centers produced to develop gold nanostructures without a reducing agent via simple synthesis. Confinement is commonly observed in biological cells via the presence of cell walls holding all the biological components together and making reactions not possible in free space, possible. By understanding how confinement works and the effect it has on metals, commonly found in human body for transportation of various solutes and nutrients, we would be able to develop synthetic materials that could be used to mimic the behaviour of various molecules within confined spaces. This study expands on previously developed nanoreactors to develop gold nanostructures and attempts to control the size and environment of the structures produced for use in diagnostics or therapeutic applications. The gold nanostructures are extensively characterized in this study by using various methods including UV-Vis, IR and TEM.

Materials and methods used in the study

Chapter 2 discusses the computational and experimental methods used to study the metal-polymer interaction. The computational modelling helps us not only to predict the experimental behaviour but sometimes also explain and support the results. Due to the complexity of the system, it is essential to understand the leading atomic interaction modelled through Density Functional Theory along with experimental characterization. Density Functional Theory (DFT) provides high accuracy solutions for systems, while requiring minimal computational time compared to other alternative methods. Spectroscopy is also extensively used and discussed for experimental characterization. Indeed, UV-Vis provides one with a convenient method to identify molecular species and monitor the change in their structure. It is used in this study to monitor the growth of various gold nanostructures within the template. Comparatively, IR is used to identify the specific presence of bonds and interactions such as sulfur-gold or amide bond. TEM is used mainly for the visualization of the nanostructures produced, specifically to study the size and the morphology of the structures. Due to the size of the gold nanostructures, a combination of methods are used together to cover the length scale necessary for a complete characterization.

Control of the active centers produced by SMA

Chapter 3 focuses on the development of nanoreactors with gold active centers and attempts to mediate the interaction between the polymeric template and gold by providing external energy and altering the nature of the polymer. A slight alteration in the polymeric structure is found to have huge impact on the sizes of the gold nanocrystals, whereas providing external energy is found to completely alter the crystal structure of gold nanostructures.

Chapter 4 expands on the previous results to add one more level of control by using a coupling agent such as thiophene. The strong and stable sulfur-gold interaction is exploited to further add another level of control on shapes and hence the properties of the gold nanocrystals and clusters. Various orders of mixing and synthesis techniques have been explored with the coupling agent to mediate the interaction and produce various sizes of gold crystals and clusters. Both Chapter 3 and 4 deal with the development and control of the system whereas the final two chapters in the thesis attempt to demonstrate the unique properties of this system or explore potential for drug delivery applications.

Enhanced catalytic capabilities of the nanoreactor

Chapter 5 expands on the pyrrole polymerization demonstrated by Groves *et al.*[15], and demonstrates an even faster pyrrole polymerization with the presence of gold nanostructures and determines the exact activation energy required for the pyrrole polymerization to begin in various systems. This chapter also takes the results from Chapter 3 and applies them by providing the sample with external

energy and studying the difference in the kinetics of pyrrole polymerization. Finally, Chapter 6 deals with computational modelling and preliminary experimental characterization of attaching a linker to SMA, specifically methionine and cysteine for enhanced biocompatibility and potential drug delivery applications.

Overall, this thesis focuses on novel development of environmentally friendly easy synthesis of gold nanostructures along with many levels of control on the type and the size of the various structures. This thesis also demonstrates the unique properties of this novel system by enhanced pyrrole polymerization and attempts to add a linker, an amino acid, for enhanced biocompatibility and drug delivery applications.

2. Materials and Methods

2.1 Introduction

There are several factors that can influence the formation of gold crystals within nanostructures including the atomic forces that dominate at the nanoscale as well as the forces that exist at a micro scale such as the effect of solvent or the concentration. In order to account for all of the forces at the micro and the nano-scale a combinatory approach must be used including *ab initio* simulations as well as the frequently used experimental characterization techniques.

Computational chemistry uses mathematical functions to calculate the electronic properties and stability of atoms and molecules in a system.[83] It is especially helpful for analyzing complicated systems as assumptions can be made to simplify the system, while retaining the accuracy and it can also contribute towards time and cost savings.[84] It also enables one to know the system at the atomic scale to better predict or justify experimental results.[84] Computational chemistry has proven to provide accurate and reliable results for systems involving SMA and gold.[79] Hence, computational chemistry is used in this study to predict and support experimental results. Specifically, it is used to determine the preferred interaction of gold with the hydrophobic or the hydrophilic cavity, the influence of monomethyl ester on this interaction and the influence of thiophene on the SMA-gold system. Computational chemistry is also used to determine the suitability of amino acids with SMA for the creation of the nanoreactor and study its interaction with gold at the atomic scale. Specifically, SMA monomers and trimers are optimized with cysteine and methionine to determine their suitability with the formation of the nanoreactors. Cysteine and methionine were chosen due to the presence of sulfur creating a strong bond with gold as mentioned earlier. In general, molecular modelling simulations have proven to be a powerful tool for prediction and characterization of organic and inorganic atomic interactions.[79,85–87] In the simulations performed, each dihedral angle was first optimized to determine the global minimum of the studied system followed by the optimization of the whole structure.

Although, molecular simulations are useful for understanding the forces that dominate at the atomic scale, they fail to provide a full picture of all the involved interactions in a system. This is mainly due to the missing solvent and limitations associated with the size of the system that can be effectively modelled within a reasonable time frame generating a need for experimental characterization. Few characterization techniques including UV-Vis, IR and TEM have been proven to provide accurate results for nano-systems. [65,72] UV-Vis provides us with a simple yet effective method for studying the formation of various gold structures within

the template over time. Typically, a UV-Vis spectrum was recorded over many time points to monitor the gold crystal or cluster formation. Comparatively, IR was used to support the results obtained by UV-Vis, specifically to study the interaction of thiophene with the SMA-gold system. Contrary TEM uses transmission of electrons enabling the visualization of various structures formed within the nanoreactors providing information regarding the shape, size and the specific crystal structures.

Hence, computational chemistry enables one to study the interactions at the atomic scale while experimental results provide results after accounting for all of the interactions with other materials such as the solvent. A combinatory approach has frequently been employed with studying the nanostructures of gold and has produced accurate and reliable results. This chapter deals with outlining the main methods used computationally including the *ab initio* simulations and experimental characterization including UV-Vis, IR and TEM results.

2.2 Computational Methods

The presence of negatively charged electrons around the nucleus consisting of protons and neutrons stabilizes the whole system. The movement of one electron around the nucleus is influenced by other electrons and results in correlated motions. In a multi-electron system with correlated motions, developing wavefunctions, modelling the movement of an electron can become very complex generating the need for approximations that simplify the system. Quantum mechanics introduces approximations that temporarily assume that the motion of electrons is not correlated and attempts to develop wavefunctions for independent particles.[88] Quantum mechanics describes the behaviour of energy and matter at the subatomic level. The field is mainly based on the notion that certain properties occur only in discrete amounts called quanta.[88] Quantum mechanics gives mathematical descriptions of the electrons, however, the mathematical equations provided by quantum mechanics have never been solved except for the hydrogen atom. Therefore, computational chemistry is mainly used for modelling large systems including biomolecules, drugs, inorganic and organic molecules using approximations.

Computational chemistry uses two main approaches including *ab initio* methods where the results obtained are purely based on theoretical calculations and semi empirical where results obtained utilize some experimental results for faster calculations.[90] *Ab initio* methods are commonly used for better accuracy. There are two types of ab initio methods including Hartree-Fock and Density Functional Theory.[90]

2.2.1 Schrödinger equation and its development

Hartree-Fock method calculates the total energy of the system using Schrödinger's equation (1) from wavefunctions where $\hat{H}$ is the Hamiltonian operator representing the kinetic and potential energy of the system and Ψ represents the amplitude function providing the energy of the molecule.[91] E is the electronic energy and $\Psi = \Psi(x_1, x_2, \ldots, x_n)$ such that x_i represents a position in spin orbital space.

$$\hat{H}\Psi = E\Psi \tag{1}$$

Hamiltonian operator (2) includes electron kinetic energy, nuclear kinetic energy, nuclear-electron attraction, electron-electron repulsion and nuclear-nuclear repulsion in the order of different terms in the equation.[83] This equation can then be simplified depending on what one is trying to solve. Moreover, the equation (2) cannot be solved for multi electron systems creating the need for various assumptions as mentioned earlier.

$$\hat{H} = -\sum_{i=1}^{N} \frac{\hbar^2}{2m_e} \bar{V}_i^2 - \sum_{I=1}^{M} \frac{\hbar^2}{2M_1} \bar{V}_I^2 - \sum_{I=1}^{M}\sum_{i=1}^{N} \frac{Z_I e^2}{4\pi\varepsilon_0 r_{Ii}} + \sum_{I=1}^{N-1}\sum_{j>1}^{N} \frac{e^2}{4\pi\varepsilon_0 r_{ij}} + \sum_{I=1}^{M-1}\sum_{J>1}^{M} \frac{Z_I Z_J e^2}{4\pi\varepsilon_0 r_{IJ}} \tag{2}$$

Before the Schrödinger equation many other theories were developed and improved upon. The foundation for quantum mechanics was laid with blackbody radiation, the radiation in thermal equilibrium with a body that absorbs and emits without favoring any range or frequencies. Later, Wilhem Wien, Lord Rayleigh and James Jeans, in order to explain the characteristics of black body radiation and its derivatives, developed various equations. The equation developed by Wien is accurate only for high frequencies whereas the Rayleigh-Jeans equation is accurate for low frequencies (3).[88] The equation, however, suggests that regardless of the temperature, there should be an infinite energy density, *p,* at very short wavelengths leading to the ultraviolet catastrophe as termed by Ehrenfest.

$$p^{Wein}(v.T) = av^3 e^{-\beta v/T} \qquad\qquad p^{Rayleigh-Jeans}(v.T) = \frac{8\pi v^2}{c^3}kT \tag{3}$$

This was followed by the contribution from Plank who proposed that the oscillation of electromagnetic field of a certain frequency, *v* can only be excited by a certain amount, *hv* where h was known as the Plank's constant. Einstein used Plank's theory and realized that photons could be treated as particles and waves both to develop an equation relating energy, *E,* and mass, *m,* directly.

$$E = hv \qquad\qquad E = mc^2 \qquad\qquad mc = \frac{h}{v} \qquad\qquad (4)$$

De Broglie then proposed that particles can also be treated like waves and generalized velocities below the speed of light to produce an equation for the wavelength, λ of particles with momentum p and by using $E=K+V$, sum of kinetic and potential energies where $K=(1/2)mv^2$

$$mv = p = \frac{h}{\lambda} \qquad\qquad \lambda = \frac{h}{\sqrt{2m(E-V)}} \qquad\qquad (5)$$

All of this was then used by Erwin Schrodinger to develop a wave equation to describe small particles which was improved to finally provide the Schrödinger equation used today for all energy calculations.

2.2.2 Approximations
Since the Schrödinger equation cannot be solved for multi-electron systems, approximations need to be made and will be discussed in the next section.

2.2.2.1 Born-Oppenheimer Approximation
One of the approximations is the Born-Oppenheimer approximation, which expands on the fact that electrons are much lighter than the nuclei and so are much faster as well. Therefore electrons can adjust to a change in nuclear position instantaneously and can be considered as moving in a field of fixed nuclei. Therefore, from equation (2) the nuclear kinetic energy and nuclear repulsion is ignored and just the electronic components are focused (6). Equation 6 consists of the kinetic energy, the interaction with the external potential and the interaction between electrons. Moreover, the approximation tries to separate electronic and nuclear components (7) of the wavefunction to simplify the system and enable the calculation for the Schrödinger equation[83]

$$\hat{H} = \sum_{i=1}^{N}\left(-\frac{1}{2}\nabla_i^2\right) + \sum_{i=1}^{N} v(\boldsymbol{r}_i) + \sum_{i<j}^{N}\frac{1}{\boldsymbol{r}_{ij}} \qquad\qquad (6)$$

where x_i represents a position in spin orbital space co-ordinate r_1 and the binary spin coordinate s_i. The Hamiltonian, $\hat{H}$ operator comprises of three-dimensional kinetic energy of *I electrons*, the external potential field produced by system nucle and the inter-electron repulsion energy

$$\Psi(\vec{r}, \vec{R}) = \Psi_{nuc}(\vec{R})\Psi_{elec}(\vec{r}, \vec{R})$$

(7)

2.2.2.2 Independent Particle Approximation

More approximations are still required in order to find an adequate solution to the Hamiltonian. Independent particle approximation temporarily ignores the "electron-electron interaction" or electron correlation and assumes that individual electrons are moving within an average field of other electrons. Slater determinant is used to describe the wavefunction of a multi-electron system and ensures that Pauli's exclusion principle is followed by only allowing anti-symmetric combinations. Some of the properties of the Slater determinant include the change of sign if the electrons are exchanged within the same orbital and the fact that molecular orbitals are obtained by linear combination of atomic orbitals (8). In order to solve equation 8, first a trial function is chosen that is a linear combination of functions and then the variational principle is used to modify the coefficients, c_{kn} representing the contribution of its corresponding atomic orbital to the whole molecular orbital, and minimize the energy associate with the orbitals, ϕ_n .[83] The equation in general represents the probability distribution for the location of electrons in a field of stationary nuclei.

$$\psi_k = \sum_n c_{kn}\phi_n$$

(8)

2.2.2.3 Variational Principle

In order to determine the coefficients corresponding to the lowest energy state in equation 8, variational principle is used. Schrödinger equation provides us with one wavefunction that corresponds to every possible energy state where the lowest energy configuration is known as the ground state energy E_0, with all of the other energy values, E_k higher than the ground state, $E_k > E_0$. Starting from the Schrödinger equation and multiplying both sides by ψ, integrating both sides and solving for energy gives equation 9 and upon substitution of equation 8 into 9 gives the molecular orbital theory equivalent expression equation 10.[83] Equation 10 states that the energy calculated from an approximate (trial) wavefunction with an exact Hamiltonian is larger than the true energy; every improvement made to the wavefunction produces a lower energy. Therefore, the total electronic energy , *E,* calculated from the many-electron wavefunction is minimized until it is as close as possible to the exact solution of the Schrödinger equation. It is crucial to

understand that although, we may not be able to find the energy corresponding to the exact ground state, MO theory and variational methods bring it very close to the real solution.

$$E[\Psi] = \frac{\int \Psi \hat{H} \Psi dx}{\int \Psi^2 dx} \tag{9}$$

$$[\psi_k] = \frac{\sum_k |c_k|^2 E_k}{\sum_k |c_k|^2} \tag{10}$$

2.2.3 Hartree Fock Theory

Hartree-Fock (HF) theory attempts to solve Shrödinger's wavequation to find the energy of the system.[92] HF theory is an application of the variational method as discussed above. In order to find the energy, E_k, one must solve for the wavefunction composed of molecular orbitals. This, however, brings up the electron-electron interaction problem discussed earlier, during the application of hamiltonian to the wavefunction. Since electrons are all "equally" negatively charged, the distance between the two electrons must be adjusted to minimize the repulsive energy in a set. The coloumb energy J is a classical term for a pair of electrons separated by a certain distance r_{12}.[83] The calculation of this becomes very complex when many electrons are involved and therefore, requires further simplification. Two electronic interactions that play a major role in influencing the energy include the exchange and correlation. Exchange energy deals with the fact that electrons are indistinguishable and antisymmetric whereas correlation implies that the motion of each electron must be highly synchronized for the energy minimization.

In order to minimize the calculations required for complex systems with more than two electrons, a Fock operator is used. The Fock operator $\hat{F}$ gives the energy for a single electron moving in an effective field composed of the various forces generated by nuclei and other electrons in the system. The equation for the Fock operator can be seen in equation 11, where $\hat{h}$ accounts for the nuclear energy contributions

$$\hat{F} = \hat{h} + \frac{J - K}{2} \tag{11}$$

J is the potential energy of an electron in a charge field:

$$J_i\psi(\pmb{x_1}) = \left(\int g(1,2)\psi_i(\pmb{x_2})\psi_i^*(\pmb{x_2})\, d\pmb{x_2}\right)\psi(\pmb{x_1})\tag{12}$$

K is the exchange energy for each electron pair:

$$K_i\psi(\pmb{x_1}) = \int g(1,2)\psi_i(\pmb{x_1})\psi_i^*(\pmb{x_2})\psi(\pmb{x_2})\, d\pmb{x_2}\tag{13}$$

It is important to understand that the difference *(J-K)* is taken to compensate for the exaggerated columbic repulsion and prevent double counting. After the application of variational principle, the coulomb and exchange integrals are written as operators and the introduction of the Fock operator allows calculation of associated orbital energies through each spin orbital ψ_i[8]:

$$\hat{F}\psi_i = \varepsilon_i\psi_i\tag{14}$$

Moreover, a Fock matrix is used to simplify the system even more and provides one with more information about the orbitals. In general the procedure to solve equation 11 is iterative, starting from guessing the molecular orbitals, calculating the Fock matrix, solving the Fock equation for new MO's and then building a new Fock operator. The process goes back and forth between solving the Fock equation and building a Fock operator until self-consistency is achieved. Therefore, when revising the original Hartree Fock equation based on the Fock operator, it gives the electronic energy of the system which can be approximated as the sum of all spin-orbitals:

$$\hat{H}_F\psi_i = \sum_i \hat{F}\psi_i = E_F\psi_i\tag{15}$$

In general, HF theory uses a self-consistent field (SCF) method where the process begins with a set of approximate orbitals for all electrons in the system.[93] A very simplified version of the general steps in HF can be observed in Figure 18. Each electron is then examined individually and the distribution of all the other electrons is frozen and instead their average distribution is considered. Later, the potential corresponding to a particular electron and the solution to Schrödinger's equation discussed above is calculated. Once the cycle is completed, a new set of electronic orbitals are produced improving the wavefunction. The cycle is then repeated until self-consistency is achieved. The cycle constantly varies the structure of the molecule very slightly and calculates the new energy. The system attempts to move the molecule slightly, calculate the energy and move towards lower energy states until the closest possible answer to the true system is obtained. It is important to realize that even after all the assumptions and approximations, the Hartree-Fock method still neglects correlation energy and therefore will always return a total energy greater than the true value. Electron correlation is very

important when dealing with atoms or molecules other than hydrogen because in multi-electron systems, there is significant repulsion between the electrons. This repulsion causes electrons to move away from each other in order to minimize interactions and stabilize the system. Therefore, electron motions are highly correlated. HF theory does not account for this correlation and so becomes inaccurate when analyzing large systems containing tens to hundreds of electrons. In order to study larger systems, other quantum mechanical theories have been developed that account for electron-electron interaction. The other wave-based methods are configuration interaction, Möller-Plesset perturbation theory and the coupled cluster.[94] This study will focus on an electron density based method called density functional theory (DFT), which is useful for large systems containing heavy metals because of the balance between accuracy in the energy value as well as the amount of time required to optimize the system.
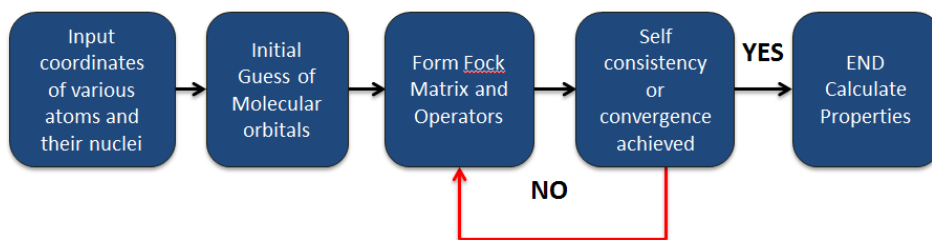
Figure 18: Simplified flowchart of the Hartree Fock method

2.2.4 Density Functional Theory

Density functional theory (DFT) calculates the total energy of the system based on electronic density instead of the multi electron wavefunction.[90] If an atom had n number of electrons then $p(\vec{r})$ represents the total electron density at a point in space $\vec{r}$ (3). The electron density in the equation can be represented by the number of electrons per unit volume in a given state. The equation describes the probability of finding any number of n electrons in a volume element $d(r)$ (16). This equation was developed based on the Thomas-Fermi model that proposed a uniform distribution of electrons into small cubic volumes such that each volume element ΔV contains ΔN electrons.[95] The Thomas-Fermi model, with modification, could adequately model atomic energies but failed at the molecular level since it could not account for the existence of chemical bonds. Although Thomas-Fermi model helped in the development of DFT, the real predecessor of modern DFT was the Slater method formulated in 1951, which developed an approximate solution to HF equations where the HF exchange was approximated by exchange energy, E_{Xa} (17). It is important to realize that equation 17 is purely dependent on the density for spin up and spin down electrons respectively.[95]

$$p(r) = N \int \ldots \int |\psi(x_1, x_2, \ldots x_N|^2 ds_1 ds_2 \ldots . d_{xN} \tag{16}$$

$$E_{Xa[p\uparrow,p\downarrow]} = -\frac{9}{4} a \left(\frac{3}{4\pi}\right)^{\frac{1}{3}} \int \{p^{\frac{4}{3}}(r)(\uparrow) + p^{\frac{4}{3}}(r)(\downarrow)\} dr \tag{17}$$

2.2.4.1 Hohenberg-Kohn Theory

The advances of the Thomas-Fermi model were followed by the development of Hohenberg-Kohn theory.[83,95,96] As discussed earlier, the Born-Oppenheimer approximation states that the ground state of the system of electrons is a result of the position of the nuclei, since everything else rearranges itself to minimize the total energy based on the nuclear position. The kinetic energy of electrons, the interactions between electrons and their density adjust themselves to the external potential that develops because of the nuclear position. To demonstrate that a functional of electron density is the same as the wavefunction it needs to map each electron density function to only one energy level and ensure that every permissive energy level is being paired with exactly one electron density. In general, this theory proposes and proves two theorems. The first theorem states that the electron density determines the external potential (within an additive constant). This implies that the external potential is a unique function of density and that the potential fixes the Hamiltonian and all of the information about the electrons can be obtained from only density by integration over space as observed in equation 18 where N represents the number of electrons and $p(r)$ represents the probability of finding an electron in a volume element to determine the nuclear potential, *v(r)*.

$$N = \int \rho(\boldsymbol{r}) d\boldsymbol{r} \tag{18}$$

Therefore, only electron number density is required to obtain all of the information about the Hamiltonian operator and hence the wavefunction. Moreover, the first theorem also demonstrates that the energy is a function of the density. The proof begins by considering two potentials $v(\boldsymbol{r})$ and $v'(\boldsymbol{r})$, with their associated wavefunctions ψ and ψ' that could give rise to the same electron density function $\rho(\boldsymbol{r})$. The $v(\boldsymbol{r}) = v'(\boldsymbol{r})$ correspond to two different wavefunctions ψ and ψ' producing different Schrödinger equations giving rise to Hamiltonians $\hat{H}$ and $\hat{H}'$ and system energies E and E' accordingly. The ground state is the lowest energy state for a given electronic system and for different Hamiltonians can be defined as:

$$E_0 = \langle\langle\psi|H|\psi\rangle\rangle \qquad\qquad E'_0 = \langle\langle\psi'|H'|\psi'\rangle\rangle \tag{19}$$

Since ground state energy is always the lowest energy state:

$$E_o < \langle\psi'|H|\psi'\rangle = \langle\psi'|H'|\psi'\rangle + \langle\psi'|H - H'|\psi'\rangle = E'_o + \int p(r)[\hat{V}_{ext} - \hat{V}'_{ext}]dr \qquad (20)$$

$$E'_o < \langle\psi|H|\psi\rangle = \langle\psi|H'|\psi\rangle + \langle\psi|H' - H|\psi\rangle = E_o - \int p(r)[\hat{V}_{ext} - \hat{V}'_{ext}]dr \qquad (21)$$

Upon adding the two equations we get: $\qquad E_o + E'_o < E'_o + E_o$

This leads to a contradiction since it cannot be true. Therefore, it can be concluded that $v(r)$ is a unique functional of $\rho(r)$ and that the electron density function contains information equivalent to the wavefunction. The density alone is sufficient to determine all of the properties according to equation 22 where $T_e[p]$ is the kinetic energy, $U_{ee}[p]$ is the interaction among electrons and $\hat{V}_{ext}[p]$ represents the external potential[95]:

$$E[p] = T_e[p] + U_{ee}[p] + \hat{V}_{ext}[p] \qquad (22)$$

The second theorem combines the energy with the variational principle while stating that the functional that delivers the ground state energy of the system delivers the exact energy only if the input density is the true ground state density. Furthermore, the theorem states that for a trial density $\tilde{p}(r)$ such that $\tilde{p}(r) \geq 0$ and $\int \tilde{p}(r)$ dr=N the ground state energy must be the lowest energy associated with the system:

$$E_0 \leq E[\tilde{p}] \qquad (23)$$

This equation where $E[\tilde{p}]$ is the energy functional produces equation 24 which restricts the density functional theory to studies of the ground states.

$$\langle\tilde{\psi}|H|\tilde{\psi}\rangle = E[\tilde{p}] \geq E[p_o] = E_o \qquad (24)$$

In general, the two theorems confirm the existence of a functional relating the electron density and the energy of the system. It is important to understand that we cannot obtain the exact form of functional and therefore approximations need to be as close as possible to the true value.

2.2.4.2 The Kohn-Sham method

All of the methods presented earlier have tried to minimize the energy by changing the corresponding density. The Kohn-Sham method relates the kinetic energy to the density by combining the wavefunction and density approach.[97] Kohn-Sham method, instead of finding the full relationship between the energy and

density, treated the majority of the kinetic energy exactly, leaving a small correction calculated separately.[95,97] They introduced a system of *N* non-interacting electrons to be described by a single determinant of the lowest number of N orbitals, yielding the same electron density as the exact interacting electron system with potential *v*. This implies that there must be a local single-particle potential *v(r)* such that the exact ground state density of the interacting system equals the ground state density of a problem for any interacting system. Furthermore, the method separates the kinetic energy term into one part that can be calculated exactly, which considers electrons as non-interacting particles and an electron-electron interaction correction. The exact electron density and expectation value of kinetic energy can be expressed as:

$$\rho(\boldsymbol{r}) = \sum_i^N \sum_s |\psi_i(\boldsymbol{r}, s)|^2 \tag{25}$$

And the kinetic energy of non-interacting electrons can be expressed as:

$$T_s[p] = \sum_i^N n_i \langle \psi_i | -\frac{1}{2} \bar{\nabla}^2 | \psi_i \rangle \tag{26}$$

Therefore, equation 22 can be rewritten and rearranged to obtain the new energy functional (equation 27) where T_s is the kinetic energy of non-interacting electrons, J_s accounts for the nuclear-electron interactions and columbic repulsions between the electrons and E_{xc} is the exchange correlation term which includes all other energy contributions not accounted for in the previous terms such as electron exchange, electron correlation and many more.

$$E[\rho] = T_s[\rho] + J_s[\rho] + E_{xc}[\rho] \tag{27}$$

The biggest challenge with DFT is the description of $E_{xc}[\rho]$ term requiring various constraints and methods to achieve proper accuracy. In general, after setting appropriate constraints on ρ or the molecular orbitals ψ leads to the development of the Kohn-Sham equations that minimizes the orbital energies.

$$\left[-\frac{1}{2}\nabla^2 + v_{\text{eff}} \right] \psi_i = \varepsilon_i \psi_i \tag{28}$$

where

$$v_{\text{eff}}(\boldsymbol{r}) = v(\boldsymbol{r}) + \int \frac{\rho(\boldsymbol{r}')}{|\boldsymbol{r} - \boldsymbol{r}'|} d\boldsymbol{r}' + v_{xc}(\boldsymbol{r}) \tag{29}$$

It is important to note that the Kohn-Sham orbitals are very similar to the eigenfunctions of the HF method. HF method is an approximate method whereas Kohn-Sham method is exact in principle. Both of the methods must be solved in an iterative method starting from an initial guess charge density, determined from superposition of the atomic densities of the molecule. An approximation for the functional that describes the dependence of E_{xc} on the electronic density is then used to calculate v_{eff} (equation 30). Later, equation 29 or the Kohn-Sham equation is solved providing an initial set of Kohn-Sham orbitals. The solution to the orbital is finally used to calculate an improved density based on:

$$p(r) = \sum_i^N \sum_s |\Psi_i(r,s)|^2 \tag{30}$$

Moreover, the potential v_{xc} can be expressed as the functional derivative of the exchange correlation energy:

$$v_{xc}^{LDA}(r) = \frac{\delta E_{xc}}{\delta \, p(r)} \tag{31}$$

The entire process, as depicted in Figure 19, is repeated until the density and the exchange correlation energy have met certain convergence criterion. In the cases where potentials are very important, DFT offers a very accurate approximation as an alternative to wavefunctions. The energy equation 28 can be rewritten as equation 32 after approximations are used for $E_{xc}[\rho]$. It is important to understand that Kohn-Sham orbitals do not have any physical meaning and are not real orbitals. The main role associated with the Kohn-Sham orbitals is to provide proper mapping between energy and density.[83]

$$E[\rho] = T_s[\rho] + J_s[\rho] + E_{xc}[\rho] + \int v(r)p(r)dr \tag{32}$$
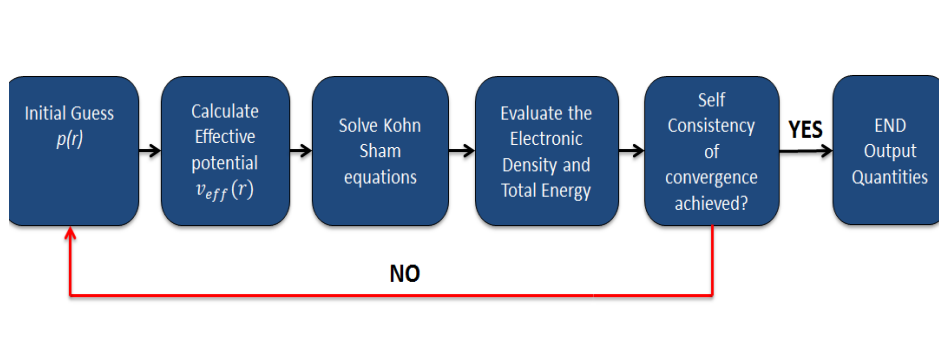
Figure 19: Simplified flowchart of the Density Functional method

2.2.4.3 Local Density Approximation(LDA)

The exchange-correlation energy, $E_{xc}[\rho]$, can be divided into two separate terms: an exchange, E_x associated with the interaction between electrons of the same spin, and a correlation term, E_c associated with the interaction between electrons of the opposite spin.[83]

$$E_{xc}[p] = E_x[p] + E_c[p] \tag{33}$$

The local density approximation (LDA) assumes that the exchange-correlation energy at any point in space is a function of the electron density at that point in space only and can be given by the electron density of a homogeneous electron phase of the same density.[98] The LDA can be expressed in equation 34 where $\varepsilon_{xc}(p)$ is the exchange-correlation energy per electron in a homogeneous electron gas with a constant density[95].

$$E_{xc}^{LDA}(p) = \int p(r)\varepsilon_{xc}(p)dr \tag{34}$$

Upon applying the KS method to the LDA the equation for exchange potential (equation 31) can be rewritten as:

$$v_{xc}^{LDA}(r) = \frac{\delta E_{xc}}{\delta\, p(r)} = \varepsilon_{xc}(p(r)) + p(r)\frac{\delta\, \varepsilon_{xc}}{\delta\, p} \tag{35}$$

Overall, LDA is very effective to determine $E_{xc}(p)$ but still encounters some errors mainly due to inhomogeneity in both the negative and positive electric charge fields in the actual molecule. A correction factor is typically added to

correct for the gradient of the density. Some of the other deficiencies of this method include inadequate cancellation of self-interaction contributions, underestimating the atomic ground state and ionization energies whereas overestimating the binding energies. Whether this approximation is good for one`s system depends on many factors and must be determined system by system. For example, LDA is generally worse for smaller molecules and typically improves with the size of the system. It is usually good for systems with slowly varying densities as well as with relatively large density gradients.

2.2.4.4 General Gradient Approximation

One of the main problems with LDA as discussed above is that it treats the whole system as a homogeneous electron gas when most of the molecules are partially heterogenous. General Gradient Approximation (GGA) tries to fix this by making the exchange and correlation energies depend on both density and the gradient of the density. This in general represents a significant improvement over many other methods discussed above.

Both LDA and GGA try to derive the density function to account for the electron exchange and correlation energies. They are generally very accurate since they underestimate the exchange energy, while overestimating the correlation energy therby cancelling out the error that is introduced. One of the other ways to increase accuracy of DFT method is to use hybrid functionals.

2.2.5 Functionals

Hybrid functionals are approximations for the exchange-correlation energy functional that combine part of the exact exchange energy calculated by HF theory with estimates of $E_{xc}[\rho]$ from DFT. Hybrid functionals incorporate the best of Hartree Fock theory along with other ab initio methods.[99]

2.2.5.1 B3LYP

The most common hybrid functional used is B3LYP (Becke, 3-parameter, Lee-Yang-Parr). Hybridization with Hartree Fock enables one to improve properties including atomization energies, bond lengths and vibration frequencies which are not described as well in pure functionals. B3LYP calculates the exchange-energy functional by combining the Becke exchange energy and Lee-Yang-Parr gradient correction energies.[100,101] The equation used by B3LYP for the calculation of exchange-correlation energy can be represented by equation 36 where $a_0, a_X \; and \; a_C$ are constants:

$$E_{XC} = E_{XC}^{LSDA} + a_0\left(E_x^{HF} - E_X^{LSDA}\right) + a_X\left(E_x^{B88} - E_X^{LSDA}\right) \qquad (36)$$
$$+ a_C\left(E_C^{LYP} - E_C^{LSDA}\right)$$

2.2.5.2 B3PW91

This method is used for many systems today due to very high accuracy for many molecules. One of the other common hybrid functionals used is the B3PW91. The major difference between the two functionals includes the difference in the correlation term. There is currently a debate in terms of which functional is better for many systems, especially the ones with metals.[87] Indeed, some researchers have tested different functionals to determine which one suits their system and provides the most accurate results compared to experiments.[102] Therefore, our study was initially carried out by using both combination, B3LYP and B3PW91 to determine which one provides the most accurate results for this system. Once it was determined that both the hybrid functionals showed similar trends, only B3LYP was chosen to study other systems.

2.2.6 Basis sets

A basis set is a mathematical description of orbitals of a system that is used to approximate theoretical calculations or modelling.[83] The choice of the basis set is crucial to maintain the accuracy of the calculations. A basis set is a set of functional building blocks that are stacked to produce the required features. Stacking refers to adding things after multiplying with its own constant as observed in equation 37 where k is the size of the basis set, ϕ_1, ϕ_2, ... ϕ_k are the basis functions and a_1, a_2, ... a_k are the normalization constants. The general form of a basis function is Ne^{-ar} where N is the normalization constant, α is the orbital exponent and r is the atomic radius

$$\Psi = a_1\Phi_1 + a_2\Phi_2 + \ldots + a_k\Phi_k \tag{37}$$

The development of basis set was done by John Slater who did orbital computation using basis sets called Slater Type Orbitals (STO`s). STOs are an accurate representation of the electron density in the valence region and farther, but are much less accurate near the nucleus. STOs were originally used because of their similarity to atomic orbitals. They describe orbitals using spherical coordinates (r, θ, ϕ) along with the angular moment, $Y_{l,m}$, and the principle, n, angular, l and magnetic, m, quantum numbers

$$\Phi_1(a, n.l, m; r, \theta, \Phi) = Nr^{n-1}e^{-ar}Y_{l.m}(\theta, \Phi) \tag{38}$$

Later, Gaussian type orbitals (GTO`s) were introduced by Frank Boys[101] as a method of modifying the wavefunction. GTO`s contain the exponential $e^{-\beta r^2}$ instead of e^{-ar} making it easier to evaluate.[103] Although, GTO`s are easy to evaluate, they do not represent the real electronic density of the real situations. GTO's are not orbitals but simplified forms of functions. A typical Gaussian function looks like:

$$g = Ne^{(-\beta r^2)} \tag{39}$$

In order to use multiple GTO's, they are sorted into separate functions each consisting of several GTO's combined linearly with fixed coefficients. For example a GTO (3G) basis function is given below where the values of c_1, c_2, c_3, β_1, β_2, and β_3 are fixed and those numbers are included in the designation.

$$GTO\ (3G) = c_1 e^{(-\beta_1 r^2)} + c_2 e^{(-\beta_2 r^2)} + c_3 e^{(-\beta_3 r^2)} \tag{40}$$

The calculation of c and β is typically done by fitting the 3G expression to a STO using a least squares analysis method. Some of the other methods that are used involve varying c and β in the atomic calculations to minimize energy. It is only possible to produce one GTO basis function for each principle quantum level.

2.2.7 Types of Basis sets

2.2.7.1 Minimal Basis sets
Minimal basis sets are the most simple basis set and allow for faster calculations.[83] Although, calculations are fast, usually the results are not very accurate for many research studies. In a typical minimal basis set, one basis function is selected for every atomic orbital that is required to describe the free atom. This is the main reason for which minimal basis sets are also referred to as single-zeta basis sets. In this type of calculation, only ground state electrons are included. For example, for hydrogen just one 1s and two 1s for helium are included in calculations. The most common minimal basis sets are the STO-nG basis sets, which contain a linear combination of n GTOs fitted to each STO. The individual GTOs are called primitive orbitals, while the combined function is referred to as contracted.

2.2.7.2 Split-Valence basis sets
The Split-Valence (SV) basis sets are an expansion of basis sets making the total function more accurate and reliable.[83] SV basis sets use multiple functionals for orbitals in the valence shell and one functional for all the other orbitals resulting in good computational time. There are two main categories of SV basis sets including double-zeta and triple-zeta. Double-zeta (DZ) basis sets use two basis functions for each valence atomic orbital whereas Triple-zeta basis sets use three basis functions. The smallest DZ basis set is 3-21G. It uses a three primitive expansion for the 1s orbital and then splits the valence orbitals into a two basis function, the inner function being a contraction of two Gaussians and the outer function being just a single Gaussian. The most common TZ basis set is 6-311G, which contains a single three-GTO basis function for the core orbitals and three basis functions for the valence orbitals where one basis function is composed

of three GTOs and the other two basis functions contain one GTO each. The 6-311G basis set is a triply split valence basis set providing it with the flexibility to arrange according to the bonding requirements of molecules and allows orbitals to change size.[83]

2.2.7.3 Polarized basis sets

Polarized basis set takes the calculations and accuracy one step further by adding a set of basis functions one unit higher in angular moment compared to what is present in the ground state of the atom.[83] This increases the flexibility of basis set in the valence region in the molecule proving more flexibility and distorting away from spherical symmetry. When bonds are formed in molecules, the atomic orbitals are distorted from their original shape to produce optimal bonding. The polarization function significantly improves the description of molecular geometries (bond lengths and angles) and molecular relative energies. It is important to note though that this does not imply that the other levels are occupied, the function simply provides more accurate description of electron density and bonding characteristics. For example, 6-31G(d) or 6-31G* signifies that d type functions have been added whereas 6-31G(d,p) or 6-31G** indicates that p type functions have been added.

2.1.7.4 Basis sets for Transition metal elements

The basis sets described above work for most of the elements except the transition metals such as gold due to the large number of electrons present in the system.[83] In this system previously-determined effective core potentials are used to describe the core electrons in the transition metals, while minimal or double-zeta basis sets are used to describe valence electrons. This allows enough flexibility of the valence electrons to accurately represent bonding and other interactions, while the frozen core potential does not drastically increase computation time. A common basis set used for transition metals is LANL2DZ. LANL2DZ allows the use of pseudopotentials replacing the atomic electron potentials such that the only valence electrons, participating in the reaction are described. This allows one to greatly minimize the computational time associated with the optimization

2.2.8 Computational Methods used in this study

All of the optimization results were obtained using the Gaussian 09 software.[104] Density functional theory was chosen for this study because it is very accurate, widely used and the least computationally expensive *ab initio* method. Optimization of the of SMA or SMA$_m$ monomers without the gold were modelled using Density functional theory using B3PW91 and B3LYP hybrid functional and 6-31G basis set whereas if gold was involved, the optimization was conducted with LANL2DZ basis set instead of 6-31G. The optimization for SMA$_m$ and thiophene was conducted using the same method, DFT, B3LYP hybrid functional and 6-31G basis set.

Choosing LANL2DZ for systems involving gold allows the use of pseudopotentials replacing the atomic electron potentials such that the only valence electrons, participating in the reaction are described. This allows one to greatly minimize the computational time associated with the optimization. It is important to note that for all of the systems requiring comparisons with the systems involving gold, they were also run with LANL2DZ. The study was optimized with 6-31G without any polarization to minimize the computational time.

The polarized basis set has been tried earlier with just pure SMA and did not show any significant improvement in the energy value. Moreover, there is currently a debate in terms of which functional is better for many systems, especially the ones with metals.[87] Therefore, some researchers have opted to use many different methods to determine which one suits their system and provides the most accurate results.[102] As mentioned earlier, originally the study was carried out with two hybrid functionals, B3LYP and B3PW91 to determine which one provides the most accurate results for this system. Later, all other structures were only optimized with B3LYP determined to provide accurate results. Overall computational modelling was used to predict and support experimental behaviour, since it cannot account for all of the interactions involved as discussed earlier. *Ab initio* simulations also do not provide a reliable method to study the gold crystal growth within the template, generating a need for experimental methods.

2.3 Experimental Methods

Spectroscopy is a set of techniques that study the interaction between matter and energy. It produces a spectrum that shows the magnitude of the interaction of a compound as a function of incident energy. UV-Vis provides one with a convenient method to identify molecular species and monitor the change in their structure. It is used in this study to monitor the growth of various gold nanostructures within the template.

2.3.1 Ultraviolet-Visible (UV-Vis) Spectroscopy

Molecules that have π electrons or non-bonding electrons absorb UV or visible light enabling them to excite the non-bonding electrons to higher levels. The easier it is for a molecule to excite its electrons signifies a lower HOMO-LUMO gap, thus absorbing at longer wavelengths of light. This can be seen in equation (41) where E is the energy, h is the planks constant, c is the speed of light and λ is the wavelength.[26]

$$\Delta E = \frac{hc}{\lambda} \tag{41}$$

The proportion of the light that is not transmitted due to the scattering interactions is known as the absorbance. The absorbance, *A,* of a particular molecule is dependent on its electronic density and the chemical environment.Moreover,

absorbance is directly proportional to the path length as can be seen in Beer's law (42) where ε is the molar absorptivity coefficient, b is the path length and c is the concentration.

$$A = \varepsilon * b * c \tag{42}$$

The interaction of gold nanostructures with light is dictated by three main factors including its size, environment and physical dimensions. When an electromagentic radiation of wavelength larger than the diameter of nanostructures hits the particles, it induces coherent oscillations of metal free electrons. These resonant oscillations lie in the visible frequency resulting in strong optical and scattering properties known as surface plasmon resonance (SPR).

According to the Mie`s theory, the diameter of spherical gold colloids in water can be predicted based on the correlation of its radius to wavelength of its plasmon band.[50] The cross section of a spherical particle with radius R can be estimated as a function of its diameter d for a specific wavelength λ. k is a wavefactor of the incident light with respect to the dielectric constant ε_m and wavelength L, a_L and b_L are in terms of Riccoti Bessel functions as discussed in *Haiss et al.*

$$\sigma = \frac{2\pi}{|k|^2}(2L + 1)Re(a_L(d,\lambda) + b_L(d,\lambda)) \; where \; k = \frac{2\pi\sqrt{\varepsilon m}}{\lambda} \tag{43}$$

The calculation limit for the equation is from 5-80 nm with various other assumptions as will be discussed in the next chapter. The formation and polymerization of gold nanostructures can be very easily observed with UV-Vis through the change in peak amplitudes.

To measure the absorbance via UV-Vis, the sample is placed in the beam path between the radiation source, deuterium arc (λ=190-400nm) and the detector. The sample solution is analyzed in comparison with a reference solvent. As seen in Figure 20, light from two source lamps, hydrogen for UV and tungsten for visible region is passed simultaneously through the sample after which the beam is separated into monochromatic components via a prism before passing through the cuvette. A blank is first run with the solvent; water in this case, to account for any background absorbance. The difference of absorbance between the blank and the sample is what specifically gets measured by the instrument. The valence electrons in a sample absorb light for transition between ground state to excited state (Figure 21). When the wavelength of absorbed light matches the difference in two states, absorption occurs and a peak is observed. In this study, UV/Vis light spectroscopy was carried out in 1mm quarts cuvette in an Agilent 8453 PDA spectrometer and analyzed with ChemStation software v.B.04.02. UV-Vis method is a very quick, simple and effective method to study the presence of various types of gold structures in the sample or to observe the polymerization growth of gold crystals or clusters with their respective domains. UV-Vis is also used in this study to observe

thiophene and pyrrole polymerization within the hydrophobic cavity or the hydrophilic domain, respectively.
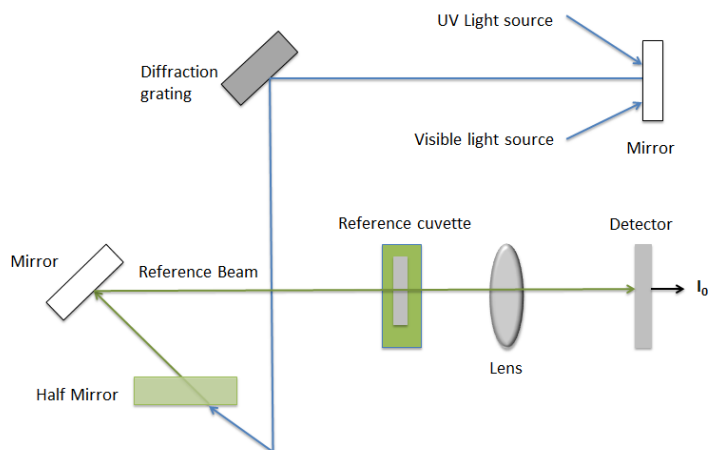
Figure 20: Schematic diagram of UV-Vis spectroscope
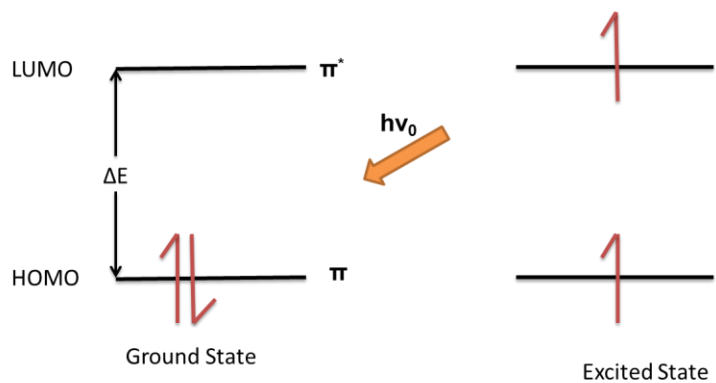
Figure 21: Electronic excitation observed in UV-Vis showing the HOMO LUMO band gap

2.3.2 Infrared Spectroscopy (IR)

The IR spectrum refers to 14000 to 10 cm^{-1} wavenumbers from wavelengths 0.78 to 1000 μm. The method takes advantage of every molecule absorbing specific frequencies depending on their structures. Every molecule in the sample is vibrating. When the frequency of the vibration in a molecule matches the frequency of IR radiation, the molecule absorbs. It produces absorption spectra with wavenumbers or wavelengths where wavenumbers are the number of waves per unit length and are directionally proportional to the frequency. IR is absorbed by the molecules and converted into energy of molecular vibration either by stretching or bending. Different bonds or functional groups absorb IR at different wavelengths and IR spectra in the end are obtained by detecting changes in transmittance intensity as a function of wavenumber.

Typically, Infrared Spectrometer consists of four parts (Figure 22) including the source for infrared light, the fixed mirror, the moving mirror and the detector. At the intersection of all of the components lies a beam splitter responsible for transmitting half the radiation and reflecting the other half. Hence, the light that is transmitted by the beamsplitter strikes the fixed mirror ,whereas the light that is reflected strikes the moving mirror. The two beams are then reflected from their respective mirrors, recombined at the beam splitter and pass through the sample and finally reach the detector to be interpreted for analysis through a computer software.

In this study, a liquid sample was freeze dried overnight and then mixed with potassium bromide (KBr) and pressed to make pellets. The pellet was then loaded on to Perkin Elmer FT-IR spectrometer model Spectrum 65 to take IR measurements. IR for this system provides information about peaks located at certain wavelengths matched through literature review. In this study, IR is mainly used to pin-point the exact functional groups giving rise to the polymerization observed in UV-Vis.
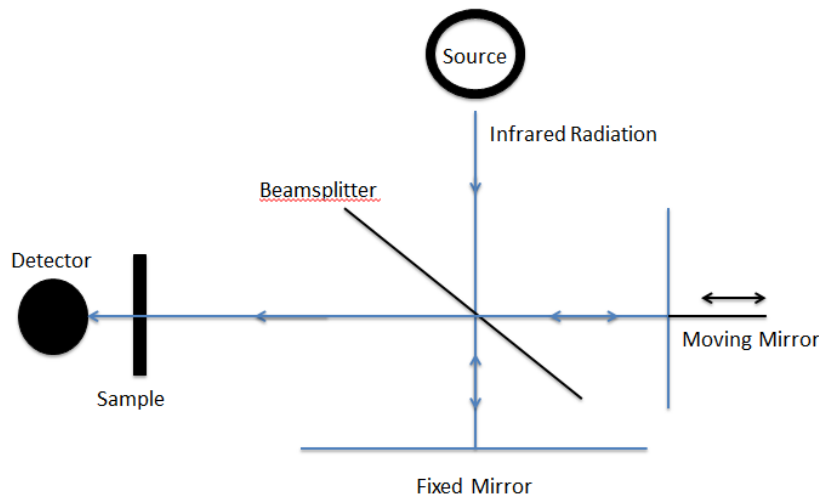
Figure 22: Simplified schematic diagram of an Infrared Spectrometer

2.3.3 Transmission Electron Microscopy (TEM)

An electron beam is passed through a series of lenses penetrating the sample deflected or undeflected, forming an image of the sample on a detector (Figure 23). The TEM instrument is maintained under high vacuum to prevent the electron beam from scattering. TEM from 80-300 KeV produces electron probe beam wavelengths from 4.33-2.24 pm producing images at the nanoscale. The high magnification of TEM can be associated with the combination of electron wavelengths, λ, as observed by the deBroglie relationship (equation 44) where m and q are the electron mass and charge respectively, h is the plank's constant and V is the potential difference via which electrons are accelerated. Overall, the electrons are generated by the electron gun and emitted by a cathode. The cathode is located at the top of the 2 meter long cylindrical tube. The electrons are then accelerated by the anode followed by passing through a small aperture resulting in a beam. The electrons are then focused onto the sample and interact with regions differently. The electrons are at the end collected on fluorescent film, which generates an image of the specimen. The beam that reaches the film consists of different amounts of electrons that pass through the sample producing in contrast.

$$\lambda = \frac{h}{\sqrt{2mqV}} \tag{44}$$

TEM can also be used to produce 2D electron diffraction pattern by taking the image at the back focal plane in reciprocal space (distance measured in 1/distance from the center of the beam). The diffraction pattern produced can then

be compared with previously studied diffraction patterns through literature review and interpreted according to standard crystallographic practice. The diffraction patterns that are produced are based on the pattern of single crystals including the specific points at distances and relative angles according to the interplanar distances and crystal structure. The results of previously studied crystal structures have been identified and well-studied. For example, gold is usually stable in a face centered cubic crystal structure (fcc), however, it has recently been found that for gold crystals with at least one dimension under 6nm, hexagonal close packing (hcp) becomes dominant.[105] A map of diffraction patterns of (111) face centered cubic plane and (0001) hexangonal close packed crystals can be found in Figure 24. The Miller indexed formula to calculate the interplanar distances for face centered cubic, where a is the lattice constant and d is the distance.

$$d_{hkl} = \frac{a}{\sqrt{h^2 + k^2 + l^2}} \tag{45}$$

and hexagonal close packed where a and c are both lattice constants and d is the distance

$$d_{hkl} = \frac{a}{\sqrt{\left(\frac{4}{3}\right)\left[\frac{h^2 + k^2 + hk}{a^2}\right] + (\frac{1}{c})^2}} \tag{46}$$
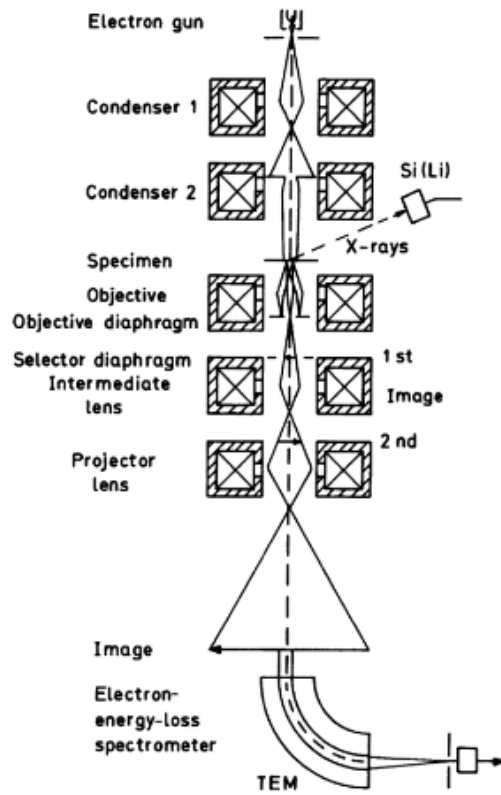
Figure 23: Schematic ray path for TEM with additional X-ray and electron energy-loss spectroscopy (Reprinted from Ref. [106] with permission)

A)
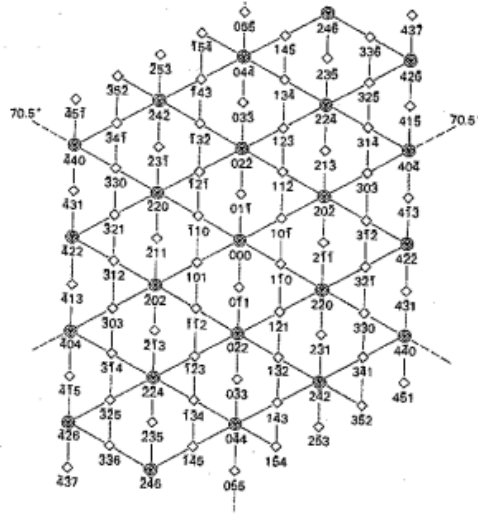
B)
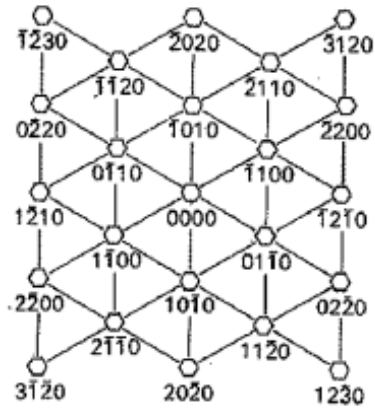
Figure 24: a) Map of electron diffraction points of the (111) crystal plane for face centred cubic (black dots), diamonds (diamond), and body centered cubic (circles) b) Map of miller indexed electron diffraction points for hexagonal close packed crystal structure (Reproduced from Ref. [107] with permission)

Analysis of diffraction patterns therefore consists of matching the pattern obtained experimentally to the one permitted via literature reviews. In this study, Transmission electron microscopy (TEM) was performed on FEI High resolution TEM Titan 80-300 LB TEM at the Canadian Center for Electron Microscopy at McMaster University. A drop from the sample was placed onto copper grids and left to air-dry at room temperature before loading it on to the machine. The images taken were then analyzed by using ImageJ software.[108] In this study TEM is used to visualize the shape and the size of different structures present in the sample and to study the exact crystal structures via diffraction patterns. It is important to realize that no one method is sufficient to draw any conclusions and needs to be used in a combination with other methods to draw valid and reliable conclusions.

2.4 Conclusion

This chapter outlined various computational and experimental methods used to effectively understand and control various interactions involved in the development and control of gold nanoreactors. The following two chapters will discuss the computational and experimental results obtained for the formation of gold reactions and control of this interaction via sonication, altering the nature of the polymer and by using coupling agents such as thiophene. Moreover the enhanced catalytic capabilities of the nanoreactors are also demonstrated by faster pyrrole polymerization.

3. Role of template-metal interactions and external energy in mediating the gold nanoparticle growth within the nanoreactor

Vishva Shah designed and performed the experiments and prepared the manuscript.

3.1 Introduction

Nanomaterials have gained large interest from the scientific community due to the fact that materials at the nanoscale exhibit unique electronic, magnetic and optical properties when compared to the bulk material.[89] The main advantage associated with nanostructures originates from higher surface to volume ratio leading to an altered catalytic capability and the domination of molecular or atomic interactions at the nano-scale.[109] These unique properties allow the development of efficient nanoreactors with metal active centers synthesized in-situ by environmentally friendly methods.[79,80] The nanoreactors can be tailored for specific reactions and applications. The optimization involves three components: (1) the selection of a template, which should allow confinement effect to occur improving the thermodynamics of the reaction by reducing entropic cost; (2) the selection of a metal center as catalyst for the reaction and (3) the selection of a hydrophobic or hydrophilic environment for the reaction. All three components are crucial for the development of tailored nanoreactors and involve an extremely challenging control of the conformation and properties at the molecular scale.

A precise method to obtain defect-free monodisperse nanoarchitectures is the bottom-up method.[110] Bottom-up approach is carried out in a controlled environment and builds the products from the dominating atomic or molecular interactions by self-assembly.[110] Self-assembly refers to the spontaneous association of components via many interactions including hydrogen bonding, van der walls or electrostatic forces to form a large functional unit.[110,111]

The self-assembly of block copolymers produces different nanoarchitectures in selective solvents.[17] Generally most diblock copolymers associate to form spherical micelles[18], however, they also have access to other morphologies. This is especially true for polymers that have an insoluble amorphous block longer than the soluble block and some of the other morphologies produced include lamella, nanotubes[18] or nanocages[112]. The nanoarchitectures obtained by block copolymers can be modified by varying factors including chain length, ratio of block lengths, polydispersity, temperature, time or concentration.[18] The size and the properties of the cavities produced by various morphologies is crucial in determining potential applications especially in drug delivery. Typically, block copolymers are known to produce larger nano or micro structures when compared to alternating copolymers and hence produce larger cavities.[17] For

example, the diameter of the cavities produced in nanotubes by block copolymer and alternating copolymers were found to be 9 nm[18] and 3 nm[19] respectively. The large cavity of the structures produced using block copolymer prevents confinement effects, which play a significant role in influencing the reactivity inside the polymeric template.[20] Indeed, the confinement effect commonly observed in systems such as carbon nanotubes or biological systems has been observed to initiate unfavorable reactions.[113–115] Therefore, alternating copolymers were selected to produce the template of the nanoreactors by self-assembly.

Poly(styrene-*alt*-maleic acid) (SMA) is an amphiphilic alternating co-polymer which self assembles into highly organized nanostructures in water.[77] These nanoarchitectures include nanotubes or nanosheets creating hydrophobic and hydrophilic cavities within the structure (Figure 25). The nanoarchitechtures (nanotubes or nanosheets) were shown to be dependent on the polymer molecular weight.[79,80] It has previously been shown that SMA nanotubes are formed from the association between eight low molecular weight SMA polymer chains through π-π stacking with the diameter of the hydrophobic cavity of 3 nm and a hydrophilic domain on the outside.[78] The templates generated by SMA are unsupported and induce a confinement effect due to the small size of the cavity, promoting reactions that are not favored in bulk. Indeed, Platinum (II) chloride, under the confinement of SMA has previously been observed to produce well dispersed and stable metal platinum nanoparticles, less than 3nm in size.[16] It is important to note that no reducing agents were involved in the synthesis of platinum nanoparticles within the hydrophobic cavity, making it very stable and environmentally friendly.[16] The use of reducing agents in the solution creates problems including low catalytic activity, remaining in the solvent due to a very hard reduction process, along with toxic characteristics associated with the reducing agents narrowing the possibility of applications in biomedicine.[82] Moreover, the confinement effect in the hydrophobic cavity of SMA was found to promote the spontaneous polymerization of pyrrole.[20] Combining the two results, it was also found that using the SMA-platinum nanoreactor along with pyrrole led to faster kinetics of pyrrole polymerization and an overall threefold increase in the reaction rates.[16] Therefore, SMA as a template is a good candidate for environmentally friendly synthesis and reduction of metal salts without the use of any reducing agents for the synthesis of novel nanoreactors with metal nanoparticles as active centers.
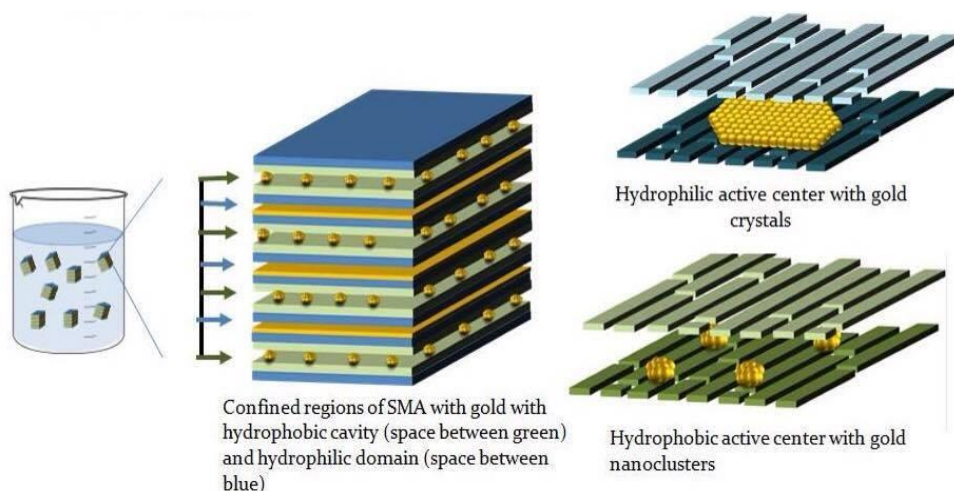
Figure 25: Schematic representation of Poly(styrene-*alt*-maleic acid) (SMA) with gold crystals and nanoclusters

Among metal nanoparticles used in nanotechnology applications, gold nanoparticles present unique optical and electronic properties. Gold nanoparticles have been extensively used in nanomedicine because of their physical properties and many applications in a variety of applications including therapeutic agent delivery, catalyst, probes, conductors or in biomedicine.[63–65,68,72] Gold is inert in bulk, however at the nanoscale gold is very reactive due to altered physical properties. In addition, the modified properties of gold under confinement effect have been observed and studied for various systems such as in SiO_2 cavities or inside siloxane nanocages.[116,117] Reduction of gold has been conducted using reducing agents such as hydrogen gas, amines or hydroquinone.[118–120] The confined conditions created by SMA makes it possible to reduce gold without any reducing agents as detailed in earlier studies by our group.[79] Similar study for reducing gold with microwave-assisted techniques have been carried out using $HAuCl_4$ as a metal precursor, water and a microwave oven.[82] This synthesis method produced gold seeds, <3nm in size but observed particle coalescence and rapid growth due to the absence of protecting agents.[82] Keeping in mind the difficulty associated with the production of stable and well dispersed gold nanoparticles without the use of reducing agents as well as the advantages that are associated with it, this study aims to develop a system that allows for a simple method of synthesis of stable and well dispersed gold nanoparticles. Moreover, unlike platinum, gold could be able to interact with the hydrophilic domain or the hydrophobic cavity simultaneously (Figure 25). Therefore, the control of the interaction of gold as an active center with the hydrophobic or hydrophilic domains of the nanoreactor will allow the

control of the environment of the reaction occurring within the nanoreactor. These unique properties will allow different reactions to occur simultaneously in the same nanoreactors within different environments.

The aim of this paper is to investigate the interaction between SMA and gold and to control the interaction with the hydrophobic and hydrophilic domain to tailor the environment of the active center of the nanoreactors. The growth of the metal active centers will be controlled by changing the nature of the polymer-metal interaction and by sonication. The interaction of gold with the SMA template will be compared to a functionalized SMA polymer, SMA_m, structurally 85-90% identical to SMA with 10-15% of SMA functionalized with monomethyl ester (Figure 26). In addition, the effect of addition of weak external energy will be investigated, as sonication disrupts the self-assembly process – one of the key elements of the nanoreactor synthesis.[121–123]Indeed, sonication has been known to disrupt the self-assembly process and promote drug release or even cause nanofibers to separate.[121–123] Therefore, the theoretical and experimental characterization of the interaction between SMA and gold is presented, as well as the influence of the presence of mono methyl ester and sonication on the growth and nature of the gold nanoparticles produced. The control of the growth of the nanoparticles within the hydrophilic or hydrophobic domains of the template will allow the development of nanoreactors with hydrophilic or hydrophobic active cavities. The nanoreactors produced are expected to present improved reactivity due to the enhanced properties of the metal catalyst at the nanoscale combined with the confinement effect within the cavities.
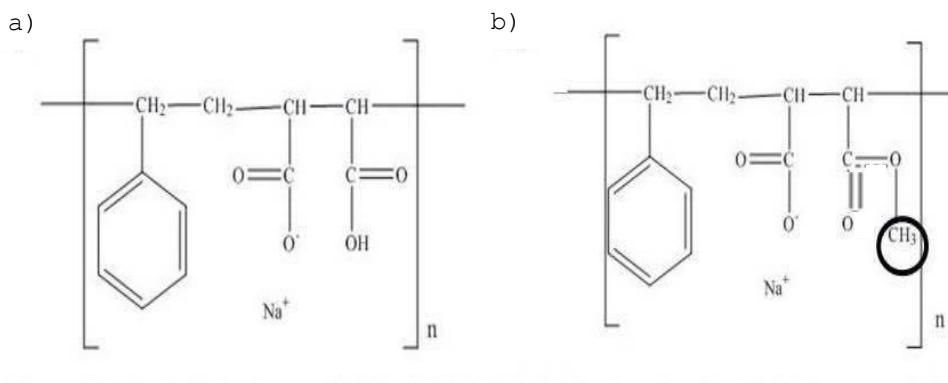
Figure 26: Chemical structures of a) SMA b) 10-15% SMA_m functionalized with monomethyl ester (highlighted in circle)

3.2 Sample Preparation and methods

Poly(styrene-*alt*-maleic acid) (SMA) sodium salt solution, 350 kDA, 13% in neutral water (liquid solution), Poly(styrene-*alt*-maleic acid) partial monomethyl ester (SMA$_m$), 350 kDA (powder) and Gold(I) chloride, 99.9% were purchased from Sigma Aldrich. SMA was diluted to 1% in DI water whereas SMA$_m$ was solubilized to make 1% solution and then neutralized to pH 7 with NaOH as required. Gold(I) chloride (AuCl) was used as received. For sample preparation, 5 ml of SMA or SMA$_m$ at pH 7 were mixed with required amount of AuCl and analyzed. The molar ratiom of 1:1 between the metal atoms and the SMA monomer was maintained. To test for the effects of sonication the sample was originally sonicated for 30 minutes to promote faster mixing and reaction rate. Unless otherwise specified, the reaction was always carried out at room temperature.

For detailed methods on computational and experimental methods used please refer to section 2.1.8 and 2.2. Experimentally, for UV-Vis, 1mm quartz cuvette was used in Agilent 8453 single beam diode array spectrometer. The data was then analyzed with UV-Visible GLP Chemstation software v.B.04.02. Moreover, Infrared spectra was obtained by using the Perkin Elmer FT-IR spectrometer model Spectrum 65. Lastly, TEM data was obtained by using FEI HR-TEM Titan 80-300 LB TEM at the Canadian Center for Electron Microscopy at McMaster University A drop from the sample was placed onto copper grids and left to air-dry at room temperature before loading it on to the machine. The images taken were then analyzed by using ImageJ software.[108]

3.3 Results and discussion

The main goals of this study include the facile, environmentally friendly synthesis of nanoreactors with gold active centers within the confined hydrophobic or hydrophilic domains provided by the polymeric template, SMA. Moreover, this study also explores the control of the production of the size of the gold nanostructures in an attempt to control the environment of the active centers and influence the properties associated with the entire system. In order to determine if gold can grow on both the hydrophobic and hydrophilic domains, characterization at the atomic level is required to study the interaction between the polymer and the metal giving rise to the need for *ab initio* molecular modelling studies.

3.3.1 Interaction between SMA and Gold- Synthesis of the gold clusters and crystals

Ab initio molecular modelling simulations have proven to be a powerful tool for prediction and characterization of organic and inorganic atomic interactions.[79,85–87] To study the interaction between SMA and gold at the atomic level, molecular modelling simulations were performed. Each dihedral angle was optimized to determine the global minimum of the studied system followed by the optimization of the whole structure. The optimized structure of SMA can be

observed in Figure 27a. The structure was optimized by using density functional theory with B3LYP and B3PW91 functionals and LANL2DZ to allow direct comparison with systems involving gold.

It has been shown in previous studies conducted by our group that gold prefers interacting with the hydrophilic domain, forming a monolayer of gold on the hydrophilic domain of SMA.[79] To confirm this computationally, gold was placed at three different sites, including beside two carboxylic acid groups (hydrophilic) and beside the styrene (hydrophobic) of an SMA monomer. The optimized structures for SMA and gold can be seen in Figure 27b and 27c where gold was placed beside carboxylic acid and styrene group respectively. Only the most stable structure with the lowest interaction energy for gold beside carboxylic acid is displayed. The structures themselves did not change after optimizations using two different hybrid functional (B3LYP and B3PW91) with only a minor change in the interaction energy values. The interaction energy of the structures with SMA-gold was calculated via equation 47 and can be observed in table 2.

$$E_{int} = E_{complex} - (E_{Au} + E_{SMA})$$ Equation (47)
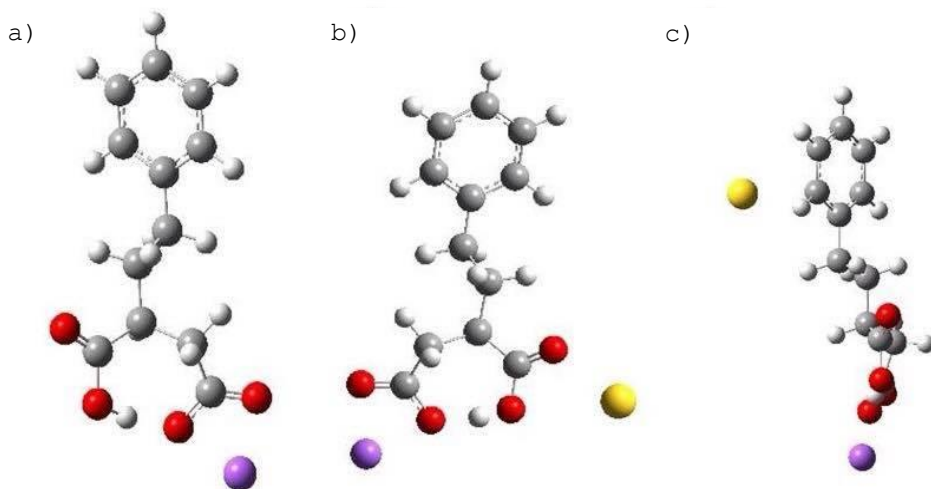
Figure 27: Optimized structures of a)SMA b) SMA with gold (yellow) SMA gold interaction with carboxylic acid c) SMA gold interaction with styrene group DFT-B3LYP/B3PW91-LANL2DZ (Gray-carbons, White-hydrogen, Red-oxygen, Purple-sodium)

Table 2: Interaction energy calculated for two structures, by DFT-B3LYP/B3PW91-LANL2DZ using equation 1

System	Structure	DFT-B3LYP-LANL2DZ (kJ/mol)	DFT-B3PW91-LANL2DZ (kJ/mol)
SMA-Au-COOH	Figure 27b	-28.23	-25.60
SMA-Au-styrene	Figure 27c	-14.50	-15.99

Good correlation can be observed in Table 2 between both functionals. It is predicted that gold will interact preferentially with carboxylic acid groups instead of the styrene group. The difference in interaction energy between gold interacting with carboxylic acid groups compared to the styrene group was found to be 13.73 kJ/mol and 9.66 kJ/mol for B3LYP and B3PW91, respectively. While it can be concluded that gold does prefer interaction with the hydrophilic domain, the difference in energy is very small. It is therefore, expected that both interactions could occur depending on the experimental conditions allowing a control of the environment of the active center.

3.3.1.1 IR spectra for SMA-gold interaction between COOH of SMA and Au

The favoured interaction between the carboxylic acid groups of SMA and gold can be observed by IR spectroscopy. The IR spectra for plain SMA can be observed in Figure 28a, with a high peak intensity at 1780 cm^{-1} corresponding to the C=O stretch from SMA.[124,125] This peak (around 1700 cm^{-1}) has previously been observed by many researchers and been attributed to C=O from the carboxylic acids adsorbed onto gold.[124,125] Indeed, the IR spectrum for SMA-gold (Figure 28b) shows a decreased intensity of a peak at 1762 cm^{-1}. The reduced intensity of the peak observed at 1762 cm^{-1} may be due to minimized interaction of gold with the COOH groups. This supports the simulation results since some gold may be interacting with the hydrophilic carboxylic acid groups whereas some gold may also be interacting with the hydrophobic styrene group instead. Although, it is important to understand that the peak intensities cannot be solely relied upon and hence a combination of results must be used to draw conclusions.
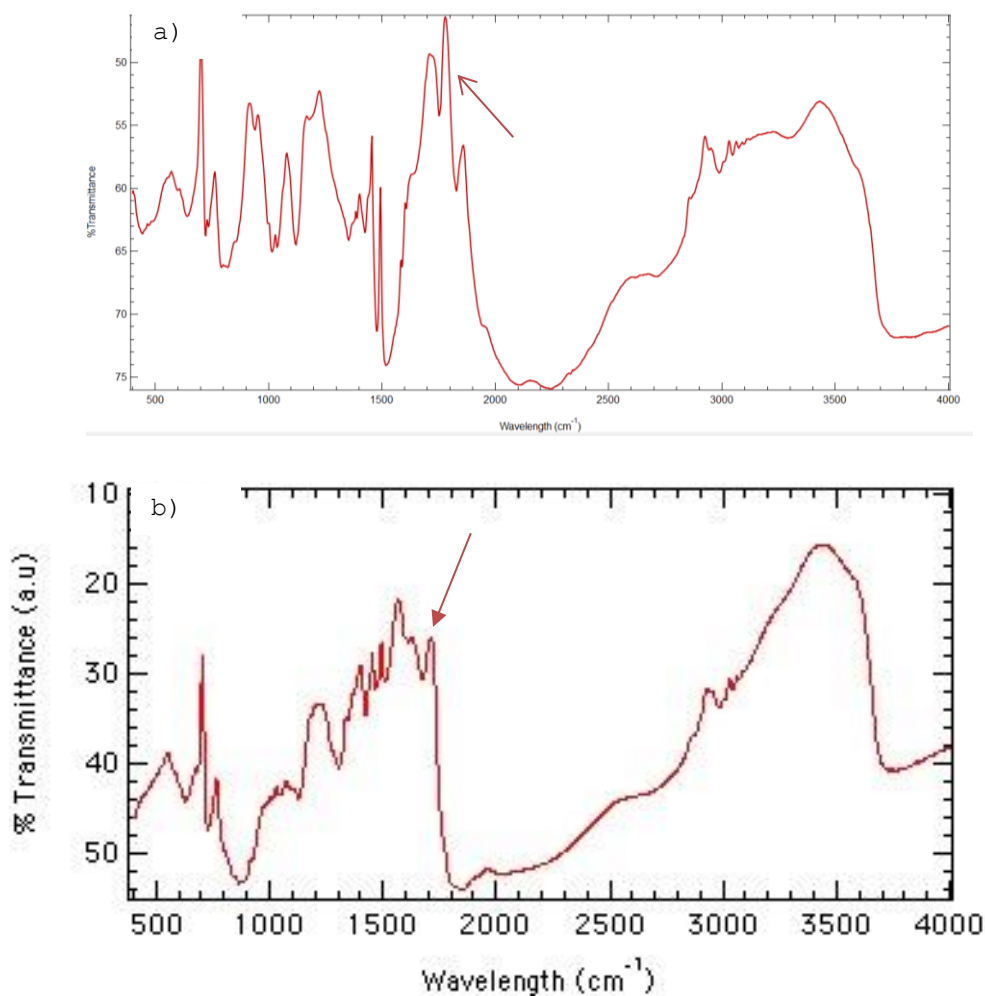
Figure 28: IR spectra for a) SMA b) SMA-gold interaction showing a decreased intensity of the peak at 1762 1960 cm^{-1} representing a deccreased interaction between COOH of SMA and Au

3.3.1.2 UV-Vis spectra for SMA-gold differentiating between gold sheets and clusters

It is predicted from simulation and IR results, that gold is interacting with the hydrophilic domain and forming gold sheets as observed by our group earlier.[79] However, the growth of the gold nanoparticles could also occur as gold clusters in the hydrophobic cavity as well, in which case the size of the gold nanoparticles would be restricted to 3 nm. The growth of gold nanoparticles can be observed by

UV-Vis as they are active in the 500 nm to 600 nm range, depending on their size and shape. This method would allow the differentiation between the sheets and clusters and provide an ability to follow their respective syntheses. Therefore, UV/Vis spectroscopy was carried out to follow the growth of gold on either the hydrophobic or hydrophilic domains. Gold chloride was added to the sample to maintain a 1:1 stoichiometric ratio with SMA monomers in 1% wt/wt solution. The sample was prepared by simple mixing as described in 2.1. Two peaks at 560 nm and 300 nm are observed in the UV/Vis spectra of SMA-gold solution monitored over 49 days (Figure 29). The peak at 560 nm develops over 11 days and then settles whereas the peak at 300 nm develops only after 16 days. A peak at 547 nm has been observed earlier by our group and other researchers and represents the formation of gold sheets.[79,126] Theoretical study conducted by Matulis *et al*. have calculated peaks around 300 nm corresponding to isomers of Au_8 clusters.[102] It can therefore be predicted that the peak at 300 nm may correspond to gold clusters instead of gold sheets. This method would therefore allow to follow the growth of the nanoparticles within the hydrophilic domain (gold sheets: ~560 nm) or hydrophobic domain (gold clusters: ~ 300 nm) in situ. Overall, from UV/Vis it can be concluded that separate nanoparticles are formed, which strengthen the hypothesis of growth both on the hydrophobic and the hydrophilic domains of SMA.
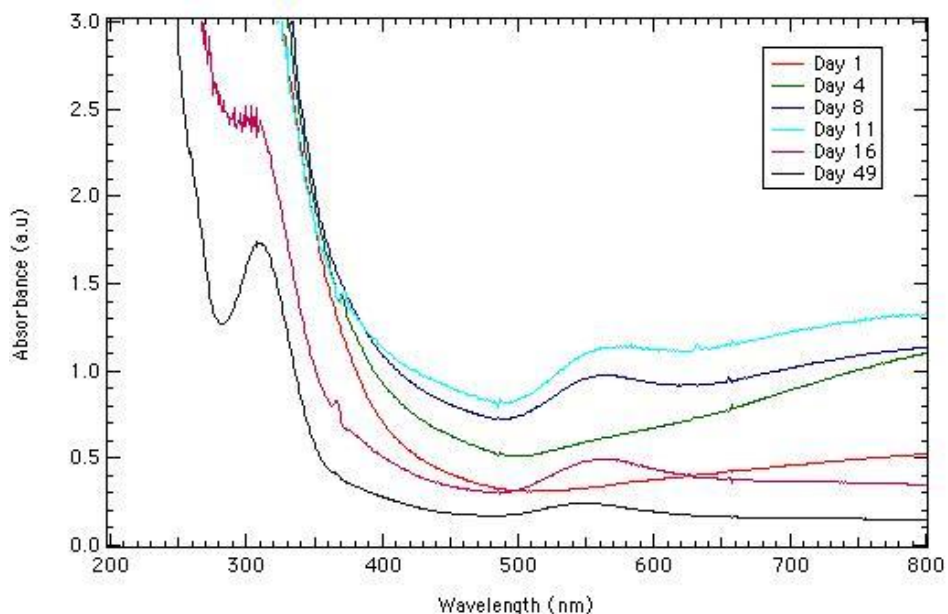
Figure 29: UV/Vis spectra of AuCl in 1% SMA solution. A peak at 560 nm develops until day 11 and then settles. Another peak at 300 nm can also be observed at day 49

Prediction of particle size via Mie's theory

In addition, according to the Mie`s theory the diameter of spherical gold colloids in water can be predicted based on the correlation of its radius to wavelength of its plasmon band.[127] In Figure 29, a peak is observed at 300 nm corresponding to a predicted diameter of the Au particles of 18 nm. However, the gold clusters are restricted by size when reacting within the 3 nm hydrophobic cavity, as observed in the case of platinum nanoclusters.[79] The discrepancy can be related to the limitation of the Mie`s theory, which gives accurate predictions only in the range of 5-80 nm assuming free spherical particles. Indeed, the nanoparticles synthesized within the nanorectors are expected to interact with the template and their diameter could be smaller than 3nm accounting for the inaccuracy with the calculated diameter.[127] Note that the particle size for the additional peak present in Figure 29 at 560 nm was not conducted due to limitations associated with Mie's theory for flat gold nanoparticles.[79] Therefore the size of the nanoparticles could not be correlated directly to the UV-Vis spectra using the Mie's theory; were instead fully characterized by high resolution TEM.

3.3.1.3 Transmission Electron Microscopy images showing gold crystals and clusters on the hydrophilic domain and in the hydrophobic cavity

In order to characterize precisely the size and shape of the nanoparticles formed as well as bridging the gap between the atomic characterization and UV-Vis observation, a high resolution TEM was performed on the SMA-Au system. The gold nanoparticles interacting with the SMA template can be observed in the images obtained through HR-TEM. Different shapes of gold crystals were observed with sizes ranging between 30-50 nm (Figure 30a,b). Crystals with similar shapes but different size have been observed in a previous study and represent the interaction of gold on the hydrophilic domain of SMA corresponding to the peak at 560 nm in Figure 29.[79] Few nanometer changes in the size of the gold crystal can lead to drastically different chemical and physical properties and therefore it is important to understand the origin of the specific shape or size of the crystal to develop. Researchers have tried to control the size and shape of the structures produced by a variety of ways including oxidative etching or restricting the size by using various DNA origami molds.[128,129] DNA origami molds take advantage of the size of internal cavity produced to restrict the size of gold nanostructures produced. Similarly, in the present study, gold clusters were observed in Figure 30c, ranging in size from 2-3 nm confirming that their synthesis occurred within the restricted hydrophobic cavity produced by SMA without any reducing agents. Moreover, a statistical analysis of the TEM images determined that approximately 11% of the area in Figure 30c was occupied by gold clusters. Because of the small size of gold clusters, it can be concluded that gold is interacting with the hydrophobic cavity of SMA and therefore corresponds to the peak at 300 nm in Figure 29.
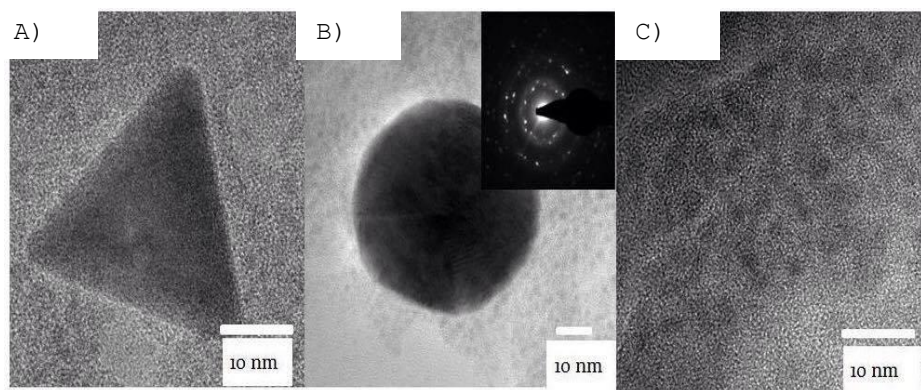
Figure 30 : TEM images for SMA with gold a) Single gold crystal of 30 nm in size b) Layered gold crystal 55 nm in size showing overlap in the corresponding diffraction pattern c) gold clusters ranging from 2-3 nm in size

Along with the shape and size of the structures produced the properties of the gold crystals produced are also affected by its crystal structure. Gold is usually stable in a face centered cubic crystal structure (fcc), however, it has recently been found that for gold crystals with at least one dimension under 6nm, hexagonal close packing (hcp) becomes dominant.[105] The diffraction pattern for gold sheets in Figure 30b can be observed in the inset. The crystal structure observed appears to be (0001) hcp plane. The Bravais-Miller system uses four indiced (*hkil*), with the constraint of *h+k+i=0*. The radial distances for the diffraction patterns were calculated from $0\bar{1}10$ and $\bar{1}100$ indedes with distances of 4.36 nm^{-1} and 4.29 nm^{-1} respectively along with the unit cell parameter of $a = 2.96\text{Å}$[105]. This different pattern is similar to the atomically thin Au layer observed previously .[79] However, there is a lot of overlap in the diffraction patterns and therefore other types of crystals structures may also be present in the background.

In this study, facile synthesis of gold nanoreactors was demonstrated with the production of gold clusters in the hydrophobic cavity (2-3 nm) and thin gold sheets on the hydrophilic domain (30-50 nm) as schematically represented in figure 25. The relative growth of the gold nanostructures was followed by UV-Vis, interactions with the polymer template characterized by IR and the structure along with the shape and size monitored through HR-TEM. As the control of the environment of the metal active center is crucial in the development and tailoring of the nanoreactors; it is important to control the ratio of gold crystals and gold clusters synthesized within the polymeric template. In order to control the environment of the nanoreactors synthesized, two methods are used: (1) the functionalization of the polymer (SMA$_m$ instead of SMA) to observe the effects of

the presence of monomethyl ester on the growth of the gold crystals and (2) sonication to characterize the effect of weak external energy on the self-assembly process and crystal growth.

3.3.2 Control of the interaction between SMA and gold by the presence of monomethyl ester

The synthesis of gold active centers within the SMA template produced both gold sheets and gold clusters. As determined in previous studies, the gold sheets or crystals interact exclusively with the hydrophilic groups of the template[79] while gold clusters grow inside the hydrophobic cavity. Therefore, modifying the nature of the polymer by functionalization could change the interaction between SMA and gold with either the hydrophobic cavity or the hydrophilic domain. SMA_m was specifically chosen because of its structural similarity to SMA with a minor modification and does not affect the self-assembly, shape and size of the polymer template. SMA_m is 85-90% the original SMA with 10-15% of SMA structure functionalized with monomethyl ester. The structural difference between SMA and SMA modified with monomethyl ester can be observed when comparing Figure 26a and 26b, respectively. It is important to note that the modified SMA (Figure 26b) constitutes only 10-15% SMA_m, whereas 85-90% is still the original structure seen in Figure 26a.

3.3.2.1 Influence of the nature of the polymer on its interaction with gold monitored via UV-Vis

SMA_m was mixed with gold chloride by the method described in 2.1 and UV/Vis spectra (Figure 31) were obtained to determine the influence of monomethyl ester on the gold nanoparticle growth. In Figure 31, a peak can be observed at 547 nm and a shoulder at 314 nm. The peak at 547 nm was found to develop for 20 days and then settle, whereas the shoulder at 314 nm develops only after 34 days. Compared to Figure 29, the intensity of the peak at 547 nm is larger, whereas the peak at 314 nm is now only a shoulder. Since the only difference between the two samples is the presence of 10-15% monomethyl ester, it can be concluded that the presence of monomethyl ester enhances the interaction of gold chloride with SMA on the hydrophilic domain. The shoulder at 300 nm develops significantly later than in Figure 29 suggesting that monomethyl ester may also be playing a part in minimizing the interaction of SMA and gold in the hydrophobic cavity. The interaction between SMA_m and gold plays a major role in controlling the synthesis of the gold nanostructures and was further investigated at the atomic scale by ab initio molecular simulation.

3.3.2.2 Influence of monomethyl ester on SMA-Au system demonstrated by ab intio simulations and molecular orbital analysis

Computational chemistry was used to understand the origin of the big difference in the polymer Au interaction on the hydrophilic domain with SMA_m. The structures were optimized using the same methods developed for SMA. Similar to SMA, gold was placed at three different sites around SMA_m including beside two carboxylic acids and styrene group. When gold was placed beside the styrene group of SMA_m, the optimization process (following the potential energy surface of the system) resulted in a strong attraction between the hydrophilic groups and Au, with the Au atom moving away from the styrene group. The optimized structures of SMA_m and SMA_m with gold are shown in Figure 32 a and b respectively. As can be observed in Figure 32b, in the presence of monomethyl ester gold strongly prefers interaction with carboxylic acid group or the hydrophilic domain. Moreover, the interaction energy calculated by equation 47 was found to be -226.07 kJ/mol and -197.99 kJ/mol by B3LYP and B3PW91, respectively. These values can be directly compared to -28.23 kJ/mol and -25.60 kJ/mol from Table 2 obtained for SMA with the same methods. Therefore, the interaction between SMA_m with gold is more favourable than SMA with gold explaining the increased intensity of the peak at 547 nm in Figure 31. Moreover, molecular orbital analysis was obtained to characterize the origin of the difference in interaction energy in the presence of monomethyl ester. From Figure 33, it is observed that gold is able to interact with only one oxygen atom of the carboxylic acid groups of SMA, while gold can interact with two oxygen atoms of the carboxylic acid groups of SMA_m. Since gold is able to interact with two oxygen atoms, instead of one in the presence of SMA_m this contributes to the stabilization of the system and to the strong interaction energy obtained for SMA_m-Au. The use of SMA_m as a template could favor the synthesis of a metal active center within a hydrophilic environment of SMA.
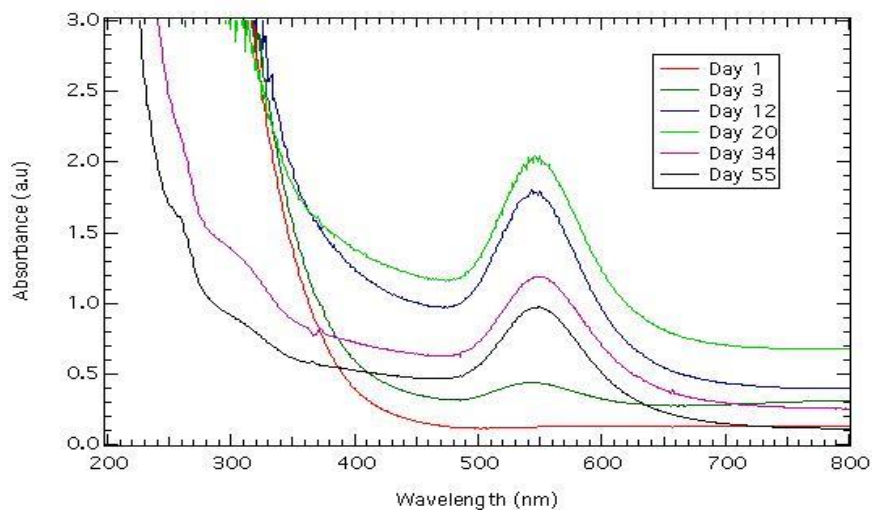
Figure 31: UV/Vis spectra of AuCl in 1% SMA$_m$ solution. A peak at 547 nm develops until day 20 and then settles. Another shoulder at 314 nm can also be observed after day 34
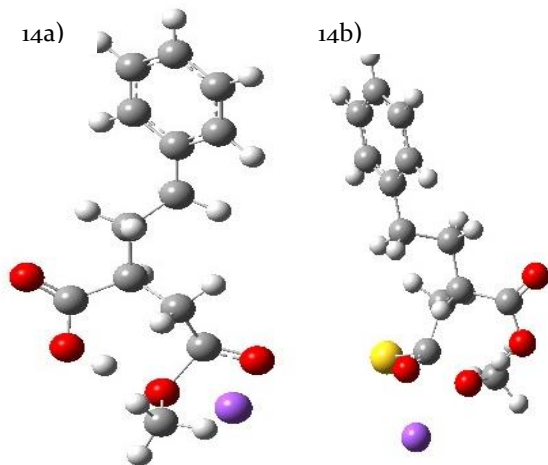
Figure 32: Optimized structures of a)10-15% SMA$_m$ b) SMA$_m$ with gold (yellow) with DFT-B3LYP/B3PW91-LANL2DZ
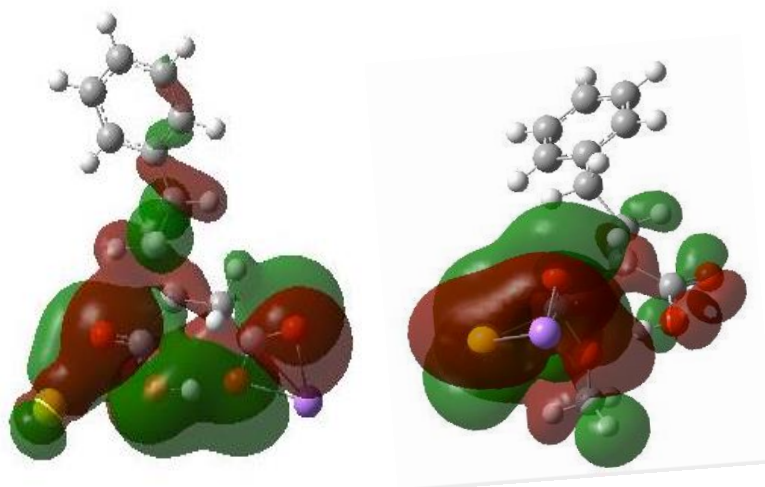
Figure 33: Molecular orbital images of a) SMA and gold, energy -0.29623 hartrees
b) SMA$_m$ and gold, energy -0.28786 hartrees obtained with iso value of 0.005

3.3.2.3 IR spectra for SMA$_m$-gold representing a stronger interaction between COOH of SMA$_m$ and Au

Infrared spectroscopy was conducted to ensure that gold in the presence of monomethyl ester was interacting with the carboxylic acid groups as predicted by the simulation and UV/Vis spectroscopy. The IR spectra for SMA$_m$ with gold in Figure 34 shows an increased intensity of the peak at 1765 cm^{-1} showing a stronger interaction of gold with two carboxylic acid group environments compared to styrene, proving a stronger interaction on the hydrophilic domain.[125,124] Indeed, the adsorption of CO onto gold surfaces is dependent on many factors including temperature and the type of surface and varies depending on the experimental conditions.[130] An extensive study on adsorption of CO onto gold surfaces revealed that low-temperature oxidation of CO onto metallic gold depends only on the presence of the hydroxyl group and that the size for the gold particles impacts the number of CO molecules it interacts with.[131] The minute differences in the IR spectra are due to the different chemical environment of the sample. It is important to note that the change in IR spectra is related to a functionalization of only 10-15% of the SMA monomers present within the SMA polymeric chain.
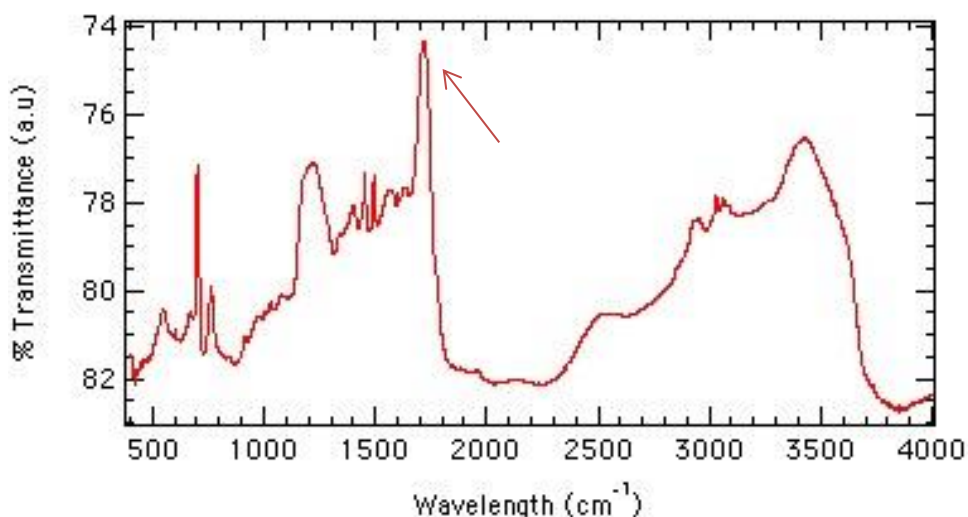
Figure 34: IR spectra for SMA$_m$ with gold showing increased intensity of the peak at two small peaks at 1765 cm^{-1} representing a stronger interaction between COOH of SMA$_m$ and Au

3.3.2.4 Transmission Electron Microscopy images showing larger gold crystals and slightly smaller gold clusters

To confirm the stronger interaction of gold on the hydrophilic domain of SMA, TEM images were taken. Larger gold sheets 70-80 nm can be observed (Figures 35a and 35b) from TEM images proving that presence of monomethyl ester intensifies the interaction between SMA and gold on the hydrophilic domain. It was predicted that monomethyl ester would minimize the interaction between SMA and gold in the hydrophobic cavity due to a shoulder being present instead of a peak at 300 nm in Figure 34. The size of gold cluster decreases in SMA$_m$-gold to 1.5-2.5 nm (figure 35c) from 2-3nm in SMA-gold suggesting that monomethyl ester does minimize the interaction to some extent. However, a significant decrease in terms of percent of area occupied, 10%, by clusters was not observed when compared to the original 11% in the case of SMA-gold. It is possible that the actual number of gold clusters present by area occupied may have been higher in SMA-gold but simply could not be accounted for due to overlapping of clusters. Moreover, the crystal structure of gold was found to be (110) face centered cubic (fcc) for figure 35a and (0001) hexagonal close packing (hcp) for figure 35b. The radial distances for the (110) fcc crystal structure were calculated by using $\bar{2}20$ and $\bar{1}11$ with indexes distance of 7.02 nm^{-1} and 4.13 nm^{-1} respectively, along with the unit cell parameter of $a = 4.08 A$ [132]. Comparatively the radial distances for (0001) hcp were calculated by using $\bar{2}200$ and $0\bar{1}10$ with indexes distance of 7.82 nm^{-1}

and 4.34 nm^{-1} with the unit cell parameter of $a = 2.96 A$ [105]. Therefore, it is important to note that the presence of monomethyl ester not only strengthened the interaction between SMA and gold on the hydrophilic domain giving clearer diffraction patterns, but it also produced a mixture of fcc and hcp type crystal structures, implying different thickness of the sheets produced.
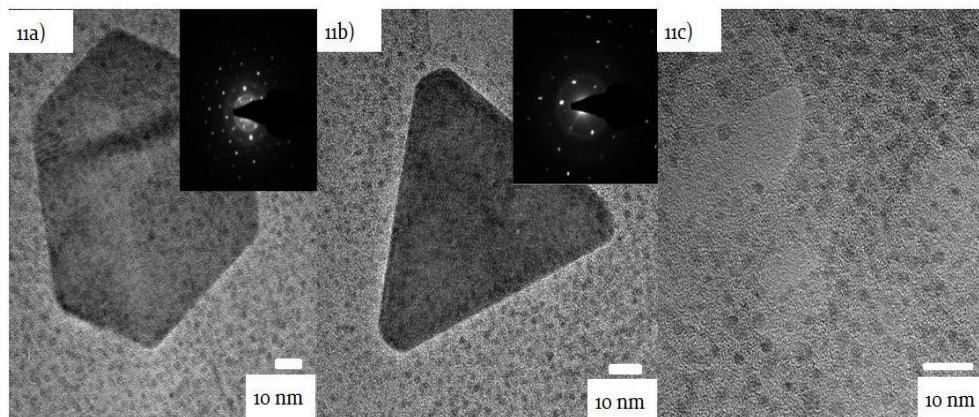
Figure 35: TEM images for SMA$_m$ with gold a) Single gold crystal of 80 nm in size and its corresponding diffraction pattern showing the (110) fcc plane b) Single gold crystal of 75 nm in size and its corresponding diffraction pattern showing (001) hcp plane c) Gold clusters of 1.5-2.5 nm in size

Furthermore, it was observed that the presence of monomethyl ester in SMA$_m$ enhances the interaction of SMA and gold on the hydrophilic domain resulting in the formation of larger gold sheets and intense peak at 547 nm in Figure 31. Monomethyl ester was also found to minimize the interaction of SMA and gold in the hydrophobic cavity resulting in slightly smaller gold clusters and a shoulder instead of a peak at 300 nm in Figure 31. One of the other ways to control this interaction even more is to provide external energy in terms of sonication to observe whether the interaction can be strengthened on the hydrophilic domain and weakened in the hydrophobic cavity due to the disruption of the self-assembly process.

3.3.3 Control of the interaction between SMA$_m$ and gold by sonication

Sonication is known to disrupt the self-assembly process and therefore may potentially force the gold to only interact with the hydrophilic domain due to disruption of the hydrophobic cavity. Only SMA$_m$ was used to measure the effect of sonication since that resulted in enhanced interaction of gold on the hydrophilic domain.

3.3.3.1 UV/Vis spectra for SMA_m-gold(sonication) showing the elimination of the formation of gold clusters

To determine the effect of sonication on the growth of the Au crystals, the sample was mixed and sonicated for 30 min before the UV measurements were obtained. The UV-Vis spectra for SMA$_m$-gold sonicated can be observed in Figure 36 and can directly be compared with Figure 31 without the sonication. A few major differences can be observed including faster growth of gold sheets on the hydrophilic domain. In Figure 31 the peak at 547 nm reached its maximum on day 20 and then settled whereas the same peak at 548nm in Figure 36 reached its maximum on day 3 and then settled. Moreover, the shoulder at 300 nm in Figure 29 representing the formation of gold clusters completely disappears in Figure 36 implying that sonication has greatly minimized the interaction of gold in the hydrophobic cavity. The results were confirmed by HR-TEM characterization (Figure 37) obtained by our group earlier showing the formation of only gold sheets of 30 nm in size when the sample was sonicated.[79] In addition, all of the gold crystals produced using this method were (0001) hcp plane as observed from $1\bar{2}10$ and $1\bar{1}00$ (inset of Figure 37) with distances of 7.94 nm^{-1} and 4.20 nm^{-1} respectively, using the unit cell parameter of $a = 2.96 A^{105}$.[79] Overall, sonication is found to be able to control the interaction between SMA and gold even more while promoting the interaction of gold on the hydrophilic domain only and eliminating its interaction with the hydrophobic cavity. Sonication also restricts the growth of monoatomic gold crystals to only (0001) hcp plane with no fcc crystals after sonication.[79]
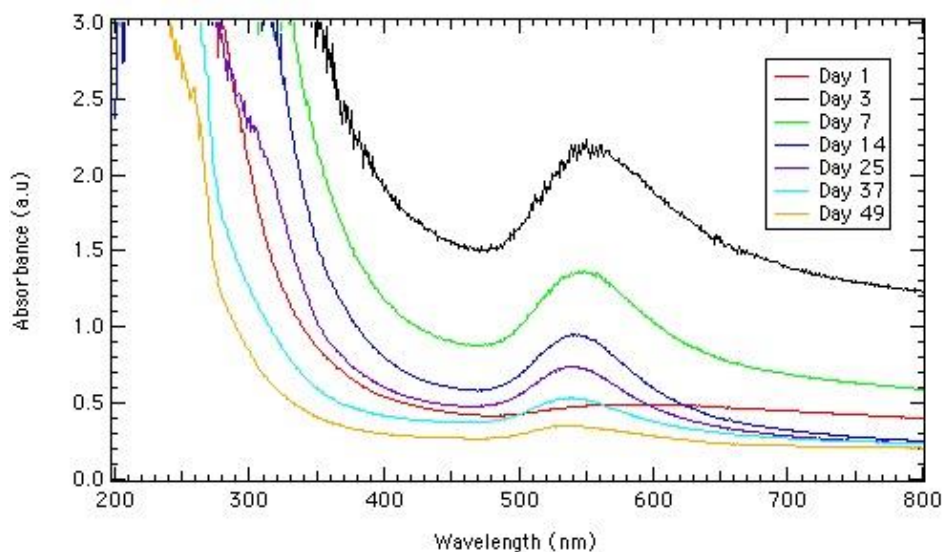
Figure 36: UV/Vis spectra of AuCl in 1% SMA_m solution sonicated for 30 mins with a strong peak at 547 nm which develops until day 3
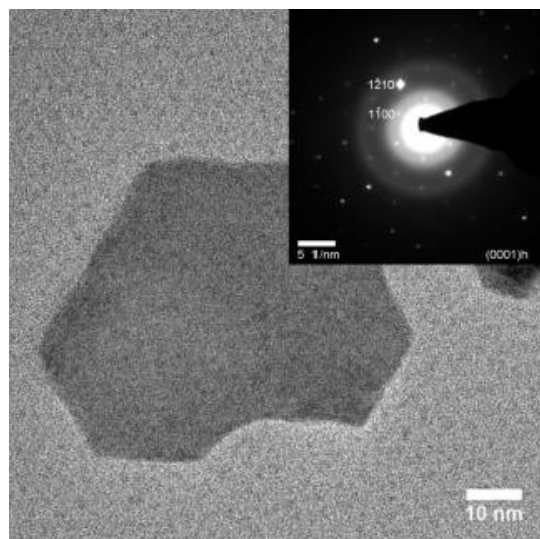
Figure 37: TEM image of AuCl in 1% SMA_m solution sonicated showing a single gold crystal approximately 40 nm in diameter with no gold clusters (Reproduced from Ref. [79] with permission) (Reprinted from Mctaggart et al. 2015)

3.4 Catalytic activity of gold demonstrated by pyrrole polymerization

The development of environmentally friendly methods for the synthesis of unsupported nanoreactor in aqueous solutions can have a significant impact on organic synthesis in hydrophobic environment without the need of organic solvents. In addition, the structure of the products obtained can be controlled at the atomic scale, a property essential for the development of efficient nanoelectronics components for example. The polymerization of polypyrrole has been observed within the confined cavity of SMA in an aqueous environment without the use of initiators.[20] Polypyrrole was specifically chosen because of its wide range of applications including high conductivity or capacity for energy storage. The UV-Vis spectra for pyrrole polymerization in SMA template initially showed a shoulder at 310 nm corresponding to pyrrole oligomers followed by the development of a peak at 470 nm corresponding to the growth of polypyrrole within the template.[20] It is important to note that, in the absence of a catalyst in the SMA template, the shoulder corresponding to polypyrrole only appears after a month indicating that it takes a significant amount of time for the pyrrole to polymerize, when the polymerization is linked solely to confinement effect.[20] The hydrophobic cavity provided by the SMA template was able to generate the confinement effect and hence promote pyrrole polymerization that is not favourable in the bulk. Moreover, the increased catalytic capabilities of the SMA template with embedded platinum nanoparticles (~2.5nm) in the hydrophobic cavities has been observed to reduce the start of the polymerization time from approximately 32 days to 8 days.[3] Hence, to characterize the potential of Au as a catalytic center for the newly developed nanoreactors, the catalytic efficiency of SMA template with embedded gold crystals and clusters on pyrrole polymerization was monitored and can be observed in Figure 38. The start of the polymerization process is observed on day 2 of the experiment with an overall faster kinetics with gold nanoparticles as catalyst. This represents a significant improvement in terms of polymerization kinetics when compared to SMA templates alone (32 days) and Pt active centers nanoreactors (8 days). Therefore, gold is very catalytically active within the unsupported nanoreactors for pyrrole polymerization in hydrophobic environment. A very steep increase in the polymerization can be observed until day 13 (Figure 38b) after which it appears to slow down slightly with polymerization still continuing up to day 44. The complete kinetics characterization of the multistep reaction will be further discussed in Chapter 5.

A)

B)
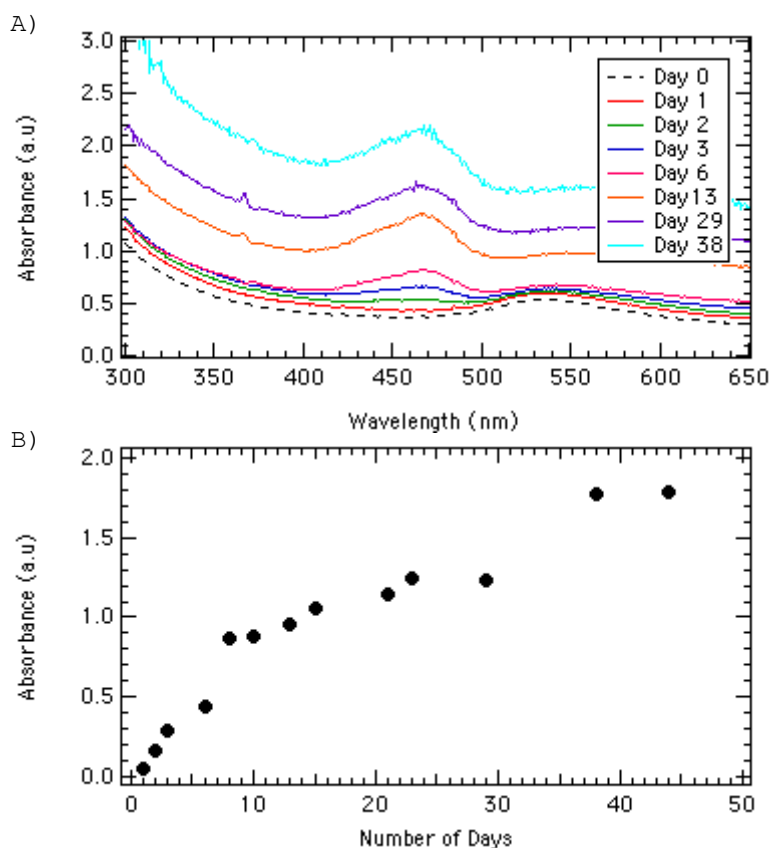
Figure 38: UV/Vis spectra of AuCl in 1% SMA solution stabilized followed by the addition of pyrrole a) strong peak at 470 nm develops on day 2 b) Percentage increase in pyrrole polymerization with respect to number of days at 470 nm.

3.4 Conclusion

In this chapter, we developed a method to characterize the growth of gold nanostructures including crystals and clusters by combining molecular modeling, IR, UV-Vis and HR-TEM. The growth of the nanoparticles was followed by UV-Vis using the different peaks generated by the clusters (300nm) and the crystals (560nm). Specifically, AuCl was found to interact with both the hydrophobic and the hydrophilic domains of SMA simultaneously, while producing gold crystals of 30-50nm in contact with the hydrophilic domain and gold clusters of 2-3 nm due to the size restriction of the hydrophobic cavity. The presence of 10-15% of monomethyl ester was found to greatly intensify the interaction of gold on the hydrophilic domain while producing larger gold crystals of 70-80 nm in diameter size and slightly smaller gold clusters with a diameter of 1.5-2.5 nm. Sonication

76

was found to effectively disrupt the whole self-assembly process and produce smaller gold crystals, 30 nm in size while completely eliminating the formation of gold clusters. This study not only allows the simultaneously interaction of gold with both the hydrophobic and the hydrophilic cavities, while using a very simple and environmentally friendly synthesis without reducing agents, but also explores different ways to control the interaction and growth on gold with the template. A mixture of gold crystals including (0001) hcp and (110) fcp were found in the presence of monomethyl ester, while just plain (0001) hcp crystals were obtained with SMA or SMA$_m$ sonicated samples.

The ability to control the interaction between gold and the polymeric template opens up many applications in drug delivery and nanoreactors development. In addition, the idea to control this interaction via other methods such as using a coupling agent, for example thiophene, will be explored in the next chapter. Thiophene is a hydrophobic molecule and has a sulfur known to form a very strong and stable bond with gold. It is expected that due to the hydrophobic nature of thiophene, it would force more gold to interact with the hydrophobic cavity producing more gold clusters. In this chapter, we were able to force majority of gold to interact with the hydrophilic domain. Developing a system that is able to do exactly the opposite will allow us to control exactly which active center gold interacts with opening tremendous potential for targeted drug delivery systems. Moreover various gold structures could also be isolated from the nanoreactor and used for diagnostic or therapeutic applications.

4. Role of Thiophene in mediating the gold nanoparticle growth within nanoreactors

Portions of this section will be submitted to a journal as: Shah V., Malardier-Jugroot C., Jugroot M. (2016) Chemistry of Materials.

Vishva Shah designed and performed the experiments and prepared the manuscript.

4.1 Introduction

Hybrid metal-polymer systems have shown great potential with their unique properties and many applications ranging from use in nano-devices such as nanowires, medical imaging agents, drug delivery agents to the development of an immunoassay.[57–59,133] The main advantage of combining the metal and polymer includes improved properties for applications in the fields including photonics[134] or electronics[135]. The advantages associated with the system arise due to the metallic composition of the material and various morphological features associated with the polymeric template.[57] Many studies have been conducted successfully combining metals and organic compounds for drug delivery systems or medical imaging applications such as using gold with hollow hybrid nanospheres for drug loading as well as a contrast agent in cancer-cell imaging.[57,61,62,134] Gold nanoparticles (GNPs) in particular have been very commonly used because of their unique properties and many promising applications in the field of biomedicine.[63–65,68,72]

Gold is inert in bulk, however, at the nanoscale its properties are altered and it becomes very reactive as summarized in Chapter 3. In addition, gold has been commonly used with thiols because of the well-known strong and stable interaction between the sulfur atom and gold.[136] Indeed, Brust-Schiffrin method, commonly used to produce metal nanoparticles, takes advantage of the strong interaction between sulfur and gold to produce thiol functionalized gold nanoparticles.[137] Moreover, self-assembled monolayers (SAM's) of thiols on gold have been extensively studied in many fields because of advantages including easy preparation or formation on objects of all sizes in many shapes such as nanowires or thin films. [138–140] Since SAM's can assemble on any surface in any size and shape, they provide the chemical functionality and thermodynamic stability for simple inorganic structures such as nanowires so that they could be used in a more complex biological system.[141] Thiophene is commonly used as the source of the sulfur atom that makes the thiol bond with gold as it is used in many technological applications including field effect transistors[141], solar cells[142], sensors[143] or synthesis of nanowires[144]. Thiophene and thiophene based materials are considered to be among the most versatile materials due to their ease of synthetic modification and environmental stability.[145] Thiophene based materials are known to have

unique chemical and physical properties including electronic, optical, redox, charge transport and self- assembly.[146]

Earlier work (Chapter 3) by our research group has shown the production of different morphologies of gold crystals and clusters upon reacting with a polymeric template, Poly (styrene-*alt* maleic acid) (SMA). SMA is an amphiphilic alternating copolymer, which self-assembles into highly organized nanostructures in neutral water.[77] The interaction between the polymeric template and gold has been discussed in detail in the previous chapter. Overall, SMA produces nanostructures in the form of a nanotube or a nanosheet, with a hydrophobic cavity of 3 nm in the middle and a hydrophilic domain on the outside.[78] Due to the small hydrophobic cavity produced in the nanostructures, confinement conditions are introduced promoting reactions that are otherwise not possible in the bulk. Gold chloride was found to interact with SMA on the hydrophilic domain without reducing agents, producing gold crystals of 30-50 nm and on the hydrophobic domain producing gold clusters of 2-3 nm simultaneously. The study was further extended, previously, to control this interaction by sonication or a slight modification of the polymer, SMA_m. SMA_m is structurally 85-90% identical to SMA with 10-15% of SMA functionalized with monomethyl ester. The characterization of the system revealed that the presence of monomethyl ester was able to enhance the interaction of gold on the hydrophilic domain while producing larger gold crystals up to 80 nm in size. Therefore, SMA_m was selected in this study as a template to enhance the control of the active center environment using thiophene as a mediating agent. The characterization of the nanoreactor active center was obtained by *ab intio* molecular modelling, high resolution transmission electron microscopy, UV-Vis and IR spectroscopy.

The aim of this chapter is to expand on the study conducted previously monitoring the interaction between SMA_m and gold to develop more stable methods for precise control of the interaction of gold with the hydrophilic or the hydrophobic domain. This paper attempts to control the interaction between SMA_m and gold by using a coupling agent, thiophene. The structure of thiophene can be observed in Figure 39. Upon the addition of thiophene in the system one of three interactions is expected (Figure 40): 1) Thiophene has been found to form a monolayer on top of a gold surface[147–149] and therefore it may also interact on the hydrophilic domain on top of the gold crystal and form a monolayer resulting in larger gold crystals 2) Thiophene itself is a hydrophobic molecule so it could force more gold to interact with the hydrophobic cavity producing a greater number of gold clusters while minimizing its interaction on the hydrophilic domain or 3) It could also give a mixture with some thiophene reacting in the hydrophobic cavity producing more gold clusters and some reacting on top of the gold crystal and forming a monolayer resulting in larger gold crystals.
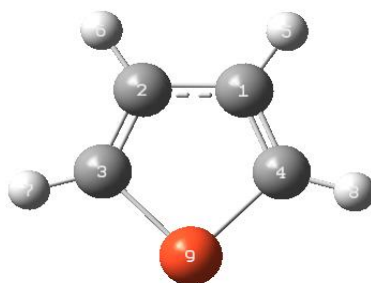
Figure 39: Chemical structure of thiophene obtained using density functional theory (DFT), B3LYP, 6-31G level of theory and visualized via Gaussview 4.1 (Orange atom represents the sulfur atom, Gray atoms represent carbons and White atoms represent hydrogens)

In order to determine how the system of SMA_m-gold responds to the addition of thiophene, we report the theoretical and experimental characterization of the interaction of thiophene with SMA_m-gold. To access all of the possibilities of the reactions three two-component systems and three three-component systems were analyzed as summarized in Table 3. All of the theoretical modelling between the two-component systems was done using *ab inito* methods. To further validate the computational results experimental characterization was done for each of the samples including UV-Vis spectroscopy to monitor the nanocrystal or cluster formation, IR spectroscopy to monitor whether gold is interacting with SMA_m or thiophene and TEM to observe the structures produced and to analyze them in terms of growth patterns as well as size. It is important to note that the interaction between the two component system, SMA-gold has already been studied and computational and experimental results pertaining to that system can be found in the previous chapter.

Table 3: Various two and three component systems analyzed in this chapter

Two-component systems	Three-component systems
SMA-gold	Addition of SMA to a gold-thiophene stabilized system
SMA-thiophene	Addition of gold to SMA-thiophene stabilized system
Thiophene-gold	Addition of thiophene to SMA-gold stabilized system

Thiophene interacts with gold on the hydrophilic
domain and forms a monolayer on top

Thiophene interacts with gold on the hydrophobic
domain and forces more gold to interact there and
form a greater number of gold clusters instead
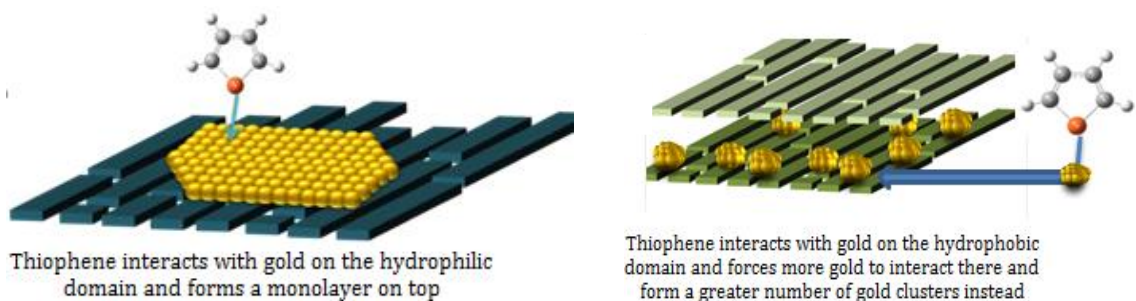
Figure 40: Schematic representation of the influence of the addition of thiophene
with SMA-gold system

4.2 Sample preparation and methods

Poly (styrene-*alt*-maleic acid*)* partial monomethyl ester SMA_m was solubilized to make 1% solution and then neutralized to pH 7 with NaOH as required. Gold(I) chloride (AuCl) and thiophene were used as received. For sample preparation, 5 mL of SMA_m at pH 7 was mixed with appropriate amounts of gold and thiophene in variable orders for various samples. The molar ratio of 1:1 between the metal atoms and the SMA monomer was maintained whereas thiophene was added in excess with respect to the volume available in the template formed by SMA_m. Unless otherwise specified, the sample preparation is the same with previous chapters and carried out at room temperature. The sample was then analyzed with various spectroscopic methods. (SMA_m), 350 kDA, Gold (I) chloride 99.9% and Thiophene 99.9% were purchased from Sigma Aldrich and used without further purification. The experimental characterization that was used was exactly the same as described in the previous chapter in section 3.2

4.3 Results and Discussion

4.3.1 Two Component Systems

4.3.1.1 Interaction between SMA_m and gold

The computational and experimental results for the interaction between SMA_m and gold can be found in an earlier chapter. Gold was found to favour interaction with the carboxylic acid groups of SMA_m compared to the styrene group with an interaction energy of -226.07 kJ/mol. The presence of monomethyl ester intensified the interaction of SMA with gold on the hydrophilic domain producing larger gold crystals corresponding to a UV-Vis peak at 547 nm, and minimized the interaction of gold in the hydrophobic cavity producing slightly

smaller gold clusters observed as a small 300 nm peak in the UV/Vis spectra. It was also discovered that the main reason for the intensified interaction on the hydrophilic domain was the interaction of gold with two oxygen atoms instead of one as was modelled and shown through molecular orbitals analysis. The results were also confirmed through IR spectroscopy showing two small peaks at 1963 cm^{-1} and 2157 cm^{-1} representing stronger interaction between the carboxylic acid group from SMA$_m$ and gold.

4.3.1.2 Interaction between thiophene and gold

The optimized structures of thiophene with gold can be observed in Figure 41. Typical distance between gold and chloride optimized with the same level of theory, functional and basis set for comparison was found to be 2.37 Å (not shown in the figure). The distance between the gold-chloride and gold-sulfur can be seen to remain constant. Thiophene is found to form clusters around gold with the interaction energy of -1280.46 kJ/mol suggesting a very favourable system (Figure 41b). Natural bond orbital analysis of the individual system revealed that electrons from valence 5d and 6s for gold, 3p for chlorine and 2p from carbons were involved in the gold-thiophene interaction. The interaction energy was calculated as follows:

$$E_{int} = E_{complex} - (E_{AuCl} + 3 * E_{thiophene}) \qquad \text{Equation (48)}$$

It is possible, however, that thiophene chooses to interact with itself and instead form polythiophene in the hydrophobic cavity created by SMA$_m$ due to the confinement effect. The modelling of polythiophene with gold was not performed as it would be computationally too expensive due to multiple gold atoms being involved. In general, as discussed above, it can be concluded that thiophene would interact with gold very strongly with the gold either forming a monolayer on top of the gold crystal (Figure 40a) or by forcing more gold to interact with the hydrophobic cavity to form more gold clusters (Figure 40b). One of the other possibilities is the formation of polythiophene (Figure 41c) in the hydrophobic cavity as was observed with polypyrrole earlier [20] Experimental characterization was not carried out for this sample since thiophene itself is very hydrophobic and does not dissolve with gold salt.
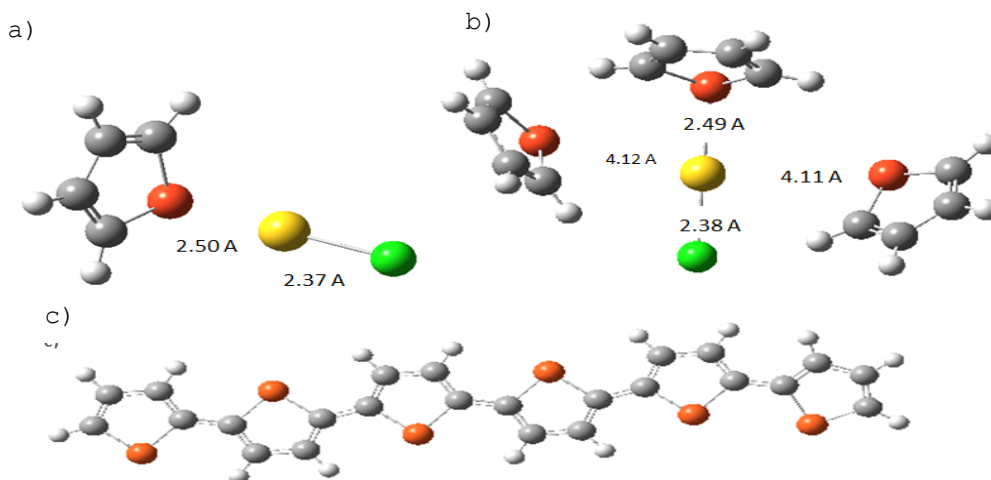
Figure 41: Optimized structures of a) thiophene with gold chloride b) three thiophene molecules with one gold chloride showing the cluster formation with DFT-B3LYP-LANL2DZ c) Poly-thiophene with DFT-B3LYP-6-31G

4.3.1.3 Interaction between SMA_m and thiophene

The structure of thiophene is very similar to pyrrole which has been found to interact with the hydrophobic cavity of SMA and hence, as thiophene is also hydrophobic similar behaviour is expected from thiophene.[20]

Molecular Modelling predictions

As described in the previous section thiophene is a hydrophobic molecule and therefore is expected to interact with the styrene present in SMA_m. When modelled through DFT with B3LYP hybrid functional and 6-31G basis set, this was not observed. Thiophene was instead found to prefer interaction with the carboxylic acid groups of the hydrophilic domain. For modelling, thiophene was placed beside both of the carboxylic acid groups present in the structure of SMA_m and beside the styrene group on both sides. When thiophene was placed beside the carboxylic acid with the mono-methyl ester (figure 42a), it was found to move away with the interaction energy of -56.74 kJ/mol whereas when thiophene was placed in a parallel direction beside the styrene group (figure 42b), it was found to orient itself in perpendicular fashion with the interaction energy of -4.21 kJ/mol. The interaction energy was calculated by equation 49:

$$E_{complex} - (E_{SMA_m} + E_{thiophene/pyrrole}) \qquad \text{Equation (49)}$$

As can be observed from the interaction energies obtained thiophene prefers interaction with the hydrophilic carboxylic acid groups. However, this was not what was expected since thiophene is hydrophobic and structurally very similar to pyrrole and pyrrole was found to polymerize inside SMA_m. The main reason associated with the discrepancy could be the missing solvent from the simulation. Since water is very dynamic, it introduces several minima in potential energy surface of the system. Therefore, addition of water or solvent would dramatically increase the computational time. In figure 42a, it can be observed that thiophene prefers interaction with the sodium and having the solvent water, present in the system may completely alter the result. Water will prefer interaction with the carboxylic acids and is expected to surround sodium preventing the thiophene from interacting with the hydrophilic component.

To further confirm this, simulations were performed with pyrrole which is known to polymerize within the hydrophobic cavity of SMA.[20] Similar trends were found with pyrrole when placed beside the same carboxylic acid site (Figure 42c) and the styrene group (Figure 42d). The interaction energy of pyrrole with the carboxylic acid was found to be -54.49 kJ/mol, whereas beside styrene was found to be -11.60 kJ/mol. The interaction energy of systems involving pyrrole were calculated by Equation 49 and show exactly the same trend with pyrrole moving slightly away in Figure 42c and turning perpendicular with respect to the styrene ring in Figure 42d. The interaction energy numbers in Table 4 show that pyrrole prefers interaction with the carboxylic acid, similar to thiophene results, however, careful experimental studies have shown that pyrrole interacts with the hydrophobic cavity of the SMA polymer template.[20] This further supports the fact that the solvent plays a crucial role in the interaction of thiophene or pyrrole with the hydrophobic or hydrophilic domain. The same trend is observed for all the other structures with the exception of between carboxylic acid 1 and 2 between pyrrole and thiophene. The slightly different interaction could be attributed to the presence of the extra hydrogen on pyrrole stabilizing its interaction with one of the oxygen's present on the carboxylic acid. It can also be concluded that the effect of the missing solvent is most likely giving rise to the discrepancy between the simulation and experimental results in the case of pyrrole and therefore, a similar effect is expected to play a significant role in the case of thiophene. Therefore, a complete study on the influence of water will be performed including the implicit and explicit solvent models and will be included in a further study.
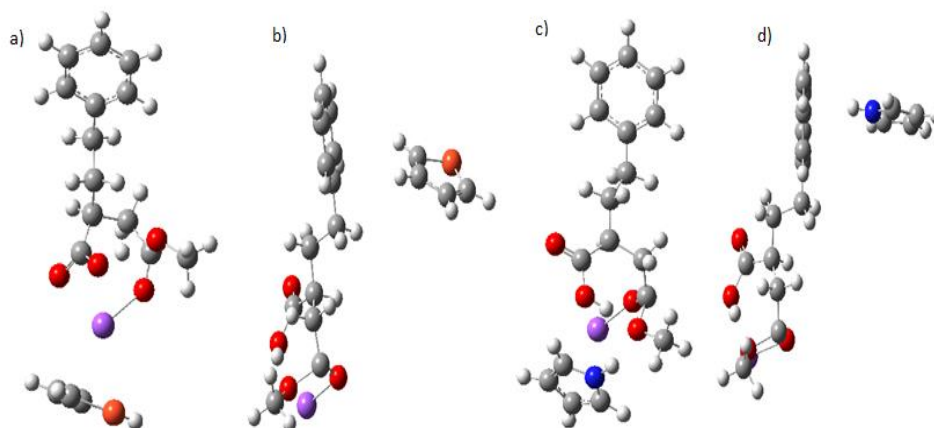
Figure 42: Optimized structures by DFT-B3LYP-6-31G of a) thiophene with SMA$_m$ placed beside COOH with monomethyl ester b) thiophene with SMA$_m$ placed beside styrene group in parallel orientation c) pyrrole with SMA$_m$ placed beside COOH with monomethyl ester d) pyrrole with SMA$_m$ placed beside styrene group in parallel orientation

Table 4: Interaction energy values for optimized molecule for thiophene placed around SMA$_m$ at various locations

	Thiophene (kJ/mol)	Pyrrole (kJ/mol)
Placed beside carboxylic acid 1 (not methyl ester) of SMA$_m$	-43.0	-94.0
Placed beside carboxylic acid 2 (methyl ester) of SMA$_m$	-56.7	-54.5
Placed beside styrene on side 1	-4.2	-11.6
Placed beside styrene on side 2	-2.4	-9.2

Experimental Characterization

Successful characterization of the gold-SMA system with the identification of the peaks corresponding to the growth of the crystals and clusters has been conducted previously using UV-Vis. Therefore, experimental characterization of SMA$_m$ with thiophene was done via UV-vis spectroscopy. For controls, first UV-vis spectra were obtained for SMA$_m$ and thiophene individually (complementary

information) with their respective peaks at 258 nm and 272 nm. A weak shoulder for poly-thiophene was also observed at 370 nm suggesting the presence of polythiophene. When thiophene and SMA_m were mixed, the UV-vis spectra (Figure 43) showed a peak at 258 nm representing SMA_m as observed in many earlier studies and a very small shoulder was observed at 369 nm suggesting the presence of polythiophene. The sample was monitored over 45 days and the equilibrium was reached at day 12 when the sample changes from cloudy to clear. Overall, UV-Vis spectra proved the presence of polythiophene, supporting the fact that thiophene indeed is more likely to interact with the hydrophobic cavity of SMA_m. Determining the properties associated with two component systems is crucial before understanding the three component systems due to the very complex interactions occurring in the system.
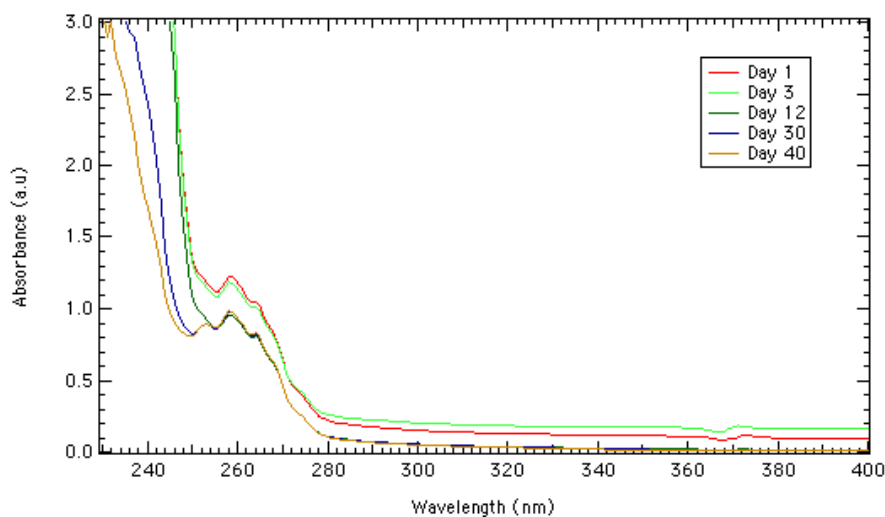
Figure 43: UV/Vis spectra for thiophene in 1% SMA_m solution. A peak at 258nm develops until day 14 and then stays the same.

4.3.2 Three Component Systems

Three component systems involving SMA_m, thiophene and gold can be computationally very expensive due to the size of the molecule involving many atoms and complex electronic structures. The study will encounter multiple minima on the potential energy surface of the polymer interacting with two free molecules (gold and thiophene) and would require a statistical dynamic analysis of the system to characterize and obtain an accurate conformation. Therefore, computational characterization of the three component system was not performed; however, experimental results will be discussed for the following three component systems including UV/Vis, IR and TEM. The results obtained from modelling two

component systems would be used to predict the properties and provide greater support for the experimental results for the three component systems.

4.3.2.1 Interaction between gold and thiophene (stabilized for 2 days) followed by the addition of SMA$_m$

To monitor the interaction between all three components, SMA$_m$, thiophene and gold were mixed in different orders which allowed the determination of any difference in terms of the structural formation. In this case, thiophene and gold were first mixed and stabilized for two days and then SMA$_m$ was added. 50 µl of thiophene was added to gold and left for two days until the solution mixed properly then 3mL 1% wt% SMA$_m$ solution was added and monitored over few days to observe the Au crystal and cluster growth. The UV-vis spectra for these interactions can be observed in Figure 44 showing a peak at 547nm representing the formation of gold crystals and a peak at 258 nm representing SMA$_m$. Moreover, the gold peak is observed to rise until day 4 and then settle until day 45 with minor fluctuations. As predicted from the simulations in Figure 41 thiophene is expected to form clusters around gold forcing it to interact with the hydrophobic cavity minimizing the interaction of gold on the hydrophilic domain. The absence of any other peak on the UV-Vis suggests thiophene pulling gold inside the hydrophobic cavity formed by SMA$_m$. Moreover, the peak at 300 nm may still be present attaributing to the gold clusters but could not be observed clearly in Figure 44. The small intensity of the peak at 547 nm represents the minimal interaction between the hydrophilic domain of SMA$_m$ and gold. This becomes especially obvious when one compares the intensity of the peak to a previous study conducted just looking at pure SMA$_m$-gold. This confirms that thiophene is disrupting the system and competing for the gold by preventing the gold to interact with the hydrophilic domain of the SMA$_m$.
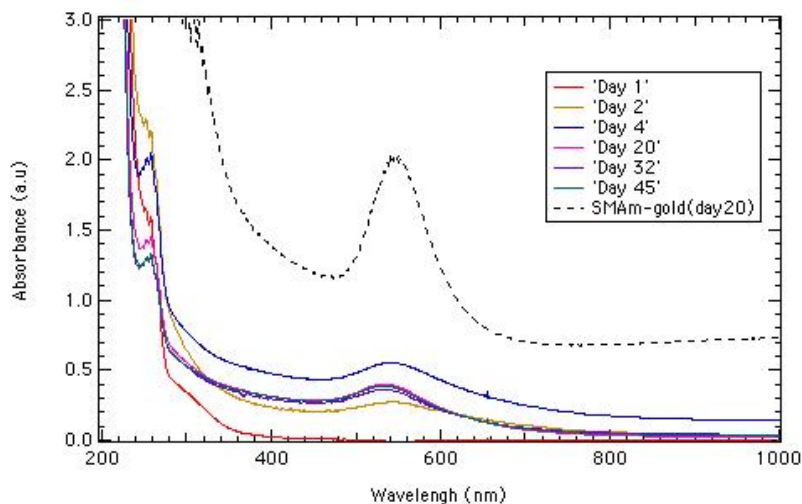
Figure 44: UV/Vis spectra of gold- thiophene (stabilized for 2 days) followed by the addition of 1% SMA_m solution. Peak at 547nm and at 258 nm develop until day 4 and then settle. SMA_{m-} gold graph (Day 20) added for comparison in terms of the intensity

      IR was performed to determine the presence of a thiol interaction between sulfur and gold. Typically the interaction between sulfur and gold is characterized by the presence or absence of sulfur and hydrogen interaction found in the range of 2560- 2590 cm^{-1}. [150] Aryal *et al.* have classified the presence of S-H group by a weak band at 2550 cm^{-1}.[150] It is essential to understand that the presence of S-H group suggests absence of S-Au. However, this may be hard to do this case, as a shoulder is already present at 2608 cm^{-1} in plain SMA as observed in Figure 28a. Hence, this shoulder cannot be used to conclusively determine the interaction of gold with sulfur. Moreover, in Chapter 3 it was determined that a high intensity peak at 1765 cm^{-1} represented a strong interaction between COOH of SMA_m and Au.[124,125] Hence, a weak intensity of the peak here would have indicated a weaker interaction of COOH with gold and, therefore, a stronger interaction with sulfur. Yet, a peak with a slight shift but strong intensity is still observed at 1720 cm^{-1}. Therefore, from the IR it cannot be concluded whether gold is, in this case interacting with the sulfur from thiophene or the carboxylic acids from SMA. It may be likely that we have a mixed interaction with some gold interacting with both of the active centers and further analyses through TEM is required to draw any conclusions.
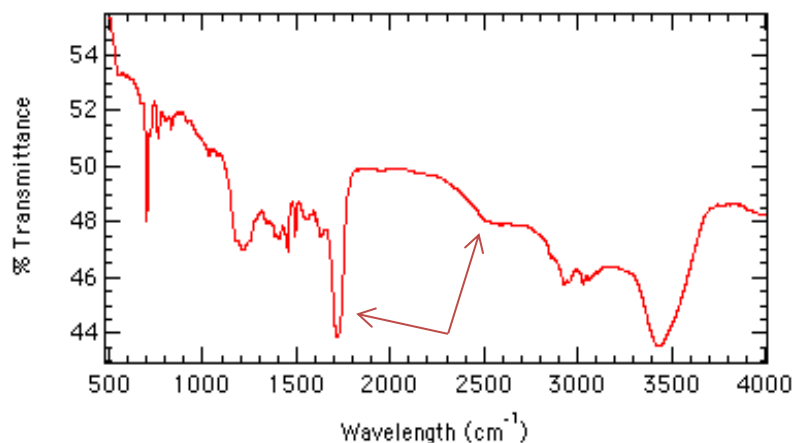
Figure 45: IR spectra for gold and thiophene (stabilized for two days) followed by the addition of 1% SMA_m solution. A shoulder present at 2506 cm^{-1} and a peak present at 1720 cm^{-1} suggests some gold may be interacting with thiophene while some still be interacting with the carboxylic acid groups

Furthermore, TEM images obtained also help support UV-Vis and IR results as a significant reduction in size (Figure 46a,b) and number (figure 46c) can be observed for gold crystals, from 70-80 nm as observed in previous study to 10-20 nm. The significant reduction in size of gold crystals representing the interaction of SMA_m and gold on the hydrophilic domain proves the disruption caused by thiophene. The crystal structures are also not very well defined proving the weaker interaction because of the presence of thiophene. It can also be seen that thiophene, indeed, did force the gold to interact with the hydrophobic domain since the percent of area occupied by gold clusters increases to 13% from 10% as observed in the previous study. The results were analyzed via calculating from three different TEM images and the percent error was determined to be approximately 1%. It is also likely that the percent area occupied in this study is actually higher since a very thick layer of clusters can be observed in Figure 46a,b suggesting that there may be a greater number of gold clusters present that simply could not be accounted for in this case. This smaller size and higher percent occupied by gold clusters could be due to the presence of thiophene forcing more gold to interact with the hydrophobic cavity and producing even smaller gold clusters. While, IR was inconclusive, TEM and UV-Vis strongly point towards thiophene forcing more gold to interact with the hydrophobic cavity and minimizing interaction on the hydrophilic domain.
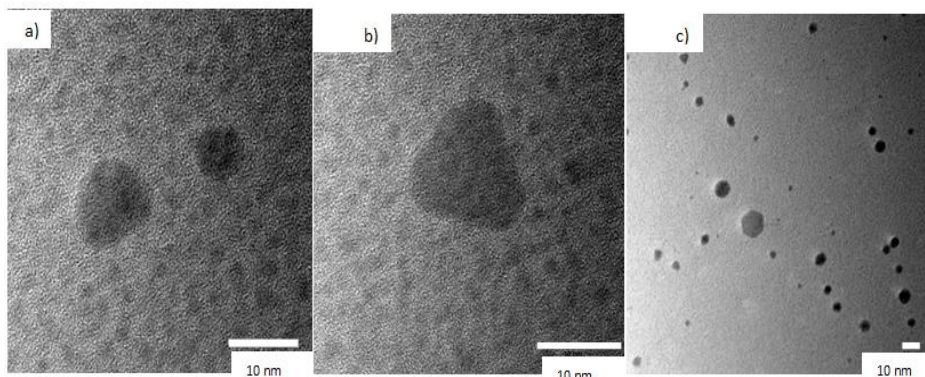
Figure 46: TEM images for gold and thiophene (stabilized for two days) followed by the addition of 1% SMA_m solution showing a/b) reduced gold crystal (10-20 nm) and cluster size (1-2 nm) c) Presence of a few number of gold crystals compared to the many gold clusters

4.3.2.2 Interaction between SMA_m and thiophene (stabilized for 12 days) followed by the addition of gold

To monitor this interaction, first a 1% wt SMA_m solution and thiophene were mixed and stabilized until the solution appeared clear as explained in section 3.1.3, then gold was added to characterize its interaction with the template once the SMA_m and thiophene structures had already stabilized. For this configuration, we could expect one of two things 1) Assuming all of the thiophene is interacting with the hydrophobic domain of SMA_m all of the gold would instead interact with the hydrophilic domain of SMA_m forming gold crystals exclusively or 2) thiophene would effectively compete with SMA_m for gold and instead would force most of the gold to interact with the hydrophobic cavity producing many gold clusters. Since the interaction energy predicted according to molecular simulations is -1280.46 and -226.07 kJ/mol for the interaction between thiophene-gold and SMA_m- gold, respectively, it is more likely that the second scenario would occur preventing the interaction of gold on the hydrophilic domain. The UV-Vis spectra produced for this interaction can be observed in Figure 47 showing one peak at 300 nm. It's important to note that a peak around 550 nm is not observed due to the interfering interaction between SMA_m and thiophene and stabilized structure. The peak at 300 nm has been discussed in the previous study and it was concluded that this peak corresponds to the isomers of gold clusters that are formed due to the strong binding between the sulfur atoms of polythiophene and gold atoms.[151]
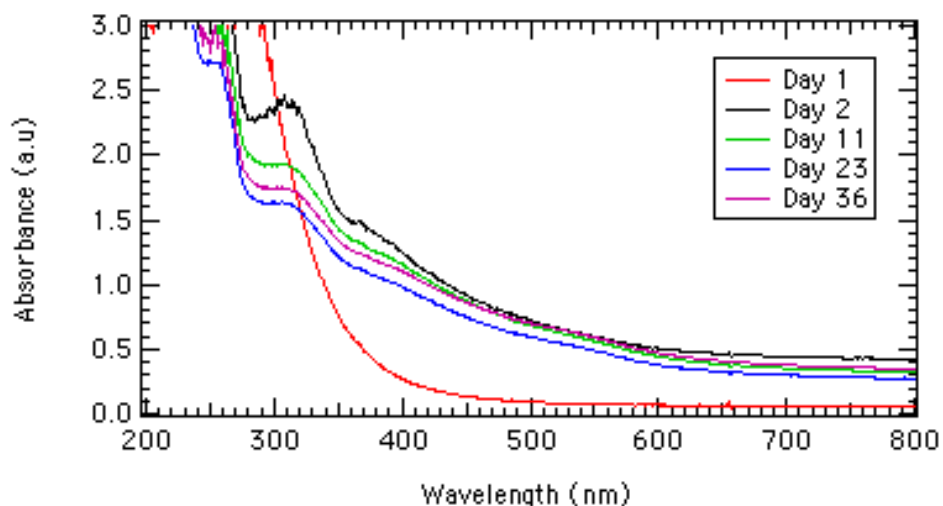
Figure 47: UV-Vis spectra for SMA_m and thiophene stabilized for 11 days (until the solution is clear) and then added gold chloride monitored over 36 days. A peak develops at 300 nm until day 2 and then settles
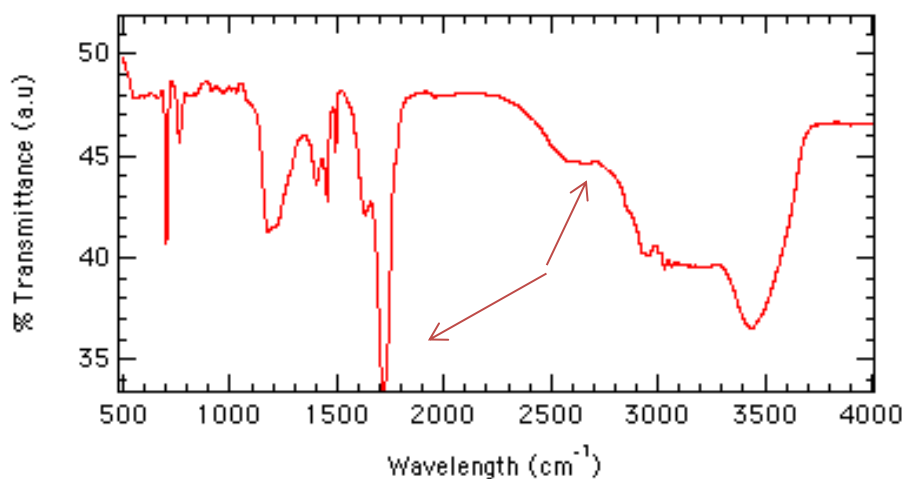
Figure 48: IR spectra for SMA_m and thiophene (stabilized for two days) followed by the addition of gold. A shoulder present at 2560 cm^{-1} and a peak present at 1706 cm^{-1} suggests some gold may be interacting with thiophene while some still be interacting with the carboxylic acid groups

To further confirm these results an IR spectrum (figure 48) was obtained. The IR spectrum obtained in Figure 48 looks very similar to the one observed in

Figure 45 with only a slight shift in the peak from 2506 cm^{-1} to 2560 cm^{-1} possibly suggesting a S-H bond and a shift from 1720 cm^{-1} to 1706 cm^{-1} representing the COOH interaction with gold.[124,125] While it may be likely that we have a S-Au interaction because of a shoulder present at 2531 cm^{-1}, this cannot be concluded as the same shoulder is present in plain SMA even in the absence of sulfur as observed in Figure 28a. The increased intensity of the peak at 1706 cm^{-1} suggests a strong interaction between COOH and Au instead. Therefore, from the IR it cannot be concluded whether gold is, in this case interacting with the sulfur from thiophene or the carboxylic acids from SMA. It may be likely that we have a mixed interaction with some gold interacting with both of the active centers and further analyses through TEM is required to draw any conclusions. It is essential to understand that while IR may be not conclusive UV-Vis results suggest a very strong interaction between thiophene and gold and it is very likely that thiophene is forcing more gold to interact with the hydrophobic cavity.

These results are confirmed with the TEM images, showing very few gold crystals (figure 49a), a reduction in the size for gold crystals 10-30 nm (figure 49b) and the number of gold clusters that are slightly larger in size from 1.5-3 nm (figure 49c). All of the TEM images also support the UV-Vis spectra suggesting an even stronger interaction between thiophene and gold. Overall, thiophene was able to minimize the interaction between carboxylic acid from SMA$_m$ and gold even more as proven by the total absence of a peak at 550 nm on UV-Vis, and TEM images showing very few smaller gold crystals. Even though gold clusters were found to be slightly larger, a change was not observed in terms of density of clusters (13%). The results were analyzed via calculating from three different TEM images and the percent error was determined to be approximately 1%. This once again could be due to the layering of gold clusters.
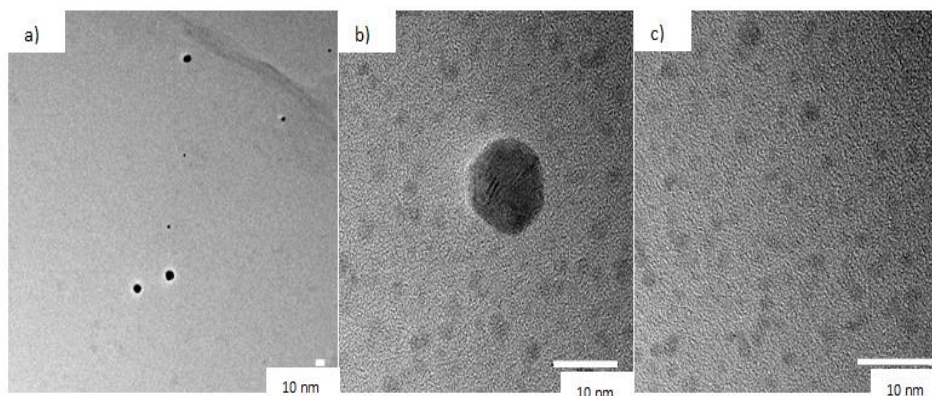
Figure 49: TEM imaged for SMA$_m$ and thiophene (stabilized for 12 days) followed by the addition of gold chloride showing a) very minimal number of gold crystals b) reduction in the size of gold crystals to approximately 10-30 nm c) the many gold clusters of 1.5-3 nm in diameter

4.3.2.3 Interaction between SMA$_m$ and gold (stabilized for 12 days) followed by the addition of thiophene

The interaction between SMA$_m$ and gold was analyzed in a previous study and the peak intensity at 547 nm on day 31 was observed to slowly start decreasing. This is the main reason the interaction between SMA$_m$ and gold was stabilized for 31 days before the addition of thiophene. Since SMA$_m$ and gold are being mixed and stabilized before the addition of thiophene, a very strong interaction between the carboxylic acid from SMA$_m$ and gold is expected. Indeed, as observed in Figure 50, thiophene was not able to disrupt the stable interaction between SMA$_m$ and gold. The UV-Vis spectra looks very similar to plain SMA$_m$ and gold with the same intensity for the peak at 547 nm representing the formation of gold crystals and at 300 nm representing the formation of gold clusters. A shift, however, is observed for the first time from 547 to 567 nm and could be due to formation of even larger gold crystals due to their interaction with thiophene as suggested in the figure 44. The previous three component systems emphasized the disruption of the SMA$_m$ (COOH) and gold interaction by thiophene forcing more gold to interact with the hydrophobic cavity and minimizing the formation of gold crystals. However, when thiophene is added stabilization of SMA$_m$-gold system, the interaction between SMA and gold seems unaltered. To further confirm that carboxylic acid is interacting with gold very strongly, IR spectroscopy (figure 51) was carried out. Figure 51, looks very similar to the two IR figures (Figure 45 and 48) observed earlier and was therefore not conclusive once again generating a need for TEM images. The slight shift in the IR peaks could be due to the altered environment of the sample.
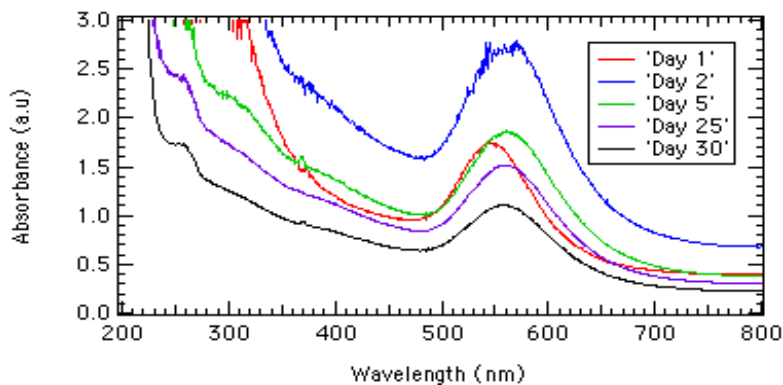
Figure 50: UV/Vis spectra of SMA$_m$ with gold (stabilized for 12 days) followed by the addition of thiophene showing a peak at 260 nm for SMA$_m$, 567 nm for SMA$_m$-gold on the hydrophilic domain and a weak shoulder at 300 nm for gold clusters on the hydrophobic cavity
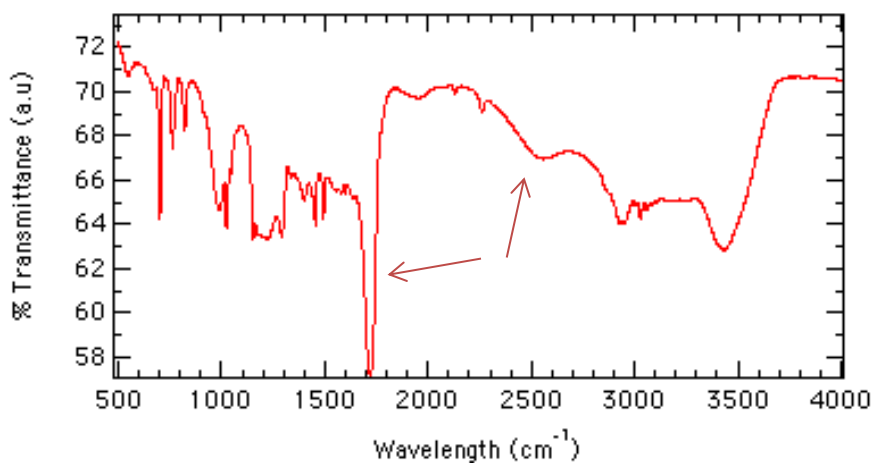
Figure 51: IR spectra for SMA$_m$ with gold (stabilized for 12 days) followed by the addition of thiophene. A shoulder present at 2510 cm^{-1} and a peak present at 1710 cm^{-1} suggests some gold may be interacting with thiophene while some still be interacting with the carboxylic acid groups

The results were further confirmed by HR-TEM characterization. Indeed, a good dispersion of gold crystals was observed (Figure 52a) with sizes between 60-100 nm. Therefore, thiophene was not able to affect the interaction on the hydrophilic domain in this case whereas it still increased the amount of gold clusters in the hydrophobic domain (Figure 52c) with a percent occupied of 12% compared to 10% for pure SMA_m. The results were analyzed via calculating from three different TEM images and the percent error was determined to be approximately 1%. The size of gold clusters was also very variable with most being under 2 nm in size. Note that the size never increases to more than 3 nm due to the size restrictions imposed by the hydrophobic cavity. It is also important to note that gold crystals along with increased size also have a more definite shape and structure of (0001) hexagonal close packing (hcp) for the big crystals (Figure 52b). Comparatively, as discussed in the previous study (Chapter 3) gold crystals without the addition of thiophene, were found to be larger around 80 nm showing a mixture of both (110) face centered cubic (fcc) and (0001) hcp. Lastly, the peak shift in the UV-Vis curve could be due to the thiophene layer created on top as observed in Figure 52b. Elemental analysis was attempted to determine the major compound in that layer but due to the very high composition of the copper from the grid and gold in the crystal it could not be detected. Overall, it can be concluded that when SMA_m and gold are mixed and stabilized first thiophene is unable to interrupt their interaction and instead interacts with the system in two ways either by forming more gold clusters in the hydrophobic cavity or by forming a layer on top of the gold crystal itself resulting in even larger gold crystals resulting in a peak shift on UV-vis curve.
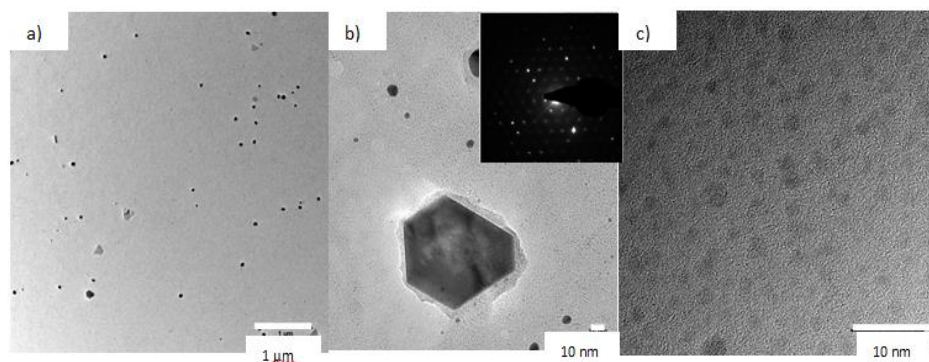
Figure 52: TEM images for SMA_m with gold (stabilized for 12 days) followed by the addition of thiophene showing a) the dispersion of gold crystals b) the variable size of gold crystals and possible layering of thiophene on gold crystals c) dispersion of gold clusters, variable in size most less than 2 nm

4.4 Conclusion

Thiophene was successfully able to control the interaction between SMA and gold by acting as a coupling agent, preferring interaction of gold with the hydrophobic cavity and minimizing its interaction on the hydrophilic domain of the polymeric template. When thiophene was stabilized with either gold or SMA before adding the third component it was found to reduce (from 70-80 nm to 10-20 nm) or completely eliminate the production of gold crystals on the hydrophilic domain. It was simultaneously also able to promote the formation of gold clusters (from 10% to 13% area occupied) without causing a size change due to the size restriction associated with the hydrophobic cavity. Contrary, when SMA and gold were mixed first before the addition of thiophene, gold crystals were much larger with a well-defined shape and (0001) hcp crystal structure. Thiophene in this case, since added later was not able to influence the interaction of SMA-gold on the hydrophilic domain to a great extent while still promoting the formation of more gold clusters from 10% to 12% in terms of area occupied. While IR could not provide conclusive results for this study, UV-Vis and TEM results were sufficient to provide proof for the different scenarios and suggested a strong interaction between thiophene and gold when that interaction was stabilized first. This study offers another level of control on the interaction between the polymer and gold earlier controlled by modifying the nature of the polymer and sonication as discussed in an earlier study. The whole nanotemplate with gold structures offers tremendous potential for applications due to its unique properties. The next chapter explores enhanced catalytic capabilities of these nanoreactors demonstrated through rapid environmentally friendly polymerization of pyrrole within the hydrophobic cavity.

5. Enhanced pyrrole polymerization by mediating the metallic active centers within the nanoreactors

5.1 Introduction

Polypyrrole (PPy) has been well known due to its promising conductive properties that can be applied to develop new technologies including its use as a potential vehicle for drug delivery, catalyst support for fuel cells and use for artificial muscles.[115,152] Some of the other applications for PPy include its applications in light emitting diodes (LED) and displays, charge dissipating films and volatile organic light sensors. The polymerization of pyrrole involves complex chemical reactions including oxidation, deprotonation and crosslinking.[152] The common feature in all of the conducting polymers includes the polyconjugation in the π-system of their backbone.[152] The many applications of polypyrrole can be attributed to its good electrical conductivity, environmental stability, easy synthesis and water soluble monomers. The conducting polymers are of a great interest to the scientific community as they have proven to be promising electrode materials for energy storage devices, electrocatalysts and biosensors, photoluminescent and electroluminescent materials, gas separating membranes, electromagnetic shields and even drug delivery applications.[153,154]

Polypyrrole has also been used for biological applications since the early nineties when it was used as a cell growth substrate for *in vitro* culture models.[154] The implantation of PPy has also been studied using animal models.[155] Researchers have demonstrated that using PPy modified indium oxide when used as a substrate for the chromaffin cells, cells that secrete neurotransitters, improves their secretory function.[156] Some other researchers have also demonstrated incorporating whole cells into the PPy matrix with a minimal amount of damage occurring during synthesis as a result of electroporation or other oxidative damage.[157] It was also found that antigens remained intact after inclusion in PPy raising the possibility of applications for use in blood group immune biosensors.[157] Moreover, advantages over bare gold was found for PPy including preferential cell growth and resolution at lower cell numbers due to better cell-material integration.[158] Research is still being conducted on alternative methods to increase the biocompatibility of PPy including developing other methods without the use of any harsh chemicals in a soluble form. [159,160] The synthesis of PPy traditionally produced an insoluble powder limiting its applications requiring polymerization in the presence of polyanions, resulting in the formation of a ternary complex and a colloidal form of PPy.[161] One of the other methods for obtaining solvent-soluble PPy is to use dopants such as dodecyl benzene sulfonic acid.[161] In general, PPy has traditionally always been synthesized chemically or electrochemically.[152] Chemical synthesis typically includes mixing a strong oxidizing agent with a monomer solution whereas electrochemical synthesis involves a positively polarized electrode proceeds via a condensation reaction between the monomer units.[154] The specific

method for synthesis is chosen based on the requirements of the experiment. For example, chemical initiation by oxidative agents might be applied if a large amount of PPy is required for the experiment, whereas electrochemical oxidation generally gives higher conductivity and better control over the structural and electrical properties of the product. PPy synthesis can also use halogens and organic compounds as electron acceptors.[152] The yield and conductivity of PPy are affected by a variety of factors including choice of solvent, chemical oxidants, initial concentration of pyrrole, duration and temperature of the reaction.[152] The various synthesis strategies for pyrrole are discussed in detail below:

Synthesis of PPy by Chemical Oxidation

Although electrodeposition is sometimes preferred for the synthesis, due to its wide choice of dopants and relatively easy synthesis, chemical oxidation methods are still preferred due to cost effectiveness, large amounts of products and no restriction in terms of the required electrode shape.[162] Chemical polymerization typically requires oxidative agents such as $(NH_4)_2S_2O_8$. H_2O_2 and transition metals such as Fe^{3+}, Ag^+, I_2, Br_2 or Cu^{2+}.[163] The reaction usually begins with dispersing pyrrole monomers in appropriate solvent followed by slow, drop-wise addition of dopant-oxidant in the appropriate solvent. The mixture is then left undisturbed for the polymerization to occur. The properties of the conducting polymer can be influenced by different ratios, dopants, reaction time, and temperature.

Synthesis of PPy by Electrochemical Oxidation

In electrochemical oxidation the monomers of pyrrole are dissolved in a solvent such as acetonitrile, propylene carbonate or water with appropriate amounts of doping salts such as sodium dodecylsulfate (SDS). The monomers are then oxidized at a moderately positive potential. Diaz *et al.,* proposed the most commonly accepted mechanism for the polymerization and stated that upon oxidation pyrrole loses one electron and becomes a radical cation.[164] The stable radical cations are then coupled with monomers in the solution where two protons are eliminated.[164] This method however also has its limitations including the maintenance of charge balance in the solution and is dependent on factors including the solvent, electrolyte, pH and applied potential. The production of PPy with targeted properties, hence, requires a strong understanding of each of the individual components.

Template mediated synthesis of PPy

Due to the presence of harsh chemical agents and complicated synthesis strategies in both the chemical and electrochemical oxidation, more research is still required to develop simpler methods for synthesis that are completely bio-compatible. Developing alternative strategies that offer more control on the

properties of pyrrole as well as polymeric morphologies remains under investigation. Template mediated synthesis provides an opportunity to manipulate the structural dimensions of the resulting polymeric architectures. For example, Martin[165] and Joo[166] et al., have synthesized polypyrrole nanostructures including tubes and wires inside the template pores ensuring that morphology follows the shape of the template. The template is then dissolved or removed leaving the material with the shape of the pores of the host membrane.[167,168] Template-directed synthesis allows for a convenient technology that provides an opportunity to manipulate the length and morphology of the products along with improved properties. This study utilizes template mediated synthesis for the synthesis of PPy and attempts to improve on the methods investigated by Xia *et al* and Groves *et al*.

To investigate or develop alternative synthesis methods for PPy, it is essential to understand the fundamentals of the chemical reaction and to determine the exact amount of activation energy that is required for the polymerization to start. Very minute alterations in terms of the synthesis strategies could result in development of completely different nanostructures. For example, Joo *et al*., used electrochemical oxidation for the PPy synthesis in Al_2O_3 templates with dopant CSA[166]. The resulting polymer was found to form PPy-nanotubes or PPy-nanowires depending on reaction time.[166] If the reaction was conducted for 2 minutes, nanowires (20 nm in thickness) were obtained whereas if it was conducted for 15- 40 minutes nanotubes were obtained. Hence, the development of altered synthesis methods required a deep understanding of the interactions at the atomic scale.

To study the polymerization of pyrrole, one can look at two different aspects including the thermodynamics and kinetics. Thermodynamics deals with whether a reaction would occur or not (i.e. favorable or unfavourable) based on the free energy whereas kinetics deals with the activation energy that needs to be overcome for the reaction to start. The difference between the kinetics and thermodynamics is described in Figure 53. The reaction is thermodynamically favourable when the gibbs free energy (difference between the reactant and the products) is negative and unfavourable when it is positive. Comparatively, the activation energy is the energy difference between the reactants and the high energy intermediate. The reaction for pyrrole polymerization without a template can be observed in Figure 53c where the ΔG value is positive meaning that the reaction is not thermodynamically favorable, but by placing it within the template and inducing the spatial confinement effect the reaction becomes favourable. Xia *et al*., conducted DFT simulations to determine that the polymerization of pyrrole is thermodynamically not favorable until a hexamer is formed.[115] The author also furthered the study by studying the effect of altering the template, the size of confinement and contact with water on the polymerization. [20] It was found that altering the template itself still results in polymerization making the polymerization a thermodynamic reaction instead of kinetic, as it deals with the question of the reaction occurring or not occurring instead of the speed at which the reaction

occurs by lowering the activation energy. [20] Pyrrole polymerization was also found to take over a month to begin in an empty polymeric template without a catalyst, SMA detailed earlier, whereas in the presence of platinum nanostructures the amount of time was reduced to eight days.[16] This study focuses on the kinetics of the reaction and attempts to investigate the different reaction rates and determines the exact activation energy of pyrrole polymerization in the presence of gold and platinum nanostructures at different temperatures. By adding metal catalysts within the template, we are reducing the activation energy required, resulting in faster polymerization of pyrrole. Similar studies have been carried out in the past by various researchers attempting to study the kinetics of polypyrrole due to fast oxidation via NMR spectroscopy using ferric chloride as an oxidant.[169] They conducted the first-order kinetics study as a function of temperature and determined the activation energy to be around 79 kJ/mol for the initiation step and 73 KJ/mol for the propagation step.[169]
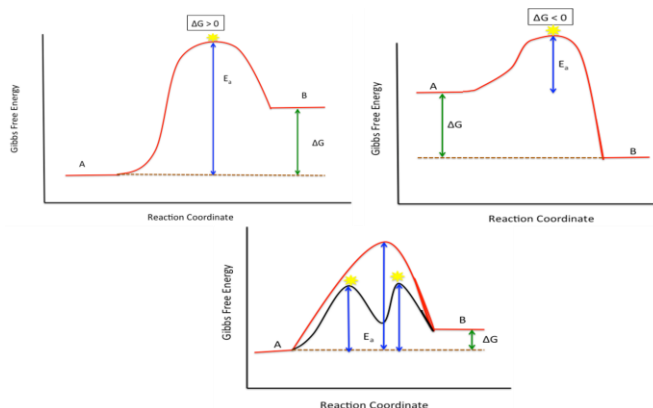
Figure 53- a) Reaction with a positive Gibbs free energy that is thermodynamically not favourable requiring high activation energy b) Reaction with a negative Gibbs free energy that is thermodynamically favourable requiring relatively lower high activation energy c) Pyrrole polymerization reaction depicted that is thermodynamically (green) not favourable where the activation energy (blue) can be reduced by using the effect of confinement to study the kinetics at play in this reaction

Along with studying the kinetics of the chemical reaction, it is essential to maximize a system's catalytic capabilities. It has been found that metal catalysts, with higher order crystallographic facets are more active provided that they have more edges and corner sites.[170] Chen et al., found that slowing the reaction rate induces the growth of the (111) crystal face of platinum structures leading to the formation of anisotropic structures.[171] Hence, the speed of reduction and formation of various nanostructures affects the structural morphology of the nanostructures.

Macromolecular crowding or spatial confinement has been observed to affect the reaction rates.[172] This increase in reaction rate due to confinement could be attributed to the reduced diffusion rate of the molecules and an increase in thermodynamic activities. The confinement produced by the polymeric template, similar to this system, is expected to increase the rate of reaction that is slow and involve transition states and slow down the rate of reaction with fast diffusion-limited association reactions.[172] Moreover, increasing temperature or providing the system with external energy is also expected to increase the reaction rate.

This chapter details a bio-compatible facile synthesis method for enhanced pyrrole polymerization when compared to plain SMA polymeric template or in the presence of metal catalyst. Specifically, this chapter investigates the different reaction rates and determines the exact activation energy of pyrrole polymerization in the presence of gold and platinum nanostructures at different temperatures. The goal of this chapter is to combine the results from previous chapter to study the kinetics of polymerization of pyrrole in various systems including SMA_m, SMA_m-gold (sonication), SMA_m-gold (no sonication), SMA_m-platinum and SMA_m-gold-platinum. In Chapter 3, it was observed that gold nanostructures greatly enhance the rate of pyrrole polymerization by lowering the activation energy and affecting the reaction rate. Similar effect has also been observed in the case of platinum nanostructures[16] and in plain SMA_m reactor as well[115]. Determining the activation energy associated with pyrrole polymerization allows us to analyze different ways to control the polymerization by using various metallic nanostructures within the nanoreactor. In the end, it would enable us to gain a deeper understanding toward the polymerization process and broaden the applications for polypyrrole nanosheets and nanorods.

5.2 Sample Preparation and methods

Poly (styrene-*alt*-maleic acid*)* partial monomethyl ester SMA_m was solubilized to make 0.1% w/w solution and then neutralized to pH 7 with NaOH as required. The results from previous chapters are combined to study the polymerization of pyrrole in various systems including SMA_m, SMA_m-gold (sonication), SMA_m-gold (no sonication), SMA_m-platinum, SMA_m-gold-platinum.

It was found earlier (Chapter 3) that external energy or sonication affects the gold nanocluster formation within the nanoreactor. Hence, the effect of external energy on pyrrole polymerization is also studied by providing the sample with external energy for 30 mins. The samples with gold and platinum nanoclusters were prepared according to the method described in section 3.2 and pyrrole was added in accordance with section 4.2. Overall, metals (gold or platinum) were received as used and added in a 1 to 1 ratio by weight to SMA_m whereas pyrrole was added in excess with respect to the volume available in the template formed by SMA_m.

Each sample was made in a replicate of four and maintained at different temperatures of 277K, 283K, 293K, 323K to study the effect of temperature on polymerization via UV-Vis. The data is then used to determine the reaction rate coefficient and activation energy via Arhenius plots. Pyrrole 99.9% was purchased from Sigma Aldrich and used without further purification. Further experimental characterization including TEM microscopy to study the shape and the size of the nanostructures formed would be explored in detail in a future study.

5.3 Results and Discussion

Pyrrole polymerization has been extensively studied in earlier studies due to many applications of polypyrrole in energy storage electrocatalysts and biosensors or drug delivery.[152,154] Various polymerization methods have been proposed and used, but most involve harsh chemicals and complex synthesis reactions.[152] Other researchers have also attempted to determine the activation energy of pyrrole polymerization.[169,173,174] Many researchers have used the radical coupling method for the formation of PPy and found the reaction to be first order with respect to pyrrole.[175,176] Planche et al. studied pyrrole disappearance by HPLC with various $FeCl_3$ concentrations and found the reaction to be first order with respect to pyrrole.[177] Similarly, Bjorklund also reported first order kinetics of the chemical oxidation of pyrrole by iron (III) chloride.[175]

The activation energy of pyrrole polymerization has been studied by various researchers under different conditions involving oxidants.[169,173,174] Tan et al., studied the polymerization of pyrrole in water and determined the activation energy to be 79 kJ/mol for the initial step and 73 kJ/mol for the propagation steps.[52] In this study pyrrole and $FeCl_3$ were added to D_2O and the depletion of pyrrole was measured through NMR.[169] Moreover, the activation energy for pyrrole polymerization in acetonitrile monitored via calorimetry was found to be 32 kJ/mol.[176] All of the methods used previously have used harsh chemicals or complex oxidation steps to study pyrrole polymerization. Hence, a novel completely bio-compatible system must be developed attempting to study the activation energy of pyrrole.

Easy, environmentally friendly synthesis of PPy was first suggested by Xia *et al.* who observed pyrrole polymerization after a month within the confined cavities of SMA_m.[20] This study also confirmed the influence of confinement on the thermodynamics of the reaction. Groves *et al.*, reported the same result with pyrrole polymerization within the plain SMA_m nanoreactor after 25 days.[16] They further extended the study by showing faster polymerization, observed after 8 days, due to the presence of platinum nanostructures. This study attempts to extend the results observed to systems including gold nanostructures as well as a mixture of gold and platinum nanostructures. The unique properties of gold at the nanoscale have been discussed in detail in earlier chapters. Platinum similarly has many applications and offers another alternative to develop efficient and tailored nanoreactors that mimic biosystems.[16] It is important to develop various methods to

control the nature and shape of active centers to optimize their surface area and catalytic efficiency.

5.3.1 Pyrrole polymerization observed by UV-Vis

A first order reaction can be defined as one where rate is determined by the variation of one concentration only. Pyrrole polymerization has been observed to be first-order by previous studies.[171-173] Consider any reaction where

$$A \rightarrow products$$
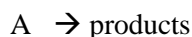
The initial concentration of the reacting substance A in g moles per litre can be represented by a and let x moles/litre of A decompose in time t. The rate of the reaction here at time t, proportional to the concentration of A at that instant, can be represented by a-x.

$$\frac{dx}{dt} \propto (a - x) \quad or \quad \frac{dx}{dt} = k(a - x) \qquad \text{Equation (50)}$$

Where dx/dt is called the reaction velocity and k is the proportionality constant also known as the first order velocity constant. After rearranging and calculating one gets equation (51) where I is the constant of integration

$$\frac{dx}{(a-x)} = k \, dt \text{ upon integration } -\ln(a - x) = kt + I \quad \text{Equation (51)}$$

When $t=0$ and $x=0$ equation (51) becomes $a= I$, which can be substituted back in the original concentration to obtain the kinetic equation for the first order reactions.

$$-\ln(a - x) = k \, t - \ln a \qquad \text{Equation (52)}$$

In some reactions, where the initial concentration is not known definitely due to the uncertaining in the time at which reaction starts, the above equation can be integrated and rewritten as:

$$k = \frac{2.303}{t} \, log \frac{c_1}{c_2} \qquad \text{Equation (53)}$$

Where c_1 and c_2 are molar concentrations of the reactant A at time t. As can be seen in the equation the value of k can be evaluated knowing the concentration of the reactant at different time intervals. In the previous chapters UV-Vis has been extensively used to monitor the intensity of the polymerization corresponding to the concentration. Hence knowing the intensity of growth which corresponds to the concentration from the UV-Vis can be used for the determination of the rate

constart, *k*. Graphically, when the equation is rearranged if resembles y=mx+b where *k* can be determined by the slope when ln (intensity) is plotted against *t*, time. The rate constants obtained at different temperatures can then be used into the Arrhenius equation where A is the pre-exponential factor for the reaction, R is the universal gas constant 8.3145J/mol K, and T is the temperature (in Kelvin). The units of the pre-exponential factor A are identical to those of the rate constant and can change depending on the order of the reaction.

$$k = Ae^{\frac{-E_a}{RT}} \text{ or } \ln k = lnA - \frac{E}{RT} \qquad \text{Equation (54)}$$

As observed in the above equations if lnk is plotted against 1/T, a straight line will be obtained and the slope value can easily be used for the calculation of the activation energy. Therefore, all of the samples after sample preparation were monitored via UV-Vis and follow the procedure described above for the determination of activation energy associated with pyrrole polymerization.

5.3.1.1 SMA$_m$ *pyrrole polymerization*

The samples were prepared according to section 5.2 and the data was analyzed as described above. First, the polymerization of pyrrole is explored within the confined conditions of SMA$_m$ at room temperature (293K), followed by altering the temperature to 277K, 283K, and 323K. At a 0.1% concentration as mentioned in the methods, polymerization was not observed at any of the temperatures implying that the concentration may be too low to detect on UV-Vis. Hence 1% SMA$_m$ solution was tested for this sample with pyrrole. Since the same confinement is present in all of the samples, the rate of reaction is simply expected to be directly proportional to temperature. The intensity of polymerization was monitored over time via UV-Vis and ln (intensity) was plotted against time. The graph resulted in a straight line and hence followed first order kinetics as predicted and observed by many researchers.[51] The formation of PPy was only observed at room temperature and all of the other temperatures resulted in no polymerization of pyrrole being observed. The polymerization of pyrrole at room temperature was observed upto 60 days and can be observed in Figure 54. The reason for which polymerization was not observed at any other temperatures could be due to a disruption in the self-assembly process responsible for the formation of nanoreactors. At lower temperatures, 277K and 283K, it is possible that that the system did not have enough energy due to lower macromolecular crowding not resulting in the formation of nanoreactors. It could also be possible that nanoreactors are formed but pyrrole does not have sufficient kinetic energy to overcome the activation energy barrier to start polymerizing. Comparatively, at higher temperatures, the exact opposite may be true implying that the system has too much kinetic energy not resulting in nanoreactor development and hence no pyrrole polymerization. Since polymerization was not observed at any other

temperatures, activation energy of this system could not be determined. This generates the need to optimize other systems with metal active centers that may further stabilize the system and encourage polymerization of pyrrole.

a)

b)
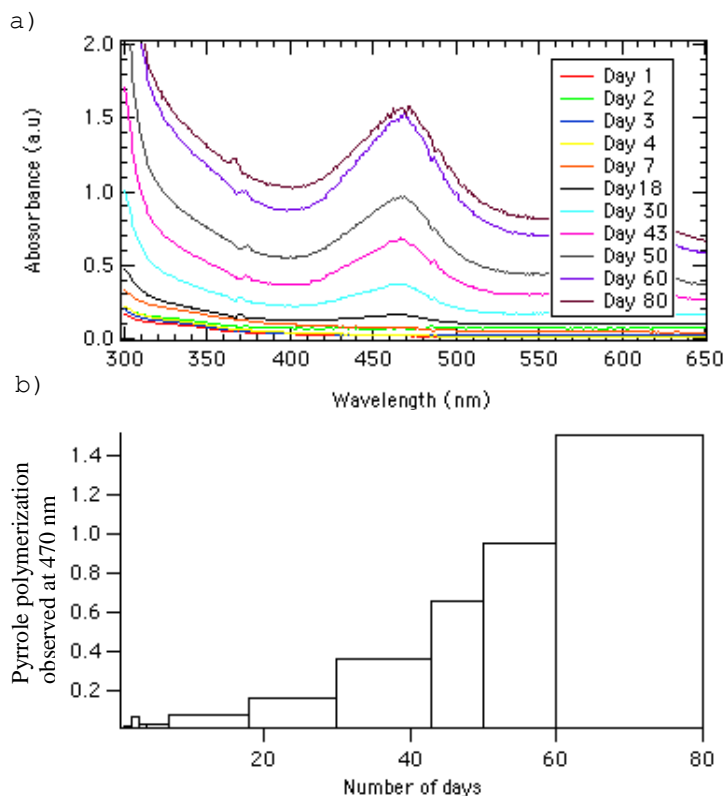
Figure 54: a) Pyrrole polymerization observed in plain SMA_m nanoreactor showing polymerization starting after 18 days upto 80 days b) Pyrrole polymerization observed at 470 nm as shown in a)

5.3.1.2 SMAm pyrrole polymerization with metal active centers

The presence of metals is expected to stabilize the system and enhance the rate of polymerization as observed earlier. Hence, 0.1% SMA_m solution is used and mixed with platinum before the addition of excess pyrrole. Polymerization was observed for all of the temperatures with increased reaction rate with temperature. To determine the rate of the reaction, ln (intensity) was plotted versus time in minutes. A sample graph for pyrrole polymerization in SMA_m-platinum system at 293K can be observed in Figure 55. The slope from this graph represents the rate constant, k value that can be used in the Arrhenius equation (equation 54) to determine the activation energy. Values of rate constants corresponding to all the temperatures were determined and an Arrhenius plot was then created by plotting

ln of the rate constants vs 1/temperature. The slope of the Arrhenius plot was used to determine the activation energy. The arhenius plots for all the systems with various metal nanostructures can be observed in Figure 56.
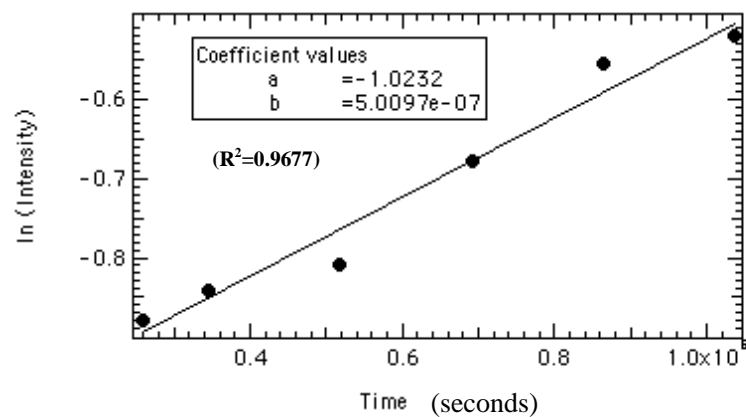
Figure 55: Determination of the rate constant of pyrrole polymerization in SMA_m - platinum nanoreactor as observed at 293K
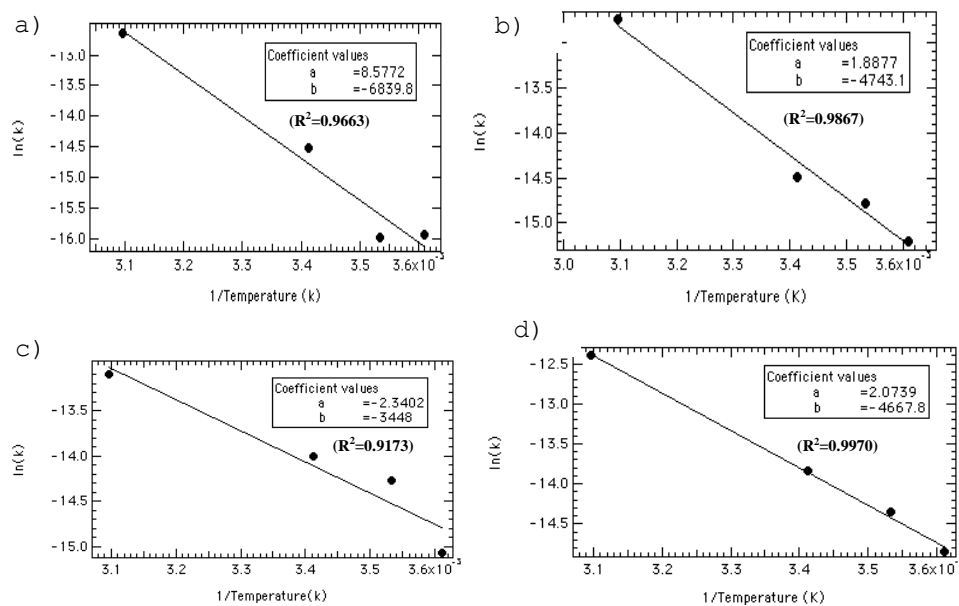
Figure 56: Arrhenius plots for pyrrole polymerization in a) SMA$_m$-platinum nanoreactor b) SMA$_m$-gold (no sonication) nanoreactor c) SMA$_m$-gold (sonication) nanoreactor d) SMA$_m$ -gold-platinum nanoreactor

The activation energy of pyrrole polymerization in various systems was determined to be 56.84 (+/- 7), kJ/mol 39.42 (+/- 3) kJ/mol, 28.65 (+/- 6) kJ/mol and 38.79 (+/- 2) kJ/mol for SMA$_m$-platinum, SMA$_m$-gold (no sonication), SMA$_m$-gold (sonication) and SMA$_m$ gold-platinum nanoreactor respectively. As observed from the activation energy numbers, the presence of any metal nanostructures within the polymeric template is found to stabilize the entire system and increase the rate of polymerization within the hydrophobic cavity. Moreover, since the analyses were only performed on one sample, it needs to be investigated further in the future. Furthermore, as discussed earlier, the activation energy associated with the polymerization of pyrrole can be further divided in two parts initiation and propagation.[165] In this system, the first few readings were ignored and only the energy associated with the propagation of the polymerization is calculated. The reaction mechanism for the polymerization in this system along with multiple samples for the determination of the same activation energy with greater accuracy will be conducted in the future.

5.3.1.3 Pyrrole polymerization within SMA$_m$-gold nanoreactors

The lowest activation energy, 28.65 kJ/mol, required for pyrrole polymerization to start was found to be in the SMA-gold system that has been sonicated for 30 mins. Sonicating the SMA$_m$-gold nanoreactor was found to alter the structure of the gold crystals, while forcing all of the gold to only interact with the hydrophilic domain in Chapter 3. This leaves the hydrophobic cavity completely open for pyrrole polymerization requiring the least amount of energy to start the polymerization. Comparatively, when the same sample has not been sonicated, without any external energy, the activation energy was found to increase to 39.42 kJ/mol. As observed in Chapter 3, this system is when we have a mixture of gold crystals and clusters. Since some of the space within the hydrophobic cavity is occupied by the formed gold clusters, pyrrole has to effectively compete for the same interaction. One of the other reasons for greater interaction energy required could be the reduced stability of the entire system due to the presence of both gold clusters and crystals discouraging pyrrole from entering the hydrophobic cavity. The altered crystal structure due to sonication of the sample was also discussed in chapter 3. It was found that sonication eliminates the formation of fcc crystals with the presence of only (0001) hcp plane crystals. The importance of crystal structure and its ability to impact the properties of a sample has also been discussed earlier. The elimination of fcc crystals with the presence of only hcp crystals could also have to do with the properties of this system when it is sonicated resulting in a lower activation energy.

5.3.1.4 Pyrrole polymerization within SMA$_m$-platinum nanoreactors

Comparatively, the activation energy of pyrrole polymerization in the SMA$_m$-platinum nanoreactor was observed to be significantly higher than gold, 56.84 kJ/mol. Mctaggart *et al*., has analyzed the formation of platinum nanostructures within the hydrophobic cavity of SMA$_m$ and found that no crystals and only clusters were present within the hydrophobic cavity. They found that platinum chloride preferentially concentrates within the hydrophobic nanodomains of the SMA$_m$ architectures with diameters of <3nm. Since only platinum clusters are present with all of the platinum interacting with the hydrophobic cavity, pyrrole effectively has to encounter greater competition for the same interaction. Although the specific crystal structure of platinum structures has not been analyzed, it could also effectively contribute towards the properties of this system resulting in a higher activation energy.

5.3.1.5 Pyrrole polymerization within SMA$_m$-gold-platinum nanoreactors

The interdependence of the confinement domain and active metal centers were explored by Mctaggart et al. This sample is prepared by individually preparing 1.5 mL of AuCl solution and 1.5 mL of PtCl$_2$ and combining the two after sonication. The UV-Vis spectra monitored was found to show two separate gold and platinum peaks indicating independent crystal growth. This suggests that

no exchange of metals occurs between the SMA_m-Pt and SMA_m-Au system. It appears in this system that gold is effectively only interacting with the hydrophilic domain or the surface of SMA_m, whereas platinum is solely interacting within the confined regions or the hydrophobic cavity. This system was also concluded to form very fast and stable bonds. Therefore it can be predicted that this system would have a lower activation energy compared to platinum but still higher than gold (sonicated). Since both gold crystals and platinum clusters are present in the same system the interaction energy is expected to be very similar to the SMA_m-gold non sonicated system. Experimentally, this is exactly what is observed with the activation energy being 38.79 kJ/mol, slightly lower than 39.42 kJ/mol found for the SMA_m -gold (non-sonicated) system. It appears that both platinum and gold nanostructures within the hydrophobic cavity behave very similarly providing effective competition against pyrrole polymerization. Due to the interaction energy numbers being so close, the more stable system cannot be established.

5.4 Conclusion

The activation energy of pyrrole polymerization was determined for various systems with active metal centers. The activation energy for the pyrrole polymerization for the various systems was found to be the lowest in SMA_m-gold (sonication) and highest in SMA_m-platinum nanoreactor. This result could be explained by the number of metal clusters interacting with the hydrophobic cavity and the crystal structure giving rise to the properties of the nanoreactors and influencing the activation energy. In general, the greater the number of nanoclusters interacting with the hydrophobic cavity, the more pyrrole has to compete for the same polymerization resulting in higher activation energy. Comparatively SMA_m-gold (no sonication) and SMA gold-platinum were found to have very similar activation energies due to the similarities in the cluster formation within the hydrophobic cavities. It appears that clusters regardless of gold or platinum within the hydrophobic cavity provided very similar competition for polymerization of pyrrole and hence resulted in very similar activation energies.

This system provides one simple example of the greater potential that lies within the unique properties of the nanoreactors. Moreover, studies have shown that greater activation energy is required for PPy even after using harsh chemicals and oxidants. This is the first study that provides an environmentally friendly alternative to the same polymerization, with much lower activation energy due to the metal active centers and favoured thermodynamics due to confinement effect. More studies need to be conducted to determine the activation energy under confinement for a deeper understanding on forces that dominate at this scale and their effect on the activation energy of reactions. The self-assembled nanostructures of the polymeric template with alternating hydrophilic and hydrophobic nanodomains allow for the development of complex nanoreactors with both platinum and gold active centers. Further characterization of the systems in detail, via IR or TEM remains an active area of investigation for future studies.

The effects of various other factors such as the effect of thickness of gold sheets or number of platinum clusters on activation energy also remain a subject of future investigation. The systems presented here offer tremendous potential for various catalytic applications or many biological applications after the isolation of PPy.

6. Investigating the effect of an amino acid attachment and its influence on the polymeric interaction with gold

6.1 Introduction

The goal of the newly developed field of nano-medicine is to mimic the complex biological systems as observed in a biological cell by creating artificial nanostructures in a rational manner. These cells have various compartments and communication between these compartments is the key for all of the biological functions including replication, mechanisms or signal transduction. Compartmentalisation or confinement of cellular components enables cells to control and optimize all of the biological processes. The cell membrane is composed of a phospholipid bilayer forming a barrier between intracellular and extracellular aqueous regions. Proteins are present in this bilayer to selectively transfer essential molecules and nutrients. The phospholipid bilayer also has negatively charged compounds making it harder to deliver hydrophobic or negatively charged compounds. To overcome the complications involved in delivering hydrophobic drugs, drug delivery systems (DDS) have been developed. DDS have some complications associated with the system including, biodegradability, biocompatibility, costs and various interactions that play a part in drug delivery.[178]

Researchers have developed various mimics of the biological cells by using the bottom up approach and many organic and inorganic materials, but, they have still been found to lack the environmental sensitivity. Many of the systems created fail to respond to the environmental stimuli and cannot communicate effectively with their surroundings. An example of natural nanostructure that is able to respond to its environment can be observed in a virus capsid. A cowpea chlorotic mottle virus (CCMV) is an icosahedral virus with 28 nm outer diameter and 18 nm inner diameter.[179] The virus capsid is also known to undergo a pH-dependent reversible swelling behaviour allowing small molecules to diffuse out in the swollen state. [179] The inside of the virus capsid provides a unique opportunity to study the effect of confinement similar to the one observed in our system by using SMA. Virus capsids therefore offer tremendous potential to be utilized as a system for drug loading and delivery applications.

In order to mimic the natural biosystems that have had many years to optimize, polymers have been frequently used in the field of drug delivery by providing controlled and sustained release of therapeutic agents for both hydrophobic and hydrophilic drugs. Environmentally responsive polymers are widely used in the field of drug delivery due to their ability to undergo a physical or chemical change, in response to an external stimulus such as pH, temperature, magnetic fields, ultrasound and light.[52,40] It has been found that SMA is pH responsive as altering the pH disrupts the linearity of the structure and hence interferes with the formation of the nanoreactor.[77] The pH responsiveness of the

polymer can be observed in Figure 57 and can be utilized for possible drug delivery applications.[180]
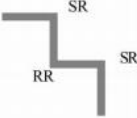
pH	Chirality	Optimised structure	Backbone
pH 3	SR RR SR		SR / RR / SR
	SR SR SR		
pH 7	SR RR SR		
	SR SR SR		
pH 12	SR RR SR		
	SR SR SR		

Figure 57: SMA chain linearity demonstrating the pH dependability due to internal hydrogen bonding (Reproduced from Ref. [180] with permission)

Polymers combined with amino acids have been found to show unique properties for use in drug delivery systems.[56,181] Long-circulating macromolecular carriers such as peptide-based molecules can exploit the enhanced permeability and retention effect (EPR).[56] EPR is a property by which molecules tend to accumulate in tissues much more than they traditionally would. SMA, as mentioned in the previous chapters is an alternating amphiphilic co-polymer. Compared to the alternating co-polymers without the polypeptide blocks, polypeptide containing ones can simulate not only the shape of the nanoreactors formed but also their biological performance.[56] Jun et al., while using cysteine based polymers, have demonstrated up to 25% drug loading and sustained release of a hydrophobic drug,

docetaxel. [56] In Contrast, another group of researchers while attempting to improve the entrapment efficiency of hydrophilic drug substances have used sodium cromoglycate inside poly(l) lactide nanoparticles and demonstrated up to 70% drug loading. [182]

Hence, the main aim of this chapter is to use a polymeric material, SMA and combine it with an amino acid for enhanced properties and biocompatibility. The selection of amino acid has two main criteria with regard to this system, including maintaining the linearity of the polymeric structure and ability to study it's interaction with gold to be effectively able to use it in the nanoreactor developed in previous chapters. Linearity is crucial for the development of the nanoreactor, whereas a strong interaction with gold ensures the formation of a stable structure while allowing us to determine how the amino acids interact with gold. Indeed, cysteine (Figure 58 a) and histidine (Figure 58 b) were chosen for this study mainly due to their effectiveness as cellular drug delivery agents as well as their structure with a sulfur atom known to form a very strong and stable bond with gold. Computational chemistry was used to ensure that the linearity of the polymer would not be disrupted due to the attached amino acid. Many systems have shown effectiveness in predicting properties related to drug delivery by using computation.[183,184] Gregg *et al*., used computational chemistry to predict the net surface interactions between nanoparticles and cell surfaces[183] whereas another group of researchers use both computational and experimental approaches to estimate the solubility and permeability in drug discovery[184]. Moreover, experimental characterization is used to support computational results as well as determine the unique properties associated with the interaction between amino acid with polymeric template and gold. Developing a nanoreactor with an amino acid that increases its biocompatibility and stability makes this reactor an ideal candidate for use in diagnostics and therapeutic applications. The hydrophillic and hydrophobic active centers with different gold structures could both simultaneously and individually be used for drug loading and delivery. After loading one can take advantage of the pH responsiveness of the system for effective drug delivery.

6.2 Sample Preparation and methods

The 13% SMA aqueous solution was purchased from Sigma Aldrich and was freeze dried to remove excess solvent. L-Cysteine and L-methionine were also purchased from Sigma Aldrich and used without further purification (Figure 58).

6.2.1 Computational analysis of optimal properties for the formation of nanoreactor

The SMA models used in this chapter were optimized starting from dihedral angles of a monomer upto a hexamer at DFT-B3LYP/6-31G as described in an earlier study using Gaussian 09 software.[104] The amino acids including cysteine and methionine were optimized by using the same level of theory and

method as described above. Firstly, each amino acids was attached to SMA monomer and their interaction with gold was studied to determine whether gold prefers interaction with hydrophillic or hydrophobic domains post attachment. It is important to note that the optimizations involving gold were optimized by using at DFT-B3LYP/LANL2DZ instead to minimize the computational time, while still obtaining accurate results as described in earlier chapters. The trimer of SMA was then chosen and modelled with amino acids to predict the linearity of the structure. Although each PSMA has four chiral centers, the geometry and linearity of the polymer backbone is independent of chirality, hence, one stereoisomer was chosen and optimized using the same procedure and theory described above. Due to the size of the system and the many electrons that need to be modelled, High Performance Computing Virtual Laboratory (HPCVL) was utilized. The results were then analyzed based on linearity and the lowest interaction energy associated with the entire system to determine the suitable candidate for experimental work.

6.2.2 Synthesis of biocompatible amino acid based polymeric nanoreactor

Amino acids (AA) including cysteine and methionine were separately dissolved in anhydrous DMSO and reacted with dicyclohexylcarbodiimide (DCC and N-hydroxysuccinimide (NHS) (AA/DCC/NHS molar ration= 1:1.2:1.2). The reaction was performed under inert nitrogen atmosphere at room temperature overnight. This was then mixed with freeze dried 1% SMA dissolved in DMSO and the reaction was carried out for 12 h under inert nitrogen (Figure 58). The solution was then dialysed against water and freeze dried. The mixture was then characterized through IR via forming a KBr pellet and ^{1}H NMR in deuterated DMSO. For detailed methods on FTIR and NMR techniques used please refer to section 2.1.8.
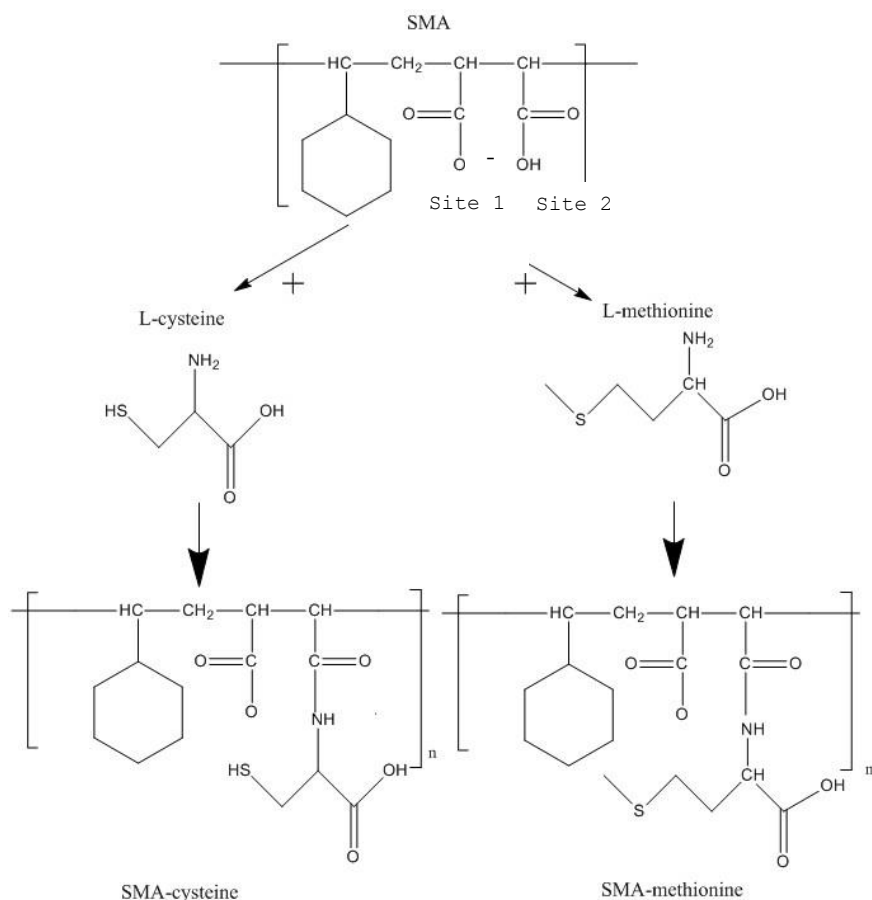
Figure 58: Structures of SMA and L-cysteine and L-methionine with SMA

6.3 Results and Discussion

The main goal of this study is to extend the easy, environmentally friendly synthesis of nanoreactors by combining it with the addition of biocompatible amino acids. As mentioned earlier, polymers with amino acids have been found to exploit the EPR affect for enhanced drug delivery. Moreover, cysteine and histidine also have a sulfur atom known to form a strong and stable bond with gold making them ideal candidates for testing with gold nanoreactors. Addition of amino acids also reduces the biocompatibility risk as they are naturally found in the human body. In order to determine the suitable amino acid that would not disrupt the linearity of the SMA structure and consequentially form the nanoreactor, *ab initio* simulations were carried out. Simulations were also performed to determine whether gold prefers interaction with the hydrophobic or hydrophilic groups.

6.3.1 Computational Interaction between SMA and amino acids

Ab initio simulations have been employed for prediction of atomic interactions for both organic and inorganic molecules.[79,80,85,86] To study the interaction between gold and SMA-AA, simulations were performed. As mentioned in section 2.1, each dihedral angle was optimized to determine the global minimum followed by the optimization of the entire structure using DFT-B3LYP-LANL2DZ. It was determined in Chapter 3 that both hybrid functional B3LYP and B3PW91produced similar trends for the results. Hence, only one hybrid functional, B3LYP is used for all of the other optimizations.

It was found and discussed in Chapter 3 that gold prefers interaction with the hydrophilic domain. The interaction of gold was found to be restricted to and amplified with the hydrophillic domain in the presence of sonication and in the presence of monomethyl ester (SMA_m) respectively. In this study SMA instead of SMA_m was used since the interaction of plain SMA-AA with gold needs to be determined first. The effect of addition of AA to the SMA- gold interaction depends on disrupting the linearity of the polymeric material and hence the formation of the nanoreactor. Since the size of amino acid is quite small relative to the polymeric material and due to the past studies commonly including polymeric materials with amino acids, it is not expected that the intrinsic properties of the polymeric material will be impacted by the presence of amino acids. To confirm this computationally, first amino acids were attached to two different sites of the polymeric compound as observed in Figure 59. Both cysteine and methionine were found to slightly prefer to form an amide bond with site 2. The optimized structures can be observed in figure 59. The difference in energy between site 1 and site 2 for cysteine and methionine was found to be -8.49 kJ/mol and -5.89 kJ/mol, respectively. Since the difference in energy is very small, in an experimental setup we expect to have an equal mixture of the two. Also, any conclusions regarding the linearity of the structure cannot be made from a monomer and require optimizations with a trimer.

a)   b)
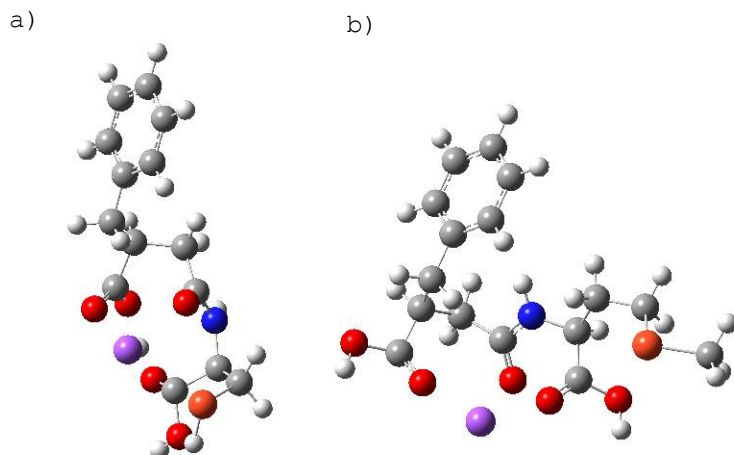
Figure 59- Optimized structures of SMA and a) cysteine b) L-methionine with DFT-B3LYP-LANL2DZ

In Chapter 4 it was demonstrated that the sulfur from thiophene forms a very strong and stable bond with gold,whereas in Chapter 3 without the presence of sulfur, gold preferred interaction with carboxylic acid groups. To determine whether gold still prefers interaction with the hydrophillic domain or the sulfur, computational modelling with the monomers was performed. Gold was placed at a variety of locations including beside the styrene group, beside the carboxylic acid groups and beside sulfur. The interaction energy values were then calculated via equation 50 and can be observed in Table 5.

$$E_{complex\,with\,gold} - (\,E_{SMA-AA} + \,E_{gold})$$ Equation 50

Table 5: Interaction energy values for various structures of SMA-AA-gold for both site 1 and site 2

	System	Site 1 Interaction Energy (kJ/mol)	Site 2 Interaction Energy (kJ/mol)
SMA-cys-gold beside	Styrene	-234.69	-153.38
	Carboxylic acid	-247.83	-153.38
	Sulfur	-263.35	-229.41
SMA-meth-gold beside	Styrene	-198.37	-250.04
	Carboxylic acid	-194.82	-294.51
	Sulfur	-387.79	-321.47

Similar trends can be observed in both cases of cysteine and methionine attached to SMA. Gold atom was placed beside its respective group and then optimized. From the interaction energy values in Table 6 it is obvious that the most favourable structure was produced when gold was initially placed beside sulfur. While gold was initially placed beside sulfur it can be observed to slightly move away and interact with both the carboxylic acid groups and sulfur in both cases. The interaction energy values for site 1 interacting with sulfur are lower, but the difference between site 1 and 2 is small. It is therefore expected that both interactions could occur depending on the experimental conditions. Only site 1 structures and their interaction with gold is displayed in Figure 60 for clarity purposes. From the interaction values alone for a monomer, it appears that the interaction in the presence of the methionine is stronger than in cysteine. This could be due to the length of the linker minimizing the steric hindrance and allowing gold to more strongly interact with the sulfur. However, this may change in larger systems due to other dominating interactions. Overall, in this system it seems initially that gold prefers interaction with the sulfur and then slowly stabilizes to allow for an interaction with carboxylic acid as well. Initially, due to the gold moving away from sulfur, it may appear that it is rather interacting with the carboxylic acid groups, however, through molecular orbital (Figure 61) images it becomes clear that although further in distance, gold is still interacting with the sulfur. It remains unclear how the gold will behave in an experimental system due to the presence of a polymer instead of a monomer and the effect of the solvent. This generates the need to optimize a larger system (i.e a trimer).
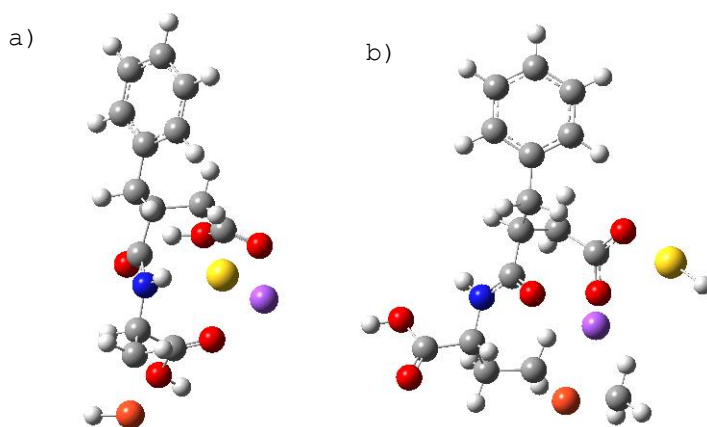
Figure 60- Optimized structures of SMA and a) cysteine b) L-methionine with DFT-B3LYP-LANL2DZ
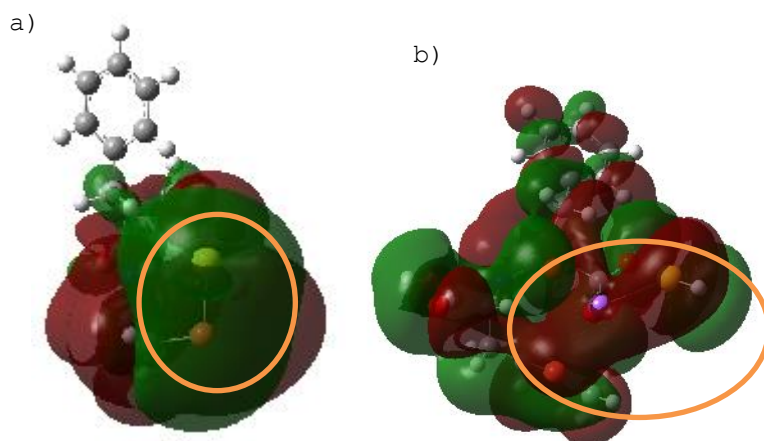
Figure 61- Molecular orbital images of a) SMA-cysteine gold, energy -0.30180 hartrees b) SMA-methionine gold, energy -0.17250 hartrees obtained with iso value of 0.001

To determine whether gold prefers interaction with the carboxylic acid groups or the sulfur atom, optimization with a trimer is required. Optimization with a trimer will also assist with determining the linearity of the structure after the addition of the amino acid. The optimization of the structure was done in the same manner as described earlier and the interaction energies were calculated by Equation 50. The interaction energy numbers for the trimers can be found in Table 6 with the most favourable molecules being site 2 for SMA-cys gold (Figure 62) placed beside sulfur and site 1 for SMA-meth-gold (Figure 63) placed beside sulfur as well. It is important to note that there is only one amino acid per trimer was modelled as the experimental functionalization is expected to be 1 amino acid per every ten monomers of SMA.

Table 6: Interaction energy values for trimers various structures of SMA-AA-gold for both site 1 and site 2

	System	Site 1 Interaction Energy (kJ/mol)	Site 2 Interaction Energy (kJ/mol)
SMA-cys-gold beside	Styrene	-267.30	-269.77
	Carboxylic acid	-233.46	-112.25
	Sulfur	-198.99	-368.34
SMA-meth-gold beside	Styrene	-224.33	-282.11
	Carboxylic acid	-226.61	-275.56
	Sulfur	-304.67	-220.68
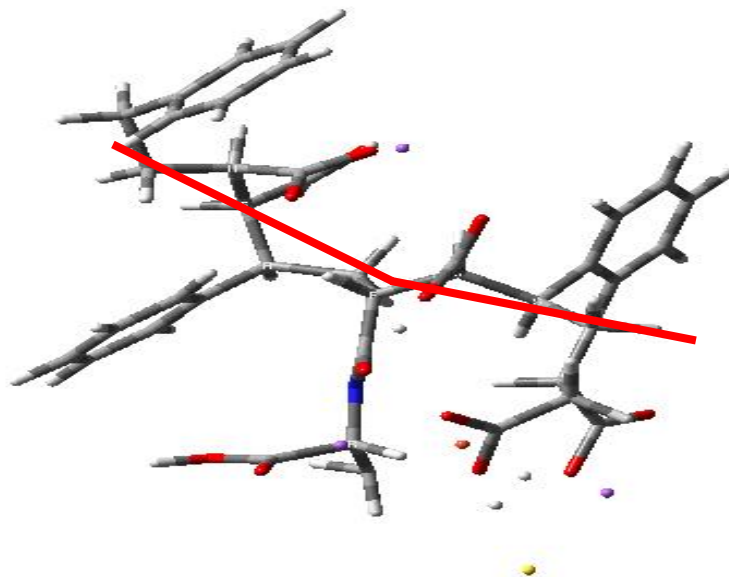
Figure 62: Optimized trimer model of a gold atom balancing the interaction between sulfur atom and oxygen rich carboxylic acid group of SMA-Cys site 2. Simulation used DFT-B3LYP-LANL2DZ level of theory

It can be observed in Figure 62 that gold, when initially placed beside the sulfur atom, slightly moves towards the oxygen rich carboxylic acid groups. Energy minimization pulls gold away from the hydrophobic regions towards the hydrophilic carboxylic acid groups, while still maintaining linearity of the structure. Gold can be observed to balance the interaction between carboxylic acids and the sulfur atom and hence it is expected that gold in this case will prefer interaction with the hydrophilic domain with some gold nanocrystal formation. Moreover, addition of cysteine and its interaction with gold does not disrupt the linearity of the polymer backbone to a great extent. It is also important to understand that experimentally larger chains will exist and only increase the linearity of the chain. Comparatively SMA-meth interacting with gold appears to be very linear in nature (Figure 63). Gold in this case appears to more strongly interact with the sulfur instead of the carboxylic acid group. One of the reasons why gold instead interacts with the sulfur atom could be that methionine is a longer amino acid compared to cysteine. This keeps the sulfur farther from the carboxylic acid group and minimizes the steric interactions. Overall, both cysteine and methionine when attached to SMA appear to maintain the linearity of SMA and could make good candidates. Since the linearity is not disrupted, it should not disrupt the formation of the nanoreactor and allow studying its interaction with

gold. A conclusion in terms of whether cysteine or methionine makes a better candidate cannot be made computationally since the interaction energy numbers are relatively close and could change depending on other experimental conditions, such as the presence of the solvent.
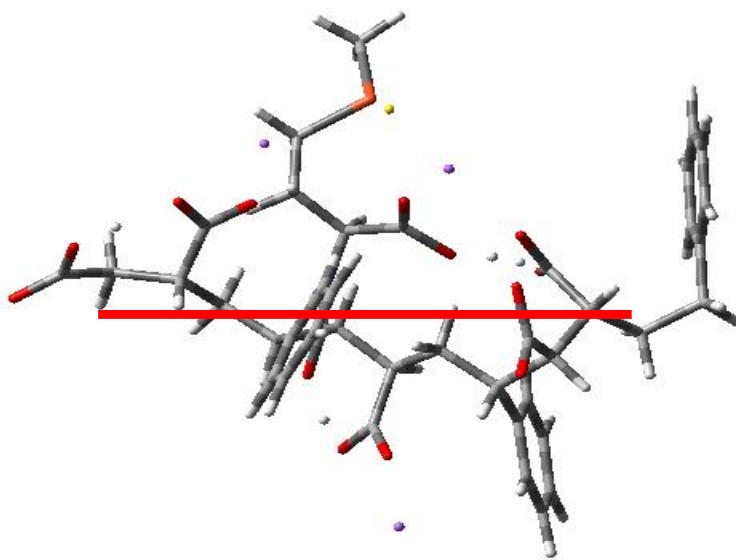
Figure 63: Optimized trimer model of a gold atom interacting with the sulfur atom from methionine attached to SMA site 1. Simulation used DFT-B3LYP-LANL2DZ level of theory

6.3.2 SMA amino acid attachment confirmed by IR

The computational simulations confirmed both cysteine and methionine would not interfere with the nanoreactor development of SMA and allow studying its interaction with gold. The reaction mechanism for the attachment can be seen in Figure 58 with detailed reaction conditions in section 6.2.2. To analyze whether the amino acids are attached with SMA, IR and NMR were performed. The IR spectra's for SMA attached with cysteine and methionine can be observed in Figure 64. As observed in Figure 64, in both of the cases an amide bond is being formed by the combination of the amine and a carboxylic acid. The presence of an amide is observed through IR with a peak at approximately 1620 and 1570 cm^{-1} representing C=0 and N-H functionalities proving the linkage between SMA and the amino acid. It is also important to note that these peaks are not observed in plain SMA, Figure 28a. Further confirmation of the attachment via NMR was also performed, however, due to the complexity of the nature of the polymer along with amino acids, conclusions could not be drawn. Hence, IR suggested that the attachment was successful due to the presence of two peaks at the same position in

the case of both methionine and cysteine whereas NMR was not conclusive. This generates the need to verify or prove the attachment via other methods such as UV-Vis.
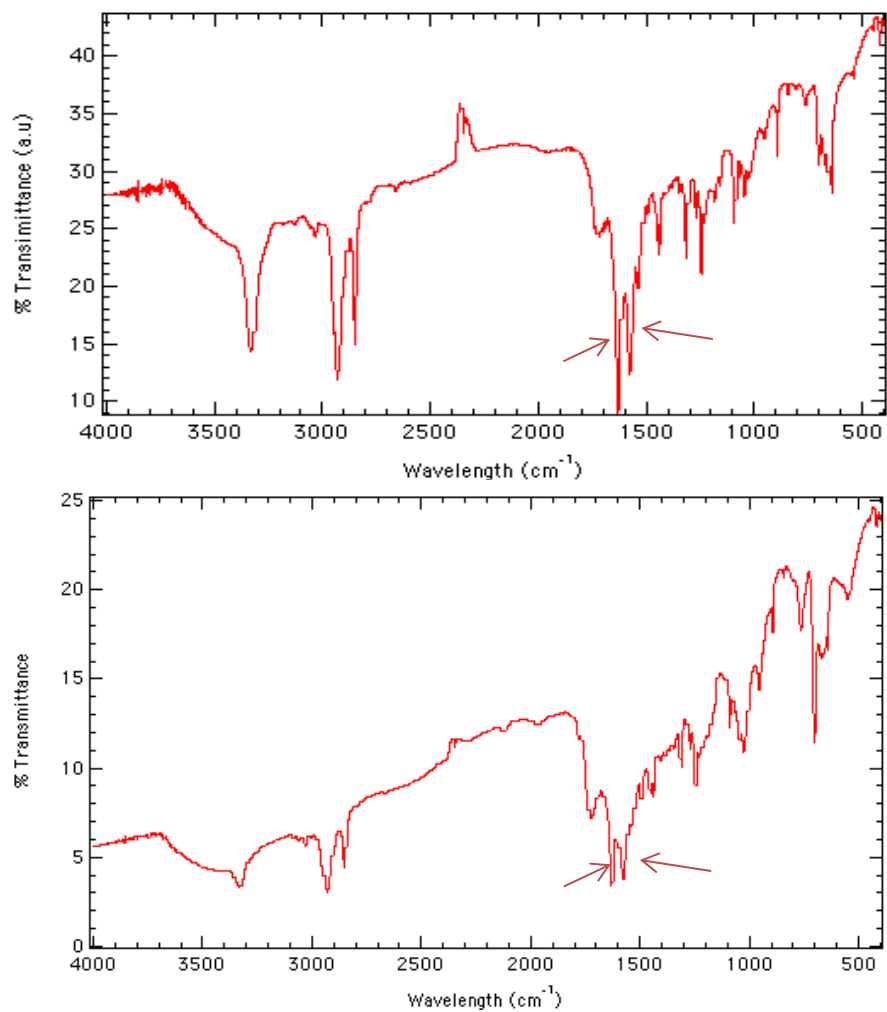
Figure 64:IR spectra for SMA and a) cysteine and b) methionine showing a peak at 1620 cm^{-1} and 1570 cm^{-1} representing C=0 and N-H bend in the newly formed amide bond.

6.3.2 Characterization of the compound performed by UV-Vis

   Although UV-vis cannot be used to directly verify the attachment, we may be able to determine the presence of various gold nanostructures present in the sample. During the sample preparation, it was found that minimal amounts of polymer were soluble in water. The sample was hence sonicated for 6 hours and left for 3 days before selecting only the supernatant. The supernatant with minute amounts of polymer dissolved was then mixed with gold and studied via UV-Vis. In Figure 65, a very stable broad peak at 300 nm can be observed for both cysteine and methionine. It is important to note that only one spectrum is shown even though the sample was monitored for many time points due to its stability for both of the compounds. The spectra were found to be very consistent with the same peak without alteration. It has previously been demonstrated in Chapter 3 and 4 that a peak at 300 nm corresponds to the formation of gold clusters. Due to the absence of the peak at 567 nm corresponding to the gold crystals, it can be predicted that, only gold clusters were formed in both of these cases. Moreover, this also supports the IR results since in the case the polymer was not attached, we would have only seen SMA- gold interaction discussed in Chapter 3 with a peak at 567 nm. In order to study the shape and the size of the gold nanostructures produced the system needs to be further studied via TEM.
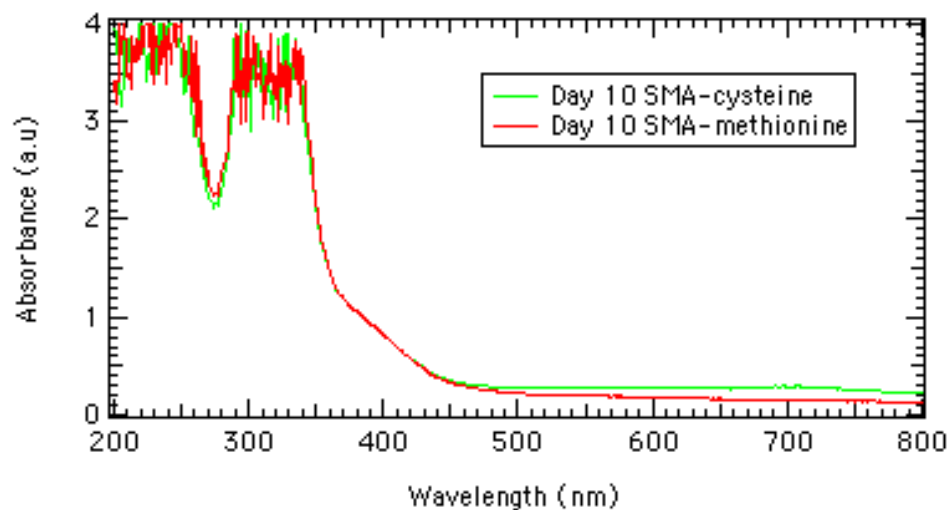
Figure 65: UV/Vis spectra of SMA attached with cysteine and methionine with gold both showing a broad peak at 300 nm

6.3.3 Presence of the gold nanostructures observed by TEM

TEM analysis was conducted on both SMA-meth and SMA-cys. Both of the samples appeared to be very similar with presence of gold nanostructures. Due to the similarity of the results, only SMA-meth images are presented in Figure 66. Figure 66 shows a good dispersion of very large gold nanocrystals upto 230 nm in size with hollow centers. Moreover gold nanoclusters between 1-3 nm can also be observed in the background. Figure 66d shows discrete Moire fringe patterns of two gold nanosheets overlapping. Although, this could be an artifact of drying, this is very unlikely as similar results have also been observed by other researchers earlier. This conformation proves that the gold nanosheets found in the sample are atomically thin and could demonstrate exceptional catalytic capabilities. The presence of many gold nanoclusters in the background corresponds to the broad peak at 300 nm observed in Figure 65. However, a peak at approximately 560 nm corresponding to the presence of gold crystals was not observed in Figure 65, potentially due to the low concentration of gold in the sample or alteration in the thickness of the gold structures. It is important to note that these are just preliminary results and further analyses on them would be done in future.
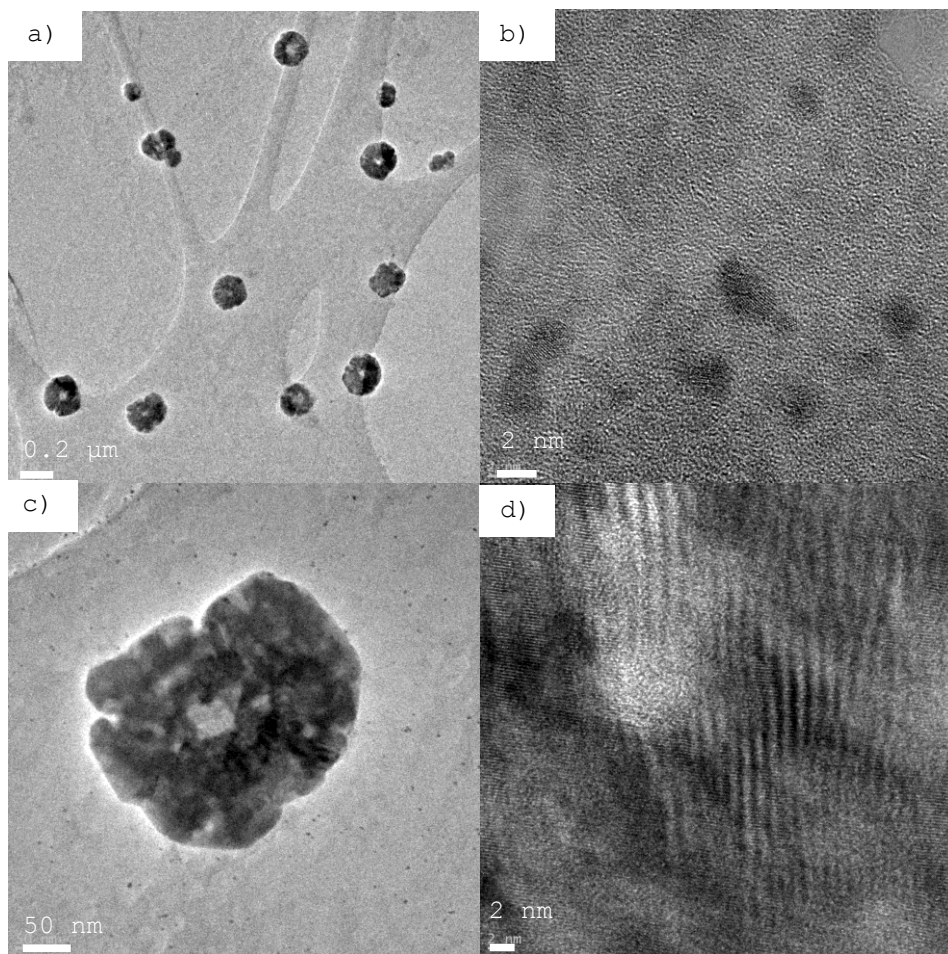
Figure 66: a/b/c) Image showing good dispersion of gold crystals (upto 230 nm) and clusters (1-3 nm) in the SMA-meth sample d) Two discrete gold sheets producing a 1 nm Moire fringe pattern by their overlap

6.4 Conclusion

It was computationally predicted that both cysteine and methionine would be good candidates for the attachment with SMA as they would allow one to study the interaction of gold with covalently attached sulfur. The addition of amino acids has been found to increase the biocompatibility of the polymeric compounds and has been commonly used for drug delivery applications. The combination of a stimuli-responsive polymer with a biocompatible polymer along with gold opens up many diagnostic and therapeutic applications. Both of the linkers when attached

to SMA were found to maintain linearity of the compound essential for the formation of nanoreactor whereas it was concluded that we will most certainly have a mixture of linkers attached on both site 1 and site 2 through interaction energy numbers. Thiols and gold have previously been found to form a very strong and stable bond, however, computationally it was observed to move away from the thiols. Through molecular orbital analysis and interaction energy values, it was predicted that gold, even if further in distance, would still prefer interacting with the thiol groups.

The synthesis was then conducted and IR was used to prove the attachment by the presence of an amide bond, peaks at 1570 and 1620 cm^{-1} representing C=0 and N-H functionalities in an amide bond. To study the kinetics of the formation of gold nanostructures, UV-Vis was conducted. One broad peak was found at 300 nm for both cysteine and methionine suggesting the formation of only gold nanoclusters with the absence of gold crystals. TEM images showed the presence of gold nanostructures with crystals upto 230 nm in size and many clusters between 1-3 nm in size. It was unclear as to why a peak was not observed at 560 nm on the UV-Vis spectra and could potentially be due to low concentration of gold within the sample. Future analyses would be performed in the future to study the shape and the size of the gold nanostructures and compare them directly with the ones discussed in Chapter 3 and 4.

This study investigated the interaction between thiol and gold in a different chemical environment due to the sulfur being covalently bonded instead of, as previously discussed free thiophene. The presence of gold nanoclusters only may offer another level of control while increasing the biocompatibility of the system for biological applications. The system needs to be characterized further through TEM enabling a direct comparison with previous systems since it appears to be restricting the interaction of gold only within the hydrophobic cavity.

7.0 Summary

This thesis was aimed to investigate the novel synthesis of nanostructures with gold active centers and various methods to control this interaction. The system developed in this thesis exploits the nanostructures produced by SMA with both hydrophobic and hydrophilic cavities and introduces various methods to mediate the growth of gold nanostructures within the nanoreactors. This thesis focused on developing completely biocompatible, easy synthetic methods for the development of gold nanostructures and established three novel ways to control this interaction. The control methods included sonication and altering the nature of the polymer that was able to force more gold to interact with the hydrophilic cavity and a coupling agent, thiophene that was able to force more gold to interact with the hydrophobic cavity instead. This thesis also demonstrated great catalytic potential of the nanoreactors with gold active centers via pyrrole polymerization and determined the activation energy for the propagation step of pyrrole polymerization. Nanoreactors have the potential to replicate processes that are currently limited to high pressure and temperatures. This study brings us one step closer to understanding the effect of confinement produced by biological enzymes also containing active centers with hydrophobic and hydrophilic regions and metalloproteins that alter their behaviour within the confined space. This study also shines light on potential applications in drug delivery or diagnostics or therapeutics applications because of the presence of atomically thin gold nanostructures.

8.0 Conclusion

The new properties of gold at the nanoscale have favoured their applications in a variety of fields from catalysis to targeted drug delivery. Although, gold nanostructures have unique electronic, magnetic and optical properties, their synthesis still uses harsh chemicals and complex mechanisms such as the citrate reduction or the Burst-Schiffrin method. This restricts the use of gold in bio-medical applications and generates a need for the development of completely bio-compatible easy synthesis of gold nanostructures.

This study is unique not only because it proposes a simple yet efficient method for the synthesis of gold nanostructures but also because it investigates three different ways to mediate this interaction. SMA is an amphiphilic alternating copolymer that self-assembles into nanostructures at neutral pH and produces inner cavity of 3 nm with a hydrophilic domain on the outside. Due to the small hydrophobic cavity produced in the nanostructures, confinement conditions are introduced generating macromolecular crowding promoting reactions that are otherwise not possible in the bulk. Gold chloride was found to interact with SMA on the hydrophilic domain producing gold crystals of 30-50 nm and within the hydrophobic cavity producing gold clusters of 2-3 nm, simultaneously. This production of gold nanostructures is conducted without any reducing agent in water making the reaction completely biocompatible.

Various methods for controlling the interaction of gold with SMA were investigated in this report including control via sonication and altering the nature of the polymer to SMA_m. SMA_m is structurally 85-90% identical to SMA with 10-15% of SMA functionalized with monomethyl ester. To truly understand the interactions at play in a complex system both computational modelling and experimental characterization was performed. Computational modelling was not only used to support the experimental results but to also to predict experimental behaviour.

Combined analyses of computational and experimental modelling revealed that the presence of monomethyl ester was able to drastically enhance the interaction of gold with the hydrophilic domain producing larger atomically thin gold crystals up to 80 nm in size. Fewer gold nanoclusters of 2-3 nm were also observed within the hydrophobic cavity. This was observed experimentally by enhanced intensity of peak signal in UV-Vis and larger gold crystals via TEM. Through molecular orbital images, it was revealed that the presence of an extra monomethyl ester completely altered the structure of the polymer allowing two oxygen atoms to interact with gold instead of one. This was the main reason for which even minute amounts of monomethyl ester resulted in increased intensity of gold on the hydrophilic domain. Moreover, diffraction patterns that were obtained revealed a mixture of both fcc and hcp type crystal structures for the gold crystals.

This interaction was further controlled by adding external energy using sonication. Sonication was found to disrupt the whole self-assembly process and

completely eliminate the interaction of gold within the hydrophobic cavity producing exclusively monoatomic hpc gold crystals. It is important to note that simply by sonicating the sample we were able to control the interaction of gold and force all of the gold to only interact with the hydrophilic domain produced by SMA. The control of the environment surrounding the active center is essential for the development of tailored nanoreactors. This study brings one a step closer to understanding the effect of confinement and reminds of the minute details that can make a drastic difference in terms of the properties of the nanoreactors enhancing the level of control obtained for the active site of the nanoreactor. Since both of the methods investigated thus far have encouraged the interaction of gold on the hydrophilic domain, we attempted to focus on a method that does the exact opposite, force more gold to interact within the hydrophobic cavity.

Control by using a coupling agent such as thiophene was also investigated. Thiophene is a hydrophobic molecule and is therefore expected to interact with the hydrophobic cavity. Thiophene also has a sulfur atom in its structure known to form a very strong and stable bond with gold. We investigated both two and three component systems. Two component systems included monitoring the interaction of SMA_m-gold, SMA_m-thiophene and gold-thiophene. While the interaction between SMA-gold had been studied previously, the interaction between thiophene and gold was only computationally modelled. Computational modelling predicted the formation of clusters by thiophene around gold strengthening the hypothesis that since thiophene itself is hydrophobic while interacting very strongly with gold, it would, indeed, force more gold to interact with the hydrophobic cavity. This two component system could not be experimentally modelled since thiophene is very hydrophobic and does not dissolve well with gold salt. After understanding the interaction between two components in detail, all three components including SMA_m, gold and thiophene were mixed in different orders.

It is important to understand that mixing all three components together creates effective competition for interaction with gold since both polymer and thiophene would want to form a strong interaction with gold. Interestingly, it was found that depending on the order the components were mixed in, they produced completely different results. For example, if SMA_m-gold were mixed first and stabilized they showed a stronger interaction with some interference from thiophene, whereas if thiophene-gold were mixed first this greatly minimized the interaction of gold on the hydrophilic domain, forcing more gold to interact with the hydrophobic cavity. Therefore, using a coupling agent such as thiophene to aid in the crystal formation appears to have various effects depending on the synthesis methods. Generally, it was demonstrated that the presence of thiophene forces more gold to interact with the hydrophobic cavity because of the highly stable sulfur-gold interaction. Hence, this thesis also highlights another level of control to force more gold to interact with the hydrophobic cavity. The ability to control the interaction offers tremendous potential for targeted nanoreactors for drug delivery applications and enhanced catalysis.

To demonstrate the catalytic properties of these nanoreactors, we attempted to improve upon the observed pyrrole polymerization within the nanoreactor. Previously the thermodynamic properties of the pyrrole polymerization have been investigated by Xia *et al.* This thesis takes another route and adds to the knowledge by instead focusing on the kinetic properties and determining the activation energy required for pyrrole polymerization to start. Various nanoreactors with metallic active centers including gold, platinum and their combination were tested to deduce the best system for applications in enhanced catalysis. The activation energy of pyrrole polymerization in various systems was determined to be 56.84 kJ/mol, 39.42 kJ/mol, 28.65 kJ/mol and 38.79 kJ/mol for SMA_m-platinum, SMA_m-gold (no sonication), SMA_m-gold (sonication) and SMA_m gold-platinum nanoreactor respectively. As observed from the activation energy numbers, the presence of any metal nanostructures within the polymeric template is found to stabilize the entire system and lower the activation energy required for the polymerization to start. It is important to note that the activation energy for pyrrole polymerization in plain nanoreactor, SMA_m could not be determined due to polymerization not being observed at any other temperatures except the room temperature. This proves the effectiveness of this nanoreactor and shows the exponential potential that exists for improved catalysis. Moreover, this study demonstrates that the changes to the reaction within the nanoreactor confined spaces are not just dependent on the thermodynamics but also the kinetics.

The reduction of gold and platinum chloride is not an energetically favourable reaction and requires strong reducing agents and complex synthesis mechanisms to proceed. The method discussed in this thesis takes away the requirement of a reducing agent making the reaction more biocompatible and simple while still producing the same monodisperse gold and platinum nanostructures. This thesis also develops and discusses novel methods to control this interaction and mediate exactly where the reaction occurs (on the hydrophobic or hydrophilic domains). This is a novel approach to control chemical reactivity to alter the properties of nanoreactors.

Nanoreactors have the potential to replicate processes that are currently limited to high pressure and temperatures. This study brings us one step closer to understanding the effect of confinement produced by biological enzymes also containing active centers with hydrophobic and hydrophilic regions and metalloproteins that alter their behaviour within the confined space. Many drug clinical trials are not successful today because one cannot accurately predict the way the drug will behave within a biological cell. The development of this nanoreactor brings us one step closer to understanding the effect of confinement making reactions that are not possible in bulk, possible. With further research we may be able to test various drugs within these nanoreactors to accurately predict their behaviour within a biological cell.

The development of this nanoreactor also alleviates some of the ethical issues and helps minimize costs considered while using whole organisms or

components of organisms for biological testing. Since the entire system is synthetic, it allows one to tailor properties towards what is required for the specific application and due to its pH-responsiveness offers great potential for drug loading and release. This nanoreactor can also be used for synthesis of atomically thin crystals of gold with desired crystal structures that can then be isolated and modified for drug delivery or therapeutic applications. Gold has many electrons and therefore it has the ability to intensely scatter and emit these electrons opening the potential for diagnostic applications related to imaging cancerous cells.

Future work

This research program should continue to develop in future and consider testing various drugs within the confined space to study their altered behaviour. The reduction of other metal salts and other polymerizations should also be studied. The use of organic solvents can be drastically reduced if the formation of gold nanostructures or other metals and polymerization such as polypyrrole can be performed in water soluble nanoreactors. Attempts must also be made to increase biocompatibility by attaching amino acid linkers or other such moiety and studying its effect on the interaction of gold and polymeric material.

The effect of confinement not only has the ability to speed up chemical reactions but also to alter the favourability of reactions. Biomimicry via polymer-metal nanoreactors is an important area of research that can open many doors to applications in bio-medicine offering environmentally friendly approaches to the synthesis of many organic compounds. Understanding the way metals behave under confinement with organic materials enables us to understand and mimic biological enzymes that incorporate selectivity, reaction rate and regulatory functions. While being able to mimic an entire enzyme may take some time, studies like this exercising control of active centers with stimuli-responsive materials offer great alternatives to target each function separately.

8. References

1. McConney, M. E., Anderson, K. D., Brott, L. L., Naik, R. R. & Tsukruk, V. V. Bioinspired Material Approaches to Sensing. *Adv. Funct. Mater.* **19,** 2527–2544 (2009).

2. Dragoman, D. & Dragoman, M. *Bionanoelectronics: Bioinquiring and Bioinspired Devices*. (Springer Science & Business Media, 2012).

3. Semmlow, J. L. *Signals and Systems for Bioengineers: A MATLAB-based Introduction*. (Academic Press, 2012).

4. Czyzewski, A. M. & Barron, A. E. Protein and peptide biomimicry: Gold-mining inspiration from Nature's ingenuity. *AIChE J.* **54,** 2–8 (2008).

5. Bywater, R. P. Membrane-spanning peptides and the origin of life. *J. Theor. Biol.* **261,** 407–413 (2009).

6. Kasper, C., Witte, F. & Pörtner, R. *Tissue Engineering III: Cell - Surface Interactions for Tissue Culture*. (Springer, 2012).

7. Stenger, D. A. *et al.* Detection of physiologically active compounds using cell-based biosensors. *Trends Biotechnol.* **19,** 304–309 (2001).

8. Gannon, J. E. & Stemberger, R. S. Zooplankton (Especially Crustaceans and Rotifers) as Indicators of Water Quality. *Trans. Am. Microsc. Soc.* **97,** 16–35 (1978).

9. Petrovick, M. S. *et al.* Rapid sensors for biological-agent identification. *Linc. Lab. J.* **17,** (2007).

10. Cormier, M. J., Prasher, D. C., Longiaru, M. & McCann, R. O. The enzymology and molecular biology of the Ca2+-activated photoprotein, aequorin. *Photochem. Photobiol.* **49,** 509–512 (1989).

11. Radhika, V. *et al.* Chemical sensing of DNT by engineered olfactory yeast strain. *Nat. Chem. Biol.* **3,** 325–330 (2007).

12. Aida, T., Meijer, E. W. & Stupp, S. I. Functional Supramolecular Polymers. *Science* **335,** 813–817 (2012).

13. Zhou, Y., Huang, W., Liu, J., Zhu, X. & Yan, D. Self-Assembly of Hyperbranched Polymers and Its Biomedical Applications. *Adv. Mater.* **22,** 4567–4590 (2010).

14. Kumar, D. & Sharma, R. C. Advances in conductive polymers. *Eur. Polym. J.* **34,** 1053–1060 (1998).

15. Hu, H., Gopinadhan, M. & Osuji, C. O. Directed self-assembly of block copolymers: a tutorial review of strategies for enabling nanotechnology with soft matter. *Soft Matter* **10,** 3867–3889 (2014).

16. Groves, M. N., Malardier-Jugroot, C. & Jugroot, M. Environmentally friendly synthesis of supportless Pt based nanoreactors in aqueous solution. *Chem. Phys. Lett.* **612,** 309–312 (2014).

17. Alexandridis, P. & Lindman, B. *Amphiphilic Block Copolymers: Self-Assembly and Applications*. (Elsevier, 2000).

18. Raez, J., Manners, I. & Winnik, M. A. Nanotubes from the Self-Assembly of Asymmetric Crystalline−Coil Poly(ferrocenylsilane−siloxane) Block Copolymers. *J. Am. Chem. Soc.* **124,** 10381–10395 (2002).

19. Lazzara, T. D., van de Ven, T. G. M. & Whitehead, M. A. (Tony). Nanotube Self-Assembly of a Styrene and Maleimide Alternating Copolymer. *Macromolecules* **41,** 6747–6751 (2008).

20. Li, X. & Malardier-Jugroot, C. Confinement Effect in the Synthesis of Polypyrrole within Polymeric Templates in Aqueous Environments. *Macromolecules* **46,** 2258–2266 (2013).

21. Saccà, B. & Niemeyer, C. M. DNA Origami: The Art of Folding DNA. *Angew. Chem. Int. Ed.* **51,** 58–66 (2012).

22. Linko, V., Ora, A. & Kostiainen, M. A. DNA Nanostructures as Smart Drug-Delivery Vehicles and Molecular Devices. *Trends Biotechnol.* **33,** 586–594 (2015).

23. Rothemund, P. W. K. Folding DNA to create nanoscale shapes and patterns. *Nature* **440,** 297–302 (2006).

24. Andersen, E. S. *et al.* Self-assembly of a nanoscale DNA box with a controllable lid. *Nature* **459,** 73–76 (2009).

25. Walsh, A. S., Yin, H., Erben, C. M., Wood, M. J. A. & Turberfield, A. J. DNA Cage Delivery to Mammalian Cells. *ACS Nano* **5,** 5427–5432 (2011).

26. Bangham, A. D., Standish, M. M. & Watkins, J. C. Diffusion of univalent ions across the lamellae of swollen phospholipids. *J. Mol. Biol.* **13,** 238–IN27 (1965).

27. Ko, S., Liu, H., Chen, Y. & Mao, C. DNA Nanotubes as Combinatorial Vehicles for Cellular Delivery. *Biomacromolecules* **9,** 3039–3043 (2008).

28. Sellner, S. *et al.* DNA nanotubes as intracellular delivery vehicles in vivo. *Biomaterials* **53,** 453–463 (2015).

29. Pattni, B. S., Chupin, V. V. & Torchilin, V. P. New Developments in Liposomal Drug Delivery. *Chem. Rev.* **115,** 10938–10966 (2015).

30. Gregoriadis, G. The carrier potential of liposomes in biology and medicine (second of two parts). *N. Engl. J. Med.* **295,** 765–770 (1976).

31. Samad, A., Sultana, Y. & Aqil, M. Liposomal drug delivery systems: an update review. *Curr. Drug Deliv.* **4,** 297–305 (2007).

32. Anada, T., Takeda, Y., Honda, Y., Sakurai, K. & Suzuki, O. Synthesis of calcium phosphate-binding liposome for drug delivery. *Bioorg. Med. Chem. Lett.* **19,** 4148–4150 (2009).

33. Lozano, N. *et al.* Liposome–Gold Nanorod Hybrids for High-Resolution Visualization Deep in Tissues. *J. Am. Chem. Soc.* **134,** 13256–13258 (2012).

34. Daniel, M.-C. & Astruc, D. Gold nanoparticles: assembly, supramolecular chemistry, quantum-size-related properties, and applications toward biology, catalysis, and nanotechnology. *Chem. Rev.* **104,** 293–346 (2004).

35. Sharma, A. & Sharma, U. S. Liposomes in drug delivery: Progress and limitations. *Int. J. Pharm.* **154,** 123–140 (1997).

36. Anada, T., Takeda, Y., Honda, Y., Sakurai, K. & Suzuki, O. Synthesis of calcium phosphate-binding liposome for drug delivery. *Bioorg. Med. Chem. Lett.* **19,** 4148–4150 (2009).

37. Whitesides, G. M., Mathias, J. P. & Seto, C. T. Molecular self-assembly and nanochemistry: a chemical strategy for the synthesis of nanostructures. *Science* **254,** 1312–1319 (1991).

38. Pillai, O. & Panchagnula, R. Polymers in drug delivery. *Curr. Opin. Chem. Biol.* **5,** 447–451 (2001).

39. Senaratne, W., Andruzzi, L. & Ober, C. K. Self-Assembled Monolayers and Polymer Brushes in Biotechnology: Current Applications and Future Perspectives. *Biomacromolecules* **6,** 2427–2448 (2005).

40. Bayer, C. L. & Peppas, N. A. Advances in recognitive, conductive and responsive delivery systems. *J. Control. Release Off. J. Control. Release Soc.* **132,** 216–221 (2008).

41. Mendes, P. M. Stimuli-responsive surfaces for bio-applications. *Chem. Soc. Rev.* **37,** 2512–2529 (2008).

42. Luzinov, I., Minko, S. & Tsukruk, V. V. Responsive brush layers: from tailored gradients to reversibly assembled nanoparticles. *Soft Matter* **4,** 714–725 (2008).

43. Liu, Z. & Calvert, P. Multilayer Hydrogels as Muscle-Like Actuators. *Adv. Mater.* **12,** 288–291 (2000).

44. Anker, J. N. *et al.* Biosensing with plasmonic nanosensors. *Nat. Mater.* **7,** 442–453 (2008).

45. Stuart, M. A. C. *et al.* Emerging applications of stimuli-responsive polymer materials. *Nat. Mater.* **9,** 101–113 (2010).

46. Motornov, M., Sheparovych, R., Lupitskyy, R., MacWilliams, E. & Minko, S. Superhydrophobic Surfaces Generated from Water-Borne Dispersions of Hierarchically Assembled Nanoparticles Coated with a Reversibly Switchable Shell. *Adv. Mater.* **20,** 200–205 (2008).

47. Samadzadeh, M., Boura, S. H., Peikari, M., Kasiriha, S. M. & Ashrafi, A. A review on self-healing coatings based on micro/nanocapsules. *Prog. Org. Coat.* **68,** 159–164 (2010).

48. Cho, S. H., White, S. R. & Braun, P. V. Self-Healing Polymer Coatings. *Adv. Mater.* **21,** 645–649 (2009).

49. Ebara, M. *et al.* Temperature-Responsive Cell Culture Surfaces Enable 'On−Off' Affinity Control between Cell Integrins and RGDS Ligands. *Biomacromolecules* **5,** 505–510 (2004).

50. Angelos, S., Yang, Y.-W., Patel, K., Stoddart, J. F. & Zink, J. I. pH-Responsive Supramolecular Nanovalves Based on Cucurbit[6]uril Pseudorotaxanes. *Angew. Chem. Int. Ed.* **47,** 2222–2226 (2008).

51. Delcea, M., Möhwald, H. & Skirtach, A. G. Stimuli-responsive LbL capsules and nanoshells for drug delivery. *Adv. Drug Deliv. Rev.* **63,** 730–747 (2011).

52. Gillies, E. R., Jonsson, T. B. & Fréchet, J. M. J. Stimuli-Responsive Supramolecular Assemblies of Linear-Dendritic Copolymers. *J. Am. Chem. Soc.* **126,** 11936–11943 (2004).

53. Kim, J.-H., Lee, E., Park, J.-S., Kataoka, K. & Jang, W.-D. Dual stimuli-responsive dendritic-linear block copolymers. *Chem. Commun.* **48,** 3662–3664 (2012).

54. Oishi, M., Hayashi, H., Iijima, M. & Nagasaki, Y. Endosomal release and intracellular delivery of anticancer drugs using pH-sensitive PEGylated nanogels. *J. Mater. Chem.* **17,** 3720–3725 (2007).

55. Lee, E. S., Kim, D., Youn, Y. S., Oh, K. T. & Bae, Y. H. A Virus-Mimetic Nanogel Vehicle. *Angew. Chem. Int. Ed.* **47,** 2418–2421 (2008).

56. Wu, J. *et al.* Hydrophobic Cysteine Poly(disulfide)-based Redox-Hypersensitive Nanoparticle Platform for Cancer Theranostics. *Angew. Chem. Int. Ed Engl.* **54,** 9218–9223 (2015).

57. Li, S. Y. & Wang, M. Hybrid polymer-metal nanospheres based on highly branched gold nanoparticles for potential medical applications. *IET Nanobiotechnology IET* **6,** 136–143 (2012).

58. Qin, W., Lohrman, J. & Ren, S. Magnetic and Optoelectronic Properties of Gold Nanocluster–Thiophene Assembly. *Angew. Chem. Int. Ed.* **53,** 7316–7319 (2014).

59. Han, D., Hwang, H. & Park, J.-K. Optoelectrofluidic behavior of metal–polymer hybrid colloidal particles. *Appl. Phys. Lett.* **102,** 054105 (2013).

60. Kong, L., Lu, X. & Zhang, W. Facile synthesis of multifunctional multiwalled carbon nanotubes/Fe3O4 nanoparticles/polyaniline composite nanotubes. *J. Solid State Chem.* **181,** 628–636 (2008).

61. Hu, Y. *et al.* Entering and Lighting Up Nuclei Using Hollow Chitosan–Gold Hybrid Nanospheres. *Adv. Mater.* **21,** 3639–3643 (2009).

62. Sánchez-Iglesias, A. *et al.* Synthesis of Multifunctional Composite Microgels via In Situ Ni Growth on pNIPAM-Coated Au Nanoparticles. *ACS Nano* **3,** 3184–3190 (2009).

63. Dykman, L. A. & Khlebtsov, N. G. Gold Nanoparticles in Biology and Medicine: Recent Advances and Prospects. *Acta Naturae* **3,** 34–55 (2011).

64. Dykman, L. & Khlebtsov, N. Gold nanoparticles in biomedical applications: recent advances and perspectives. *Chem. Soc. Rev.* **41,** 2256–2282 (2012).

65. Boisselier, E. & Astruc, D. Gold nanoparticles in nanomedicine: preparations, imaging, diagnostics, therapies and toxicity. *Chem. Soc. Rev.* **38,** 1759–1782 (2009).

66. Dreaden, E. C., Alkilany, A. M., Huang, X., Murphy, C. J. & El-Sayed, M. A. The golden age: gold nanoparticles for biomedicine. *Chem. Soc. Rev.* **41,** 2740 (2012).

67. Geuze, H. J., Slot, J. W., Van Der Ley, P. A. & Scheffer, R. C. Use of colloidal gold particles in double-labeling immunoelectron microscopy of ultrathin frozen tissue sections. *J. Cell Biol.* **89,** 653–665 (1981).

68. Giljohann, D. A. *et al.* Gold Nanoparticles for Biology and Medicine. *Angew. Chem. Int. Ed.* **49,** 3280–3294 (2010).

69. Pitsillides, C. M., Joe, E. K., Wei, X., Anderson, R. & Lin, C. P. Selective cell targeting with light-absorbing microparticles and nanoparticles. *Biophys. J.* **84,** 4023–4032 (2003).

70. Huang, C.-M. *et al.* Eradication of drug resistant Staphylococcus aureus by liposomal oleic acids. *Biomaterials* **32,** 214–221 (2011).

71. Maltzahn, G. von *et al.* Computationally Guided Photothermal Tumor Therapy Using Long-Circulating Gold Nanorod Antennas. *Cancer Res.* **69,** 3892–3900 (2009).

72. Azzazy, H. M. E., Mansour, M. M. H., Samir, T. M. & Franco, R. Gold nanoparticles in the clinical laboratory: principles of preparation and applications. *Clin. Chem. Lab. Med.* **50,** 193–209 (2012).

73. CooperáStevenson, P., others. A study of the nucleation and growth processes in the synthesis of colloidal gold. *Discuss. Faraday Soc.* **11,** 55–75 (1951).

74. Ozawa, H. *et al.* Supramolecular Hybrid of Gold Nanoparticles and Semiconducting Single-Walled Carbon Nanotubes Wrapped by a Porphyrin–Fluorene Copolymer. *J. Am. Chem. Soc.* **133,** 14771–14777 (2011).

75. Perrault, S. D. & Chan, W. C. W. Synthesis and Surface Modification of Highly Monodispersed, Spherical Gold Nanoparticles of 50−200 nm. *J. Am. Chem. Soc.* **131,** 17042–17043 (2009).

76. Huang, X., El-Sayed, I. H., Qian, W. & El-Sayed, M. A. Cancer Cell Imaging and Photothermal Therapy in the Near-Infrared Region by Using Gold Nanorods. *J. Am. Chem. Soc.* **128,** 2115–2120 (2006).

77. Malardier-Jugroot, C., van de Ven, T. G. M. & Whitehead, M. A. Linear Conformation of Poly(styrene- *a lt* -maleic anhydride) Capable of Self-Assembly: A Result of Chain Stiffening by Internal Hydrogen Bonds. *J. Phys. Chem. B* **109,** 7022–7032 (2005).

78. Malardier-Jugroot, C., van de Ven, T. G. M., Cosgrove, T., Richardson, R. M. & Whitehead, M. A. Novel Self-Assembly of Amphiphilic Copolymers into Nanotubes: Characterization by Small-Angle Neutron Scattering. *Langmuir* **21,** 10179–10187 (2005).

79. McTaggart, M., Malardier-Jugroot, C. & Jugroot, M. Self-assembled biomimetic nanoreactors II: Noble metal active centers. *Chem. Phys. Lett.* **636,** 221–227 (2015).

80. McTaggart, M., Malardier-Jugroot, C. & Jugroot, M. Self-assembled biomimetic nanoreactors I: Polymeric template. *Chem. Phys. Lett.* **636,** 216–220 (2015).

81. Garnier, G., Duskova-Smrckova, M., Vyhnalkova, R., van de Ven, T. G. M. & Revol, J.-F. Association in Solution and Adsorption at an Air−Water Interface of Alternating Copolymers of Maleic Anhydride and Styrene. *Langmuir* **16,** 3757–3763 (2000).

82. Vargas-Hernandez, C., Mariscal, M. M., Esparza, R. & Yacaman, M. J. A synthesis route of gold nanoparticles without using a reducing agent. *Appl. Phys. Lett.* **96,** 213115 (2010).

83. *Ramachandran, K. I., G. Deepa, & K. Namboori. Computational Chemistry and Molecular Modeling: Principles and Applications. Berlin: Springer, (2008).*

84. Schnecke, V. & Boström, J. Computational chemistry-driven decision making in lead generation. *Drug Discov. Today* **11,** 43–50 (2006).

85. Sillar, K. & Sauer, J. Ab Initio Prediction of Adsorption Isotherms for Small Molecules in Metal–Organic Frameworks: The Effect of Lateral Interactions for Methane/CPO-27-Mg. *J. Am. Chem. Soc.* **134,** 18354–18365 (2012).

86. Rablen, P. R., Lockman, J. W. & Jorgensen, W. L. Ab Initio Study of Hydrogen-Bonded Complexes of Small Organic Molecules with Water. *J. Phys. Chem. A* **102,** 3782–3797 (1998).

87. Cramer, C. J. & Truhlar, D. G. Density functional theory for transition metals and transition metal chemistry. *Phys. Chem. Chem. Phys.* **11,** 10757–10816 (2009).

88. Atkins, P. W. & Friedman, R. S. *Molecular Quantum Mechanics*. (OUP Oxford, 2011).

89. Martin, C. R. & Mitchell, D. T. Peer Reviewed: Nanomaterials in Analytical Chemistry. *Anal. Chem.* **70,** 322A–327A (1998).

90. Hammes-Schiffer, S. & Andersen, H. C. Ab initio and semiempirical methods for molecular dynamics simulations based on general Hartree–Fock theory. *J. Chem. Phys.* **99,** 523–532 (1993).

91. Shirley, J. H. Solution of the Schr"odinger Equation with a Hamiltonian Periodic in Time. *Phys. Rev.* **138,** B979–B987 (1965).

92. Hartree, D. R. The Wave Mechanics of an Atom with a Non-Coulomb Central Field. Part I. Theory and Methods. *Math. Proc. Camb. Philos. Soc.* **24,** 89 (1928).

93. March, N. H. *Self-Consistent Fields in Atoms: Hartree and Thomas-Fermi Atoms*. (Elsevier, 2013).

94. Møller, C. & Plesset, M. S. Note on an Approximation Treatment for Many-Electron Systems. *Phys. Rev.* **46,** 618–622 (1934).

95. Parr, R. G. & Weitao, Y. *Density-Functional Theory of Atoms and Molecules*. (Oxford University Press, 1994).

96. Hohenberg, P. & Kohn, W. Inhomogeneous Electron Gas. *Phys. Rev.* **136,** B864–B871 (1964).

97. Kohn, W. & Sham, L. J. Self-Consistent Equations Including Exchange and Correlation Effects. *Phys. Rev.* **140,** A1133–A1138 (1965).

98. Becke, A. D. A new mixing of Hartree–Fock and local density-functional theories. *J. Chem. Phys.* **98,** 1372–1377 (1993).

99. Rudolph, M. & Autschbach, J. Performance of Conventional and Range-Separated Hybrid Density Functionals in Calculations of Electronic Circular Dichroism Spectra of Transition Metal Complexes. *J. Phys. Chem. A* **115,** 14677–14686 (2011).

100. Becke, A. D. Density-functional thermochemistry. III. The role of exact exchange. *J. Chem. Phys.* **98,** 5648–5652 (1993).

101. Lee, C., Yang, W. & Parr, R. G. Development of the Colle-Salvetti correlation-energy formula into a functional of the electron density. *Phys. Rev. B* **37,** 785–789 (1988).

102. Matulis, V. E., Palagin, D. M. & Ivashkevich, O. A. Theoretical study of optical properties of gold clusters. *Russ. J. Gen. Chem.* **80,** 1078–1085 (2010).

103. Hehre, W. J., Ditchfield, R. & Pople, J. A. Self—Consistent Molecular Orbital Methods. XII. Further Extensions of Gaussian—Type Basis Sets for Use in Molecular Orbital Studies of Organic Molecules. *J. Chem. Phys.* **56,** 2257–2261 (1972).

104. M.J. Frisch, G.W. Trucks, H. Schlegel, G.E. Scuseria, M.A. Robb, J.R. Cheeseman,G. Scalmani, V. Barone, B. Mennucci, G.A. Petersson, H. Nakatsuji, M. Caricato,X. Li, H.P. Hratchian, A.F. Izmaylov, J. Bloino, G. Zheng, J.L. Sonnenberg, M. Hada,M. Ehara, K. Toyota, R. Fukuda, J. Hasegawa, M. Ishida, T. Nakajima, Y. Honda,O. Kitao, H. Nakai, T. Vreven, J.A. Montgomery, J.E. Peralta Jr., F. Ogliaro, M.Bearpark, J.J. Heyd, E. Brothers, K.N. Kudin, V.N. Staroverov, R. Kobayashi, J. Nor-mand, K. Raghavachari, A. Rendell, J.C. Burant, S.S. Iyengar, J. Tomasi, M. Cossi, N.Rega, J.M. Millam, M. Klene, J.E. Knox, J. Cross, V. Bakken, C. Adamo, J. Jaramillo,R. Gomperts, R.E. Stratmann, O. Yazyev, A.J. Austin, R. Cammi, C. Pomelli, J.W.Ochterski, R.L. Martin, K. Morokuma, V.G. Zakrzewski, G.A. Voth, P. Salvador,J.J. Dannenberg, S. Dapprich, A.D. Daniels, Ö. Farkas, J.B. Foresman, J.V. Ortiz, J.Cioslowski, D.J. Fox, Gaussian 09, Revision B.01, Gaussian Inc., Wallingford, CT,2009.

105. Huang, X. *et al.* Synthesis of hexagonal close-packed gold nanostructures. *Nat. Commun.* **2,** 292 (2011).

106. *Reimer, Ludwig. Transmission Electron Microscopy: Physics of Image Formation and Microanalysis. Berlin: Springer-Verlag, (1984).*

107. Murr, L. F. *Electron and Ion Microscopy and Microanalysis: Principles and Applications*. (Marcel Dekker Inc, 1982).

108. ImageJ. Available at: https://imagej.nih.gov/ij/. (Accessed: 13th July 2016) Abramoff, M.D., Magalhaes, P.J., Ram, S.J. "Image Processing with ImageJ". Biophotonics International, volume 11, issue 7, pp. 36-42, (2004).

109. Laroui, H. *et al.* Nanomedicine in GI. *Am. J. Physiol. Gastrointest. Liver Physiol.* **300,** G371–383 (2011).

110. Thiruvengadathan, R. *et al.* Nanomaterial processing using self-assembly-bottom-up chemical and biological approaches. *Rep. Prog. Phys.* **76,** 066501 (2013).

111. Chhabra, R., Sharma, J., Liu, Y., Rinker, S. & Yan, H. DNA Self-assembly for Nanomedicine. *Adv. Drug Deliv. Rev.* **62,** 617–625 (2010).

112. Bertrand, O., Poggi, E., Gohy, J.-F. & Fustin, C.-A. Functionalized Stimuli-Responsive Nanocages from Photocleavable Block Copolymers. *Macromolecules* **47,** 183–190 (2014).

113. Ellis, R. J. Macromolecular crowding: obvious but underappreciated. *Trends Biochem. Sci.* **26,** 597–604 (2001).

114. Hummer, G., Rasaiah, J. C. & Noworyta, J. P. Water conduction through the hydrophobic channel of a carbon nanotube. *Nature* **414,** 188–190 (2001).

115. Li, X. & Malardier-Jugroot, C. Synthesis of polypyrrole under confinement in aqueous environment. *Mol. Simul.* **37,** 694–700 (2011).

116. Henao, J. D., Suh, Y.-W., Lee, J.-K., Kung, M. C. & Kung, H. H. Striking Confinement Effect: $AuCl_4^-$ Binding to Amines in a Nanocage Cavity. *J. Am. Chem. Soc.* **130,** 16142–16143 (2008).

117. Li, C., Zhou, Q., Gu, Z., Zhao, L. & Zheng, J. Fabrication and electrocatalytic activity of single gold particles in highly ordered SiO2 cavities. *Electrochem. Commun.* **22,** 113–115 (2012).

118. Mohammadnejad, S., Provis, J. L. & van Deventer, J. S. J. Reduction of gold(III) chloride to gold(0) on silicate surfaces. *J. Colloid Interface Sci.* **389,** 252–259 (2013).

119. Mechler, A. *et al.* with Sirajuddin. The formation of gold nanoparticles using hydroquinone as a reducing agent through a localized pH change upon addition of NaOH to a solution of HAuCl4. *Colloids Surf. Physicochem. Eng. Asp.* **370,** 35–41 (2010).

120. Newman, J. D. S. & Blanchard, G. J. Formation of Gold Nanoparticles Using Amine Reducing Agents. *Langmuir* **22,** 5882–5887 (2006).

121. Yanlian, Y. *et al.* Designer self-assembling peptide nanomaterials. *Nano Today* **4,** 193–210 (2009).

122. Marin, A. *et al.* Drug delivery in pluronic micelles: effect of high-frequency ultrasound on drug release from micelles and intracellular uptake. *J. Controlled Release* **84,** 39–47 (2002).

123. Husseinia, G. A., Myrupa, G. D., Pitt, W. G., Christensena, D. A. & Rapoport, N. Y. Factors affecting acoustically triggered release of drugs from polymeric micelles. (2000).

124. Bieri, M. & Bürgi, T. Adsorption kinetics, orientation, and self-assembling of N-acetyl-L-cysteine on gold: a combined ATR-IR, PM-IRRAS, and QCM study. *J. Phys. Chem. B* **109,** 22476–22485 (2005).

125. Han, S. W., Joo, S. W., Ha, T. H., Kim, Y. & Kim, K. Adsorption Characteristics of Anthraquinone-2-carboxylic Acid on Gold. *J. Phys. Chem. B* **104,** 11987–11995 (2000).

126. He, Y. Q., Liu, S. P., Kong, L. & Liu, Z. F. A study on the sizes and concentrations of gold nanoparticles by spectra of absorption, resonance Rayleigh scattering and resonance non-linear scattering. *Spectrochim. Acta. A. Mol. Biomol. Spectrosc.* **61,** 2861–2866 (2005).

127. Haiss, W., Thanh, N. T. K., Aveyard, J. & Fernig, D. G. Determination of Size and Concentration of Gold Nanoparticles from UV−Vis Spectra. *Anal. Chem.* **79,** 4215–4221 (2007).

128. Tsuji, M. *et al.* Shape and size controlled synthesis of gold nanocrystals using oxidative etching by AuCl4− and Cl− anions in microwave-polyol process. *Colloids Surf. Physicochem. Eng. Asp.* **302,** 587–598 (2007).

129. Helmi, S., Ziegler, C., Kauert, D. J. & Seidel, R. Shape-Controlled Synthesis of Gold Nanostructures Using DNA Origami Molds. *Nano Lett.* **14,** 6693–6698 (2014).

130. Kim, J., Samano, E. & Koel, B. E. CO Adsorption and Reaction on Clean and Oxygen-Covered Au(211) Surfaces. *J. Phys. Chem. B* **110,** 17512–17517 (2006).

131. Šmit, G., Strukan, N., Crajé, M. W. J. & Lázár, K. A comparative study of CO adsorption and oxidation on Au/Fe2O3 catalysts by FT-IR and in situ DRIFTS spectroscopies. *J. Mol. Catal. Chem.* **252,** 163–170 (2006).

132. Jomni, S. *et al.* Face centred cubic cobalt ultrathin-layers in Au/Co(111) multilayers: a study by electron diffraction and by HREM. *Thin Solid Films* **370,** 186–191 (2000).

133. Ohnuma, A., Cho, E. C., Jiang, M., Ohtani, B. & Xia, Y. Metal−Polymer Hybrid Colloidal Particles with an Eccentric Structure. *Langmuir* **25,** 13880–13887 (2009).

134. Lee, J.-H., Mahmoud, M. A., Sitterle, V., Sitterle, J. & Meredith, J. C. Facile Preparation of Highly-Scattering Metal Nanoparticle-Coated Polymer Microbeads and Their Surface Plasmon Resonance. *J. Am. Chem. Soc.* **131,** 5048–5049 (2009).

135. Jung, Y., Singh, N. & Choi, K.-S. Cathodic Deposition of Polypyrrole Enabling the One-Step Assembly of Metal-Polymer Hybrid Electrodes. *Angew. Chem. Int. Ed.* **48,** 8331–8334 (2009).

136. Pakiari, A. H. & Jamshidi, Z. Nature and Strength of M−S Bonds (M = Au, Ag, and Cu) in Binary Alloy Gold Clusters. *J. Phys. Chem. A* **114,** 9212–9221 (2010).

137. Perala, S. R. K. & Kumar, S. On the Mechanism of Metal Nanoparticle Synthesis in the Brust–Schiffrin Method. *Langmuir* **29,** 9863–9873 (2013).

138. Häkkinen, H. The gold-sulfur interface at the nanoscale. *Nat. Chem.* **4,** 443–455 (2012).

139. Love, J. C., Estroff, L. A., Kriebel, J. K., Nuzzo, R. G. & Whitesides, G. M. Self-assembled monolayers of thiolates on metals as a form of nanotechnology. *Chem. Rev.* **105,** 1103–1169 (2005).

140. Xue, Y., Li, X., Li, H. & Zhang, W. Quantifying thiol–gold interactions towards the efficient strength control. *Nat. Commun.* **5,** 4348 (2014).

141. Mushrush, M., Facchetti, A., Lefenfeld, M., Katz, H. E. & Marks, T. J. Easily Processable Phenylene−Thiophene-Based Organic Field-Effect Transistors and Solution-Fabricated Nonvolatile Transistor Memory Elements. *J. Am. Chem. Soc.* **125,** 9414–9423 (2003).

142. Kim, J., Jo, Y., Choi, W.-Y., Jun, Y. & Yang, C. Thiophene-fused coplanar sensitizer for dye-sensitized solar cells. *Tetrahedron Lett.* **52,** 2764–2766 (2011).

143. Li, H., Guo, J., Zhang, X. & Chen, Z. A Novel Colorimetric and Fluorescent pH Sensor Derived from Iminocoumarin and Thiophene-Carboxaldehyde. *Heteroat. Chem.* **23,** 551–559 (2012).

144. Balzer, F., Schiek, M., Lützen, A. & Rubahn, H.-G. Self-Organized Growth of Organic Thiophene−Phenylene Nanowires on Silicate Surfaces. *Chem. Mater.* **21,** 4759–4767 (2009).

145. Rasmussen, S. C., Evenson, S. J. & McCausland, C. B. Fluorescent thiophene-based materials and their outlook for emissive applications. *Chem. Commun.* **51,** 4528–4543 (2015).

146. Handbook of Thiophene-Based Materials: Applications in Organic Electronics and Photonics, 2 Volume Set." *Wiley:*. N.p., n.d. Web. 18 Sept. 2016.

147. Matsuura, T. & Shimoyama, Y. Growth kinetics of self-assembled monolayers of thiophene and terthiophene on Au(111): An infrared spectroscopic study. *Eur. Phys. J. E* **7,** 233–240 (2002).

148. Matsuura, T., Nakajima, M. & Shimoyama, Y. Growth of Self-Assembled Monolayer of Thiophene on Gold Surface: An Infrared Spectroscopic Study. *Jpn. J. Appl. Phys.* **40,** 6945–6950 (2001).

149. Noh, J. *et al.* High-Resolution STM and XPS Studies of Thiophene Self-Assembled Monolayers on Au(111). *J. Phys. Chem. B* **106,** 7139–7141 (2002).

150. Aryal, S. *et al.* Spectroscopic identification of SAu interaction in cysteine capped gold nanoparticles. *Spectrochim. Acta. A. Mol. Biomol. Spectrosc.* **63,** 160–163 (2006).

151. Jung, Y. J. *et al.* Luminescent gold–poly(thiophene) nanoaggregates prepared by one-step oxidative polymerization. *J. Mater. Chem.* **20,** 9770–9774 (2010).

152. Vernitskaya, T. V. & Efimov, O. N. Polypyrrole: a conducting polymer; its synthesis, properties and applications. *Russ. Chem. Rev.* **66,** 443–457 (1997).

153. Stenger-Smith, J. D. Intrinsically electrically conducting polymers. Synthesis, characterization, and their applications. *Prog. Polym. Sci.* **23,** 57–79 (1998).

154. Ateh, D. ., Navsaria, H. . & Vadgama, P. Polypyrrole-based conducting polymers and interactions with biological tissues. *J. R. Soc. Interface* **3,** 741–752 (2006).

155. Wang, X. *et al.* Evaluation of biocompatibility of polypyrrole in vitro and in vivo. *J. Biomed. Mater. Res. A* **68A,** 411–422 (2004).

156. Aoki, T., Tanino, M., Sanui, K., Ogata, N. & Kumakura, K. Secretory function of adrenal chromaffin cells cultured on polypyrrole films. *Biomaterials* **17,** 1971–1974 (1996).

157. Campbell, T. E., Hodgson, A. J. & Wallace, G. G. Incorporation of Erythrocytes into Polypyrrole to Form the Basis of a Biosensor to Screen for Rhesus (D) Blood Groups and Rhesus (D) Antibodies. *Electroanalysis* **11,** 215–222 (1999).

158. Ateh, D. D. *et al.* Impedimetric sensing of cells on polypyrrole-based conducting polymers. *J. Biomed. Mater. Res. A* **83,** 391–400 (2007).

159. Fonner, J. M. *et al.* Biocompatibility implications of polypyrrole synthesis techniques. *Biomed. Mater.* **3,** 034124 (2008).

160. Zhang, X., Zhang, J., Song, W. & Liu, Z. Controllable Synthesis of Conducting Polypyrrole Nanostructures. *J. Phys. Chem. B* **110,** 1158–1165 (2006).

161. Kızılcan, N. & Ustamehmetoğlu, B. Chemical polymerization of pyrrole in the presence of ketone–formaldehyde resins. *J. Appl. Polym. Sci.* **96,** 618–624 (2005).

162. Skothiem, T. & Reynolds, J. *Conjugated Polymers: Theory, Synthesis, Properties, and Characterization* - CRC Press Taylor & Francis Group: Boca Raton, FL, 2006.

163. Kudoh, Y. Properties of polypyrrole prepared by chemical polymerization using aqueous solution containing Fe2(SO4)3 and anionic surfactant. *Synth. Met.* **79,** 17–22 (1996).

164. Genies, E. M., Bidan, G. & Diaz, A. F. Spectroelectrochemical study of polypyrrole films. *J. Electroanal. Chem. Interfacial Electrochem.* **149,** 101–113 (1983).

165. Cai, Z. & Martin, C. R. Electronically conductive polymer fibers with mesoscopic diameters show enhanced electronic conductivities. *J. Am. Chem. Soc.* **111,** 4138–4139 (1989).

166. Kim, B. H., Park, D. H., Joo, J., Yu, S. G. & Lee, S. H. Synthesis, characteristics, and field emission of doped and de-doped polypyrrole, polyaniline, poly(3,4-ethylenedioxythiophene) nanotubes and nanowires. *Synth. Met.* **150,** 279–284 (2005).

167. De Vito, S. & Martin, C. R. Toward Colloidal Dispersions of Template-Synthesized Polypyrrole Nanotubules. *Chem. Mater.* **10,** 1738–1741 (1998).

168. Martin, C. R. Membrane-Based Synthesis of Nanomaterials. *Chem. Mater.* **8,** 1739–1746 (1996).

169. Tan, Y. & Ghandi, K. Kinetics and mechanism of pyrrole chemical polymerization. *Synth. Met.* **175,** 183–191 (2013).

170. Zhang, B. *et al.* Facet-Dependent Catalytic Activity of Platinum Nanocrystals for Triiodide Reduction in Dye-Sensitized Solar Cells. *Sci. Rep.* **3,** (2013).

171. Chen, J., Herricks, T. & Xia, Y. Polyol Synthesis of Platinum Nanostructures: Control of Morphology through the Manipulation of Reduction Kinetics. *Angew. Chem.* **117,** 2645–2648 (2005).

172. Zhou, H.-X., Rivas, G. & Minton, A. P. Macromolecular crowding and confinement: biochemical, biophysical, and potential physiological consequences. *Annu. Rev. Biophys.* **37,** 375–397 (2008).

173. Otero, T. F. & Martinez, J. G. Activation energy for polypyrrole oxidation: film thickness influence. *J. Solid State Electrochem.* **15,** 1169–1178 (2011).

174. Otero, T. F. & García de Otazo, J. M. Polypyrrole oxidation: Kinetic coefficients, activation energy and conformational energy. *Synth. Met.* **159,** 681–688 (2009).

175. Bjorklund, R. B. Kinetics of pyrrole polymerisation in aqueous iron chloride solution. *J. Chem. Soc. Faraday Trans. 1 Phys. Chem. Condens. Phases* **83,** 1507–1514 (1987).

176. Cavallaro, S., Colligiani, A. & Cum, G. Oxidative chemical polymerization of pyrrole. *J. Therm. Anal.* **38,** 2649–2655 (1992).

177. Planche, M. F., Thiéblemont, J. C., Mazars, N. & Bidan, G. Kinetic study of pyrrole polymerization with iron (III) chloride in water. *J. Appl. Polym. Sci.* **52,** 1867–1877 (1994).

178. Shirazi, A. N. *et al.* Cysteine and arginine-rich peptides as molecular carriers. *Bioorg. Med. Chem. Lett.* **26,** 656–661 (2016).

179. Kim, K. T., Meeuwissen, S. A., Nolte, R. J. M. & Hest, J. C. M. van. Smart nanocontainers and nanoreactors. *Nanoscale* **2,** 844–858 (2010).

180. Malardier-Jugroot, C., Ven, T. G. M. van de & Whitehead, M. A. Characterization of a novel self-association of an alternating copolymer into nanotubes in solution. *Mol. Simul.* **31,** 173–178 (2005).

181. Yang, J., Duan, Y., Zhang, X., Wang, Y. & Yu, A. Modulating the cellular microenvironment with disulfide-containing nanoparticles as an auxiliary cancer treatment strategy. *J. Mater. Chem. B* **4,** 3868–3873 (2016).

182. Peltonen, L., Aitta, J., Hyvönen, S., Karjalainen, M. & Hirvonen, J. Improved entrapment efficiency of hydrophilic drug substance during nanoprecipitation of poly(l)lactide nanoparticles. *AAPS PharmSciTech* **5,** E16 (2004).

183. Duncan, G. A. & Bevan, M. A. Computational design of nanoparticle drug delivery systems for selective targeting. *Nanoscale* **7,** 15332–15340 (2015).

184. Lipinski, C. A., Lombardo, F., Dominy, B. W. & Feeney, P. J. Experimental and computational approaches to estimate solubility and permeability in drug discovery and development settings. *Adv. Drug Deliv. Rev.* **46,** 3–26 (2001).